Oxydation de Sr2Co2O5 par voie électrochimique

Petr Bezdicka

N° d'ordre 988

THESE

PRESENTEE A

L'UNIVERSITE BORDEAUX I

ECOLE DOCTORALE DES SCIENCES CHIMIQUES

Par **M. Petr Bezdička**

POUR OBTENIR LE GRADE DE

DOCTEUR

SPECIALITE: CHIMIE DU SOLIDE, SCIENCES DES MATERIAUX

Titre : Oxydation de $Sr_2Co_2O_5$ par voie électrochimique.

Soutenue le : 5 octobre 1993

Après avis de : M. Juan Rodriguez - Carvajal — Rapporteurs
M. Dominique Guyomard

Devant la Commission d'examen formée de :

M. P. Hagenmuller, Professeur	Président
M. M. Pouchard, Professeur	Rapporteur
M. J. Rodriguez - Carvajal, D. R., CNRS	
M. J. Etourneau, Professeur	
M. D. Guyomard, C.R., CNRS	
M. J.C. Grenier, D. R., CNRS	
M. J. Vondrák, D. R., ASCR	
M. A. Wattiaux, I.R., CNRS	

1993

Tout ce que je sais c'est que je ne sais rien

Jean Gabin

Ce travail a été réalisé au Laboratoire de Chimie du Solide du C.N.R.S. de l'Université de Bordeaux I, Talence, France.

Que Monsieur **P. Hagenmuller** veuille bien trouver ici l'expression de ma reconnaissance pour me faire l'honneur de présider ce jury de thèse.

Je remercie Monsieur **J. Etourneau**, Directeur du Laboratoire de Chimie du Solide du CNRS, pour l'accueil qu'il m'a réservé et pour avoir participé à ce jury de thèse.

Monsieur **M. Pouchard** a suivi mon travail avec toute sa compétence et sa gentillesse. Qu'il veuille trouver ici l'expression de ma sincère reconnaissance.

Monsieur **J. Rodriguez-Carvajal** a apporté son aide efficace dans le domaine de la cristallographie. Je suis aussi bien sensible à l'honneur qu'il m'a fait d'être présent à ce jury de thèse.

Monsieur **D. Guyomard** a bien voulu juger ce travail. Je lui exprime mes sincères et respecteux remerciements.

Je tiens à remercier vivement Monsieur **J. Vondrák**, qui a participé à la réalisation de ce travail. Je le remercie pour ses conseils judicieux et pour sa gentillesse.

Monsieur **A. Wattiaux** a apporté toutes ses compétences et ses qualités humaines pour m'aider à réaliser ce travail. Qu'il veuille bien trouver ici le témoignage de ma profonde amitié.

Que Monsieur **J.C. Grenier** qui a dirigé ces recherches avec patience et disponibilité tout à fait particulière, veuille bien trouver ici l'expression de ma gratitude.

Je voudrais également remercier toutes les personnes qui ont contribué par leurs discussions et leur "savoir faire" à l'achèvement de ce travail.

Table of Contents

INTRODUCTION

Pour certaines réactions chimiques l'utilisation du potentiel électrochimique peut être un outil très puissant pour obtenir de nouveaux matériaux dans des conditions inhabituelles pour un Chimiste du Solide. Elle a été récemment développée au Laboratoire de Chimie du Solide dans le cas de l'oxydation électrochimique en milieu alcalin, à température ambiante et à l'air, ce qui a conduit à préparer pour la première fois dans ces conditions des oxydes à hauts degrés d'oxydation. Cette nouvelle méthode de "Chimie Douce" a par ailleurs été adoptée par plusieurs laboratoires nationaux ou étrangers pour préparer en particulier des matériaux supraconducteurs [1-5].

L'oxydation électrochimique d'une céramique du ferrite $Sr_2Fe_2O_5$ isolant en $SrFeO_3$, composé métallique contenant uniquement du fer tétravalent [6], a permis de démontrer pour la première fois que cette réaction était à coeur. Ce résultat pouvait aussi s'interpréter comme l'intercalation d'oxygène dans un réseau déficitaire en oxygène tel celui de la brownmillerite $Sr_2Fe_2O_5$.

D'autres résultats spectaculaires ont été obtenus avec les composés du nickel et du cuivre de structure K_2NiF_4 dont le taux de surstoechiométrie en oxygène a pu être largement augmenté. Ainsi, un nouveau composé $La_2NiO_{4.25}$ ($La_8Ni_4O_{17}$) a été préparé [7]. L'affinement de sa structure a permis en outre de définitivement montrer que l'oxygène additionnel était inséré de façon ordonnée dans les feuillets La_2O_2 de la structure mère La_2NiO_4 dans un polyèdre comportant comme ligands quatre atomes de lanthane et quatre atomes d'oxygène. Une insertion d'oxygène tout à fait similaire dans les phases $La_{2-x}A_xCuO_4$ (A = Sr, Nd) a conduit à l'obtention de matériaux métalliques, supraconducteurs à basse température. Dans le cas du composé La_2CuO_4 (x=0), la température de transition T_c a pu être portée jusqu'à la valeur 44 K pour la composition $La_2CuO_{4.09}$ [1]. Ainsi, pour des structures mères ne comportant pas de lacunes anioniques, la réaction d'oxydation ne pouvait être interprétée qu'en termes d'intercalation d'oxygène dans des sites interstitiels.

Ces processus réactionnels s'effectuant à température ambiante de manière

concurrente à la réaction de dégagement de l'oxygène,

$$4OH^- \longleftrightarrow O_2(g) + 2H_2O + 4e^-$$

posent évidemment plusieurs questions non encore résolues:

- quel est le mécanisme réactionnel et quelles espèces sont mises en jeu ?

- s'il est bien connu que des cations de taille raisonnable ($r << 100$ pm) peuvent migrer assez facilement à température ambiante, dans un matériau solide, et en particulier dans des oxydes, il est plus difficile de l'imaginer pour une espèce comme O^{2-} dont la taille est de l'ordre de 140 pm.

Des études systématiques s'avèrent nécessaires; pour répondre à ces questions. Notre travail a pour but d'y contribuer, notre choix s'est porté sur un autre élément 3d que ceux précédemment étudiés, le **cobalt**.

Plusieurs oxydes de cobalt dont les structures dérivent soit de la perovskite, soit de type K_2NiF_4 sont actuellement connus. Plus particulièrement l'oxyde $Sr_2Co_2O_5$ était tout à fait attrayant dans la mesure où ce composé semble posséder trois variétés structurales liées à la configuration électronique du cobalt trivalent et/ou à l'ordre du réseau oxygéné: à basse température une structure lacunaire en oxygène dérivant de la structure de la perovskite hexagonale 2H dans laquelle le cobalt trivalent serait plutôt dans un état spin faible. A haute température, une phase de type perovskite cubique dans laquelle les lacunes d'oxygène seraient désordonnées conduisant par trempe brutale à la structure brownmillerite, métastable à basse température. Dans ces deux dernières phases, le cobalt seraient dans un état spin fort.

De ce fait, par analogie avec $Sr_2Fe_2O_5$, on pouvait espérer préparer deux variétés de la phase totalement oxydée $SrCoO_3$, l'une la perovskite cubique et l'autre hexagonale comportant des états de spin différents du cobalt.

Dans une première partie de ce mémoire nous préciserons les données cristallographiques des matériaux de départ, puis dans une deuxième partie nous étudierons leurs conditions d'oxydation et enfin caractériserons les produits oxydés. Ce travail mettra en evidence l'influence de la structure initiale sur l'aptitude à l'oxydation.

References page 4

References

1) Lagueyte N., Wattiaux A., Park J.C., Grenier J.C., Fournès L., Pouchard M., J. Phys. **III**, **1**, 1755, 1991.

2) Arrouy F., Wattiaux A., Cros C., Demazeau G., Grenier J.C., Pouchard M., Etourneau J., Physica C, **175**, 487, 1991.

3) Bennet J.C., Olfert M., Scholz G.A., Boswell F.W., Physical Review B, **44**, 2727,1991.

4) Rudolf. P., Paulus W., Schöllhorn R., Advanced Materials, **3**, 438, 1991.

5) Chou F.C., Cho J.H., Johnston D.C., Physica C, **197**, 303, 1992.

6) Wattiaux A., Fournès L., Demourgues A., Bernaben N., Grenier J.C., Pouchard M., Solid State Commun., 77, 489, 1991.

7) Demourgues A., Weill F., Grenier J.C., Wattiaux A., Pouchard M., Physica C, **192**, 425, 1992.

8) Grenier J.C., Ghodbane S., Demazeau G., Pouchard M., Hagenmuller P., Mat. Res. Bull., **14**, 831, 1979.

9) Rodriguez J., *Thèse, Université de Barcelone*, 1984.

Chapter I

STRUCTURAL REMARKS

I.1. The Perovskite structure.

The crystal structure of the perovskite (the mineral $CaTiO_3$) is a very simple one. In its idealized form it is cubic with Ti^{4+} ions (B ions, general formula ABO_3) at the corners of the unit cell, a Ca^{2+} ion (A ion) at the body centre, and O^{2-} ions at the mid-points of the edges. This first type of unit cell is shown in Fig. 1a. When the origin of the cubic unit cell is taken at the Ca^{2+} ion, then the Ti^{4+} ion occupies the body centre and the O^{2-} ions the face centres; this second type of unit cell is shown in Fig. 1 b.

Each Ca^{2+} is thus 12 - fold and each Ti^{4+} 6 - fold coordinated by oxygen neighbours, while each O^{2-} is linked to four Ca^{2+} and two Ti^{4+} ions. As expected, it is the larger metal ion which occupies the site of higher coordination. One should point out that geometrically the structure can be regarded as a close-packed array of CaO_3 planes along $[111]_c$ direction of the cubic unit cell, with the Ti^{4+} ions occupying 1/4 of the octahedral interstices.

Many ABO_3 crystals give very simple diffraction patterns that can be accounted in terms of a cubic cell containing one formula unit like $CaTiO_3$. Some of these have true cubic symmetry, whereas some have appreciably distorted atomic arrangements. It is clear that in such a symmetrical structure a simple relationship must exist between the ionic radii of the various atoms.

Ideally this relationship is

$$r_A + r_O = \sqrt{2}\,(r_B + r_O)$$

but it is found that in practice the structure appears whenever the condition

$$r_A + r_O = t\sqrt{2}\,(r_B + r_O)$$

helds. Here t is the so - called tolerance factor, introduced by Goldschmidt [1], which may lie within the approximate limiting range 0.75 -1.1 If t lies outside this range, other structures are obtained

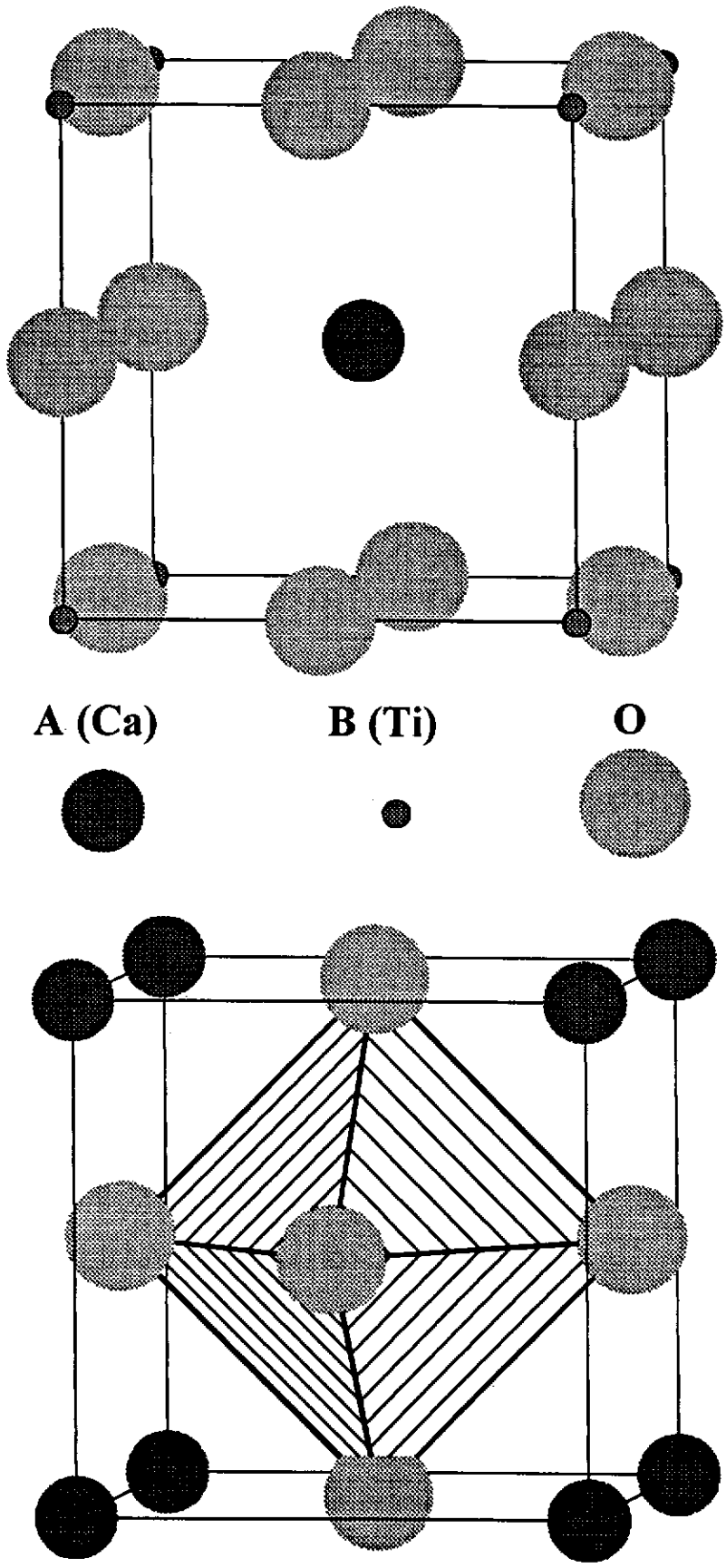

Fig. 1. Ideal perovskite structure: a) B cation at origin, b) A cation at origin

References page 16

In all the perovskite compounds, the A ions are large (e.g. K, Ca, Sr, Ba, La) and comparable in size to the oxygen or fluoride ions, as expected, since both the A and O (or F) ions form a close - packed array. Similarly, the B ions are small, since they must have a radius appropriate for a 6 - fold coordination by oxygen (or fluorine). These conditions are merely another expression of the fact that the radii have to satisfy the relation of the tolerance factor t within the quoted range.

According to these previous considerations, oxides adopting the perovskite structure may be divided into three principal classes:

1) if $t \cong 1$, the cubic symmetry is observed.

2) for $0.75 < t < 1$, according to the t value the symmetry becomes rhombohedral or orthorhombic. More especially, when the A cation is too small ($r_A <$ 90 pm) to accommodate twelve nearest neighbours, a structure in which the A and B cations are both six-coordinated becomes competitive.

In fact the same influence on the distortion of the ideal cubic structure may be caused by changes in the B cation radii. The electronic configuration and subsequently the ionic radius of the B cation may be expressed in terms of deformation of BO_6 polyhedra leading to the same type of distortions caused by changes in the ionic radii of the A cations. For example, when the radius of the B cation in octahedral site increases ($r_{Ni^{3+}_{LS}} = 56$ pm $< r_{Fe^{3+}} = 65$ pm) a distortion appears: $LaNiO_3$ ($t = 0.96$) crystallizes in the $R\bar{3}c$ system and $LaFeO_3$ ($t = 0.94$) in the Pnma one, respectively.

3) for $t > 1$, when the A cation is too large, the close packed AO_3 layers tend to change their stacking sequence from cubic to hexagonal. However, the change from the all-cubic stacking to the all-hexagonal stacking (2H) goes via some intermediate steps, as it will be discussed later.

An important property of the oxides having the perovskite - type structure is that of nonstoichiometry. There are basically three types of nonstoichiometry: The

cation nonstoichiometry concerned with the A site or B site and the oxygen nonstoichiometry, respectively.

I.2. A - site cation vacancies

As the skeleton of corner sharing octahedra is stable, it is possible to remove the A cations without destruction of the BO_3 network. In the case of ReO_3 the structure remains cubic. WO_3, on the other hand, exhibits several low - temperature phases characteristic of different degrees of the distortion of the perovskite structure (distortion of B - O -B angle). Another typical example of this category of compounds is that of tungsten bronzes. The perovskite - type structure appears with an A_xWO_3 formulation either for small values of x or for very large ones (x close to 1) [3].

I.3. B - site cation vacancies

The B - site vacancies are almost unknown in the cubic perovskite and seem to appear only in hexagonal perovskites as a result of strong repulsions through the common faces of octahedra. Due to the electrostatic character of this phenomenon, B - site vacancies are generally ordered occupying privileged sites of the hexagonal unit cell [4,5]. As B - B repulsions are strongly attenuated in corner sharing octahedra, few examples of B - cation vacancies have been reported for cubic perovskites. [6,7].

I.4. The oxygen deficiency

The oxygen deficiency in perovskite - related oxides ABO_{3-y} is quite usual and, in some cases, the amount of anionic vacancies can reach values as high as 33% ($y = 1$), the cationic sublattice being preserved.

References page 16

This oxygen deficiency involves a change in the electronic charges of the anionic sublattice and is possible owing two various factors:

-either the B cation can adopt various oxidation states.

- or a charge compensation is achieved on the cationic sublattice thanks to appropriate substitutions.

According to the nonstoichiometry coefficient (y), the defects can be isolated ($y \cong 0$), then ordered in a short range and in a long range as (y) increases. Various structural models have been proposed, more particularly for the ferrites [8].

It was thus pointed out that the way in which the oxygen vacancies are ordered, depends basically upon the electronic configuration of the cation and its stabilisation in the oxygenated ligand fields [9]. For instance cations as Fe^{3+}, Co^{3+} or Al^{3+} may adopt a tetrahedral coordination, Ni^{2+} or Cu^{3+} cations prefer a square planar sites and Mn^{3+}, Fe^{4+} or Cu^{2+} a pyramidal ones.

For minimising the electrostatic interactions oxygen vacancies are ordered; this feature was shown for the first time in 1976 by Grenier et al. [10] in $Ca_2LaFe_3O_8$ ($y = 0.33$) - related compounds. Nowadays, the most famous example is the superconducting oxide $YBa_2Cu_3O_7$ ($y \cong 0.67$).

The accommodation of the oxygen nonstoichiometry occurs through mainly two kinds of process:

- intergrowth between "line phases"

- formation of microdomains of phases having ordered vacancies.

I.5. The brownmillerite structure

A well characterized oxygen deficient phase is that of the brownmillerite (Ca_2FeAlO_5). The formulation of this compound can be expressed in terms of the $n = 2$ member of a series $A_nB_nO_{3n-1}$, ($n \geq 2$). Its structure derives from the perovskite one by the presence of one sixth oxygen vacancy. The ability of Fe^{3+} atom to adopt

either the 6-coordinated octahedral site or the 4-coordinated tetrahedral site support the creation of these tetrahedral sites as well as the ensuing vacancy ordering leading to this brownmillerite structure. This structure is represented in Fig. 2.

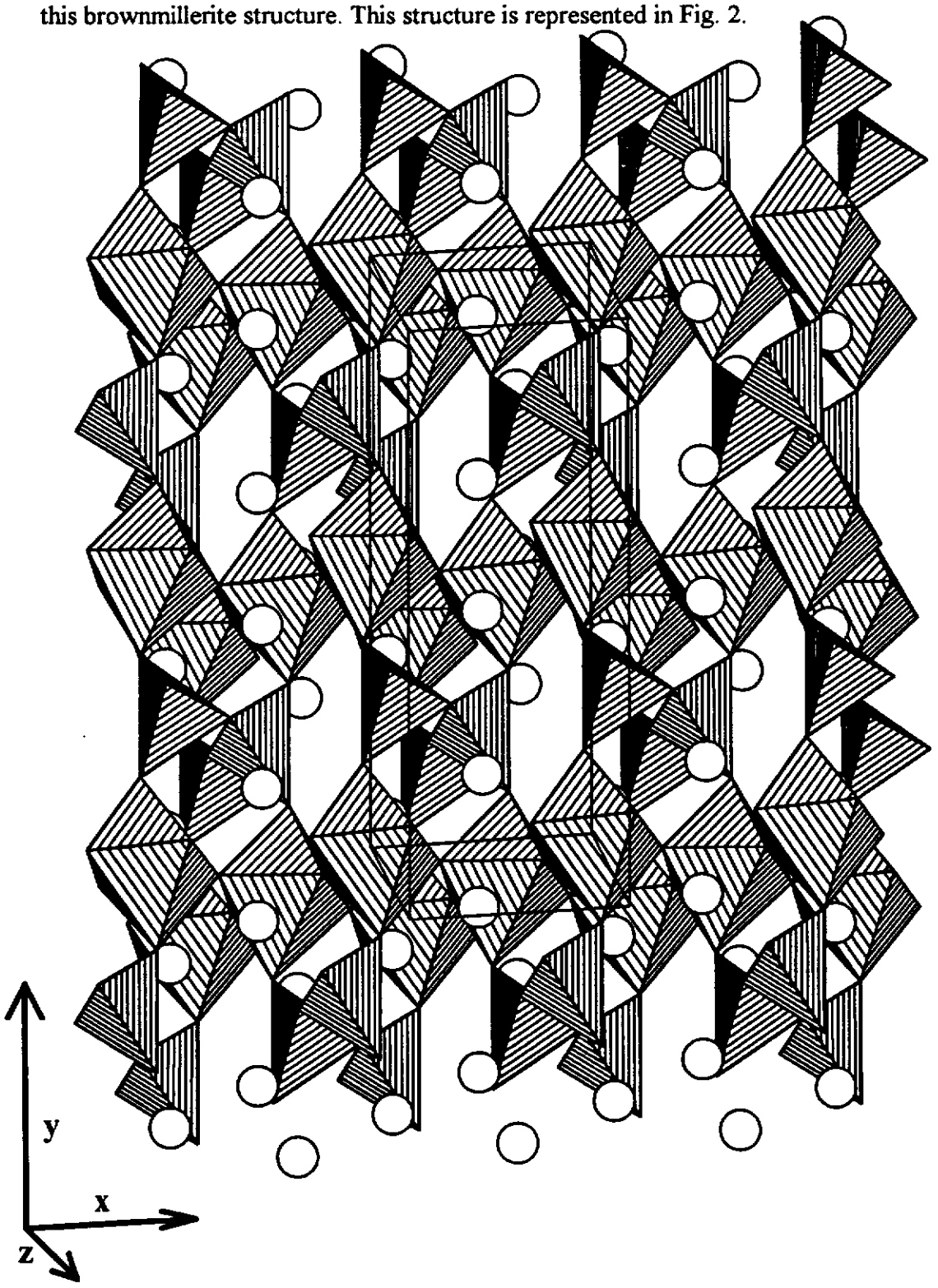

Fig. 2. Brownmillerite - type structure

References page 16

This vacancy ordering can be described as the succession of layers of octahedra and tetrahedra sharing their corners. The vacancies are in fact ordered in chains lying along $[101]_C$ crystallographic direction. This is represented by a typical sequence of polyhedra "OTOT'OTOT'...". The A cation is normally surrounded by ten oxygen atoms.

The relationship between the parameters of the brownmillerite orthorhombic supercell and the original perovskite cubic cell may be expressed as follows:

$$a_B \cong a_C \sqrt{2}$$
$$b_B \cong 4\, a_C$$
$$c_B \cong a_C \sqrt{2}$$

The coordinates of atoms forming the brownmillerite structure are represented in Table I.

Table I: Atom positional parameters for Ca_2FeAlO_5 [11].

Ca_2FeAlO_5 , (Ibm2 space group)				
Atom	Site	x	y	z
Ca	8(c)	0.0273	0.1087	0.4920
Fe, Al (O_h)	4(a)	0	0	0
Fe, Al (T_d)	4(b)	0.9283	0.25	0.9533
O (1)	8(c)	0.2523	0.9861	0.2491
O (2)	8(c)	0.0680	0.1439	0.0055
O (3)	4(b)	0.8607	0.25	0.6193

Several compounds with the general formula $A_2B_2O_5$ (A = Ca, Sr, Ba, Pb, B = Mn, Fe, Co, In, Tl) adopt this brownmillerite - type structure and can be described using Pcmn, Ibm2 and Icmm space groups.

Colville et al. [11] reported the brownmillerite Ca_2FeAlO_5 to have the space group Ibm2. The $Ca_2Fe_2O_5$ compound was described by Bertaut et al. [12] with the Pcmn space group, but Greaves et al.[13] described the structure of $Sr_2Fe_2O_5$ on the basis of the Icmm space group. More recently von Harder et al. [14] investigated the

structure of $Sr_2Fe_2O_5$ single crystals. They characterized this structure using the Ibm2 space group. Finally Battle et al. [15] studied the crystal structure of Sr_2CoFeO_5. They refined the crystal and magnetic structures simultaneously in the space groups Pcmn, Ibm2 and Icmm. The best agreement between the observed and calculated neutron diffraction patterns was achieved when the magnetic moments were constrained to lie along z, using the Icmm space group.

I.6. Hexagonal perovskite structures.

When the tolerance factor *t* becomes larger than 1 (the A cation radius increases, or the B cation radius decreases), the initial cubic closest packing (c.c.p.) sequence tends to change into the hexagonal one (h.c.p.).

This change can be elucidated from the Fig. 3.

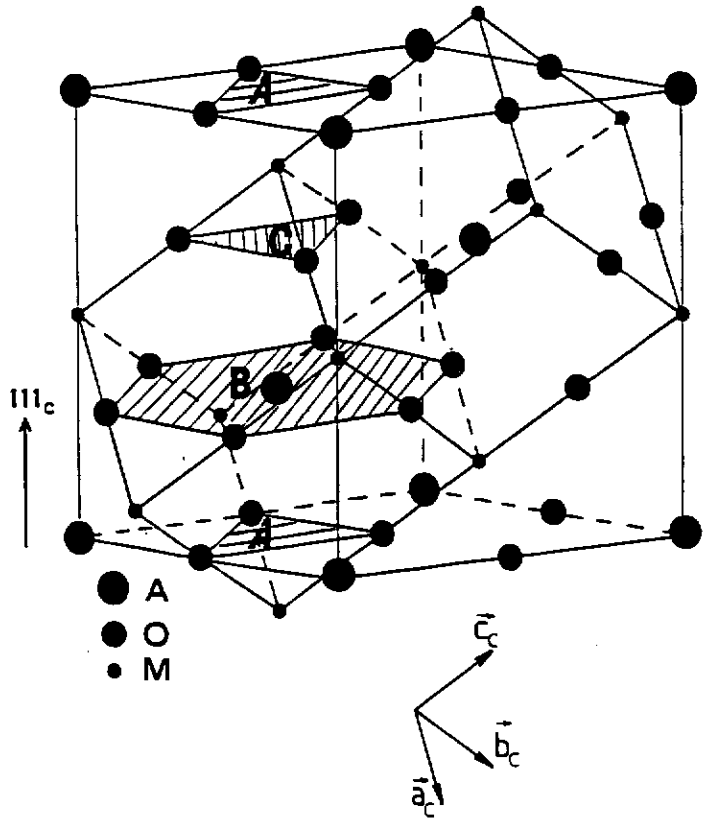

Fig. 3. Hexagonal cell for cubic closest packing.

As shown in this figure, a hexagonal cell may be constructed for cubic closest packing. This cube body diagonal $[111]_C$ becomes in such a case the hexagonal c-axis. The packing sequence of the AO_3 layers evidenced in Fig. 3 may be called as the ABC stacking sequence. According to the widely used notation this packing sequence is called 3C (Fig. 4 a).

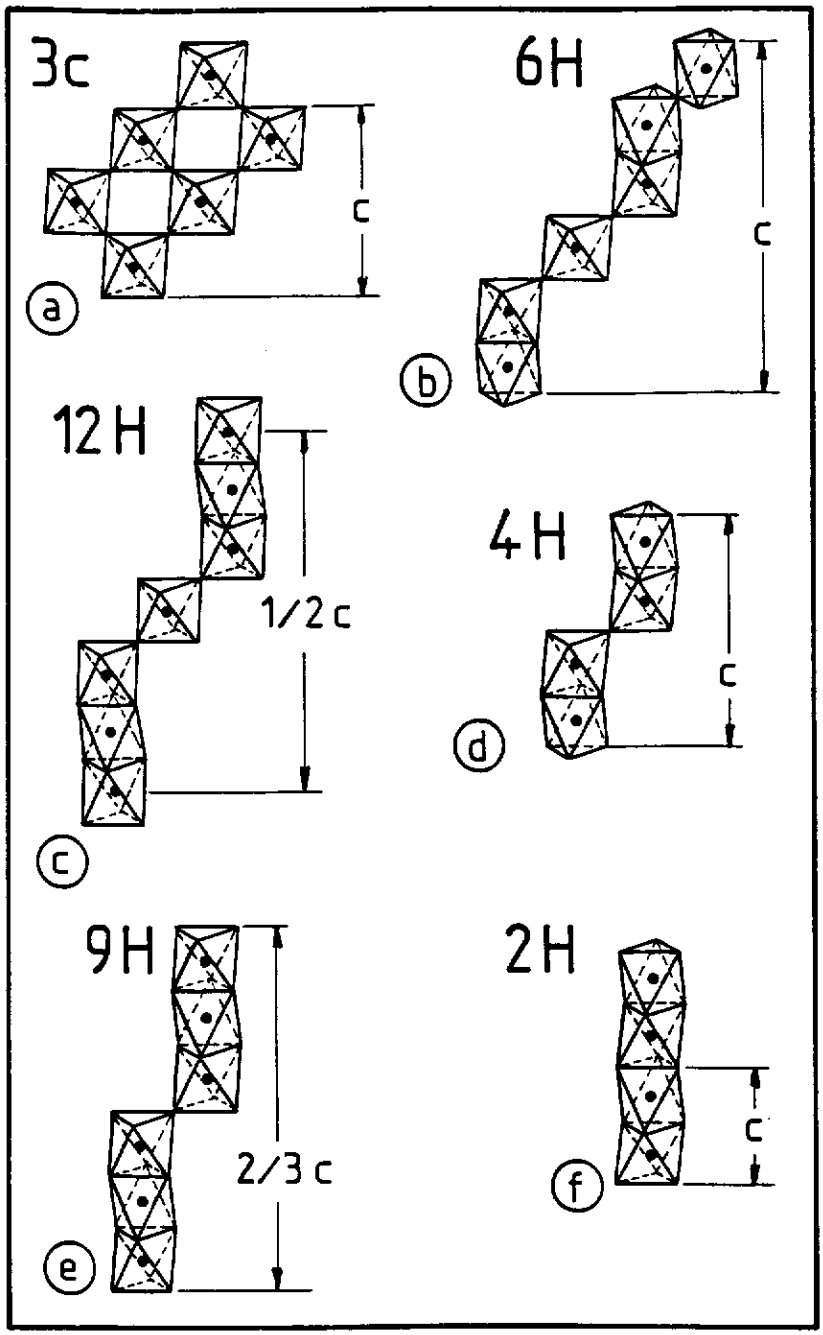

Fig. 4. Some stable intermediate structures between cubic closest packing (3C) and hexagonal closest packing (2H).

The change from the fully c.c.p (3C) to the fully h.c.p (called 2H). goes via various intermediate steps involving different kinds of structures.

The first one is that of the high temperature form of $BaTiO_3$ [16] (Fig. 4. b). It is a six layer structure (6H) with stacking sequence ABCACBA, corresponding to one hexagonal stacking out of three.

The second type is that of $BaCrO_3$ [17] (Fig. 4 c), with the sequence ABCACABCACAB (12H).

The third one is represented by the sequence ABCBA, where the unit cell (e.g. that of $BaMnO_3$) [18] contains four AO_3 layers and this structural type is called 4H (Fig. 4 d).

The fourth type called 9H is represented with the structure of $BaRuO_3$ (Fig. 4 e) [19]. It adopts the stacking sequence ABCBCACABA.

The last type is that of $BaNiO_3$ oxide [20] (Fig. 4 f) having the fully hexagonal close packing with the sequence ABAB..(2H). This structure will be described in detail in § II.2.6.2.1.

Other structures may be built up in the same way involving various sequences of A,B, or C planes [21].

References page 16

I.7. References

1) Goldschmidt V.M., Geochemische Verteilungsgesetze der Elemente VII, VIII (1927/28).

2) Hansen W.C., Brownmiller L. T., Amer. J. Sci., **15**, 224, 1928.

3) Atoji A., Rundle R.E., J. Chem. Phys., **32**, 627, 1960.

4) Poeppelmeier K.R., Jacobson A.J., Longo J., Mat. Res. Bull., **15**, 339, 1980.

5) Bontchev R., Weill F., Darriet J., Mat. Res. Bull., **27**, 931, 1992.

6) Rauser G., Kemmler-Sack S., J. Solid State Chem., **33**, 135, 1980

7) Shannon J., Katz L., Acta Cryst., **B26**, 102, 1970.

8) Hagenmuller P., Pouchard M., Grenier J.C., J. Mater. Educ., **12**, 297, 1990.

9) Hagenmuller P., Pouchard M., Grenier J.C., Solid State Ionics, **43**, 7, 1990.

10) Grenier J.C., Darriet J., Hagenmuller P., Mat. Res. Bull., **11**, 1279, 1976.

11) Colville A.A., Geller S., Acta Cryst. **B27**, 2311, 1971

12) Bertaut E.F., Blum P., Sagnières A., Acta Cryst., **12**, 149, 1959

13) Greaves C., Jacobson A.J., Tofield B.C., Fender B.E.F., Acta Cryst., **B31**, 641, 1975

14) Von Harder M., Müller-Buschbaum Hk., Z. Anorg. Allg. Chem., **464**, 169, 1980

15) Battle P.D., Gibb T.C., Lightfoot P., J. Solid State Chem., **76**, 334, 1988

16) Burbank R.D., Evans H.T., Acta Cryst., **1**, 330, 1948.

17) Chamberland B.L., Inorg. Chem., **8**, 286, 1968.

18) Hardy A., Acta Cryst., **15**, 179, 1962.

19) Donhove P.C., Katz L., Ward R., Inorg. Chem., **4**, 306, 1964.

20) Takeda Y., Kanamaru F., Shimada M., Koizumi M., Acta Cryst. **B32**, 2464, 1976.

21) German M., Kovba L.M., Zh. Neorg. Khim., **28**, 2377, 1980.

Chapter II

The $SrCoO_{3-y}$ System

Preparation, Structure and Physical Properties

II.1. A literature overview

The structures and magnetic properties of the perovskite-related compounds ABO_{3-y} where A=Ca, Sr and Ba and B=Fe and Co have been the subject of much research activity because of their wide range of possible applications, for example as electrode materials or catalysts. The basic property of these compounds which gives rise to most of these uses, is the ability of the anion sublattice to accommodate a high concentration of vacant sites so that (y) can take values in the range $0 \leq y \leq 0.5$ This oxygen nonstoichiometry depends upon the capability of the transition metal to exist as both B^{4+}, in the fully oxidized compound ABO_3, and B^{3+} in the reduced $ABO_{2.50}$ material. Compositions in-between may be regarded as mixed-valence compounds in which both B^{3+} and B^{4+} species are present. Among them the $SrCoO_{3-y}$ system is of particular interest in the study of the anion deficiency, more especially due to the fact that the Co^{3+} can adopt various spin states.

The first studies on this system were carried out by Watanabe et al. in 1957 [1] when they studied the magnetic properties of perovskites containing strontium. $SrCoO_{3-y}$ treated in vacuum was found to be antiferromagnetic and the sample treated in oxygen revealed spontaneous magnetisation below room temperature.

Later on Watanabe et al. [2] prepared the oxygen deficient $SrCoO_{3-y}$ under various conditions and studied their physical properties as a function of (y). They reported the existence of five phases. The samples prepared above 1223 K in air crystallized with the brownmillerite - type structure. When an oxygen atmosphere (101 kPa) was used instead of air, the structure was found to be of orthoferrite - type (Pnma). In higher oxygen pressures, the samples crystallized in the tetragonal system and in the cubic system (2 MPa). Powders prepared below 1073 K showed the hexagonal symmetry of the $BaNiO_3$ - type structure. But these authors did not analyse the oxygen content of those phases and hence did not clarified the relationship between structural changes and the oxygen deficiency.

The first rather extensive study on the effect of the oxygen nonstoichiometry on the physical properties of the perovskite - type $SrCoO_{3-y}$ ($0.04 \leq y \leq 0.30$) was published by Taguchi et al. [3]. They found a metallic behavior in the range 77 - 300 K for all studied compositions which was explained using the itinerant-electron model proposed by Raccah and Goodenough [4]. They also detected the presence of ferromagnetism, the Curie temperature being a function of (y) ($180 \leq T_C \leq 215$ K).

The crystalline and magnetic structure of the brownmillerite - type form of $Sr_2Co_2O_5$ ($y = 0.50$) was studied by Takeda et al. [5] who concluded that both the octahedral and tetrahedral Co^{3+} ions are in high spin state leading to G-type antiferromagnetic structure.

Rodriguez [6] contributed to the study of the $SrCoO_{3-y}$ system with a study of the $Sr_2Co_2O_5$ compound by means of X-ray and electron diffractions. He reported a Icmm space group for the description of the structure of the brownmillerite - type $Sr_2Co_2O_5$ phase.

Grenier et al. [7] prepared the high temperature (brownmillerite - type) and the low temperature ($BaNiO_3$ - type) forms of $Sr_2Co_2O_5$ and examined their magnetic behavior. The Neel temperature ($T_N = 570$ K) rather high for such a type of compound confirms that the cobalt cations are in the high spin state. In addition the brownmillerite -type material was found to be a metastable phase in the studied $Sr_2Co_2O_{5\pm x}$ system. When heated it undergoes at about 850 K a structural transition to the stable low temperature compound.

The low temperature phase was supposed to derive from the 2H perovskite - type but some additional diffraction lines were found in the X - ray powder diffractogram and could not be indexed using the $BaNiO_3$ - type cell parameters. They were attributed to the occurrence of vacancies ($y \cong 0.50$) in the material involving probably a superstructure. The magnetic properties of this oxide were explained in terms of the simultaneous presence of an intermediate spin state (S=1) and of a low spin state (S=0) of trivalent cobalt [7]. In addition the thermal analysis was performed and the structural transition between the low and the high temperature phase was

References page 91

found to be reversible, correlated to the spin transition, but with a certain hysteresis. The oxygen content was also determined as a function of the quenching temperature in the range of 973 K to 1373 K, the stoichiometric compound $Sr_2Co_2O_5$ being formed by quenching at about 1183 K.

These authors [8] studied also the $Sr_2Co_2O_5$ oxide doped with ^{57}Fe using the Mössbauer resonance spectroscopy. They confirmed the brownmillerite - type structure to be correlated with the high spin configuration of cobalt in samples quenched from temperatures above 1183 K.

The low temperature phase exhibited a paramagnetic behavior at room temperature and a magnetic ordering below 30 K. Two types of sites were found in the observed Mössbauer spectra. According to the isomer shift, site I was attributed to an octahedral site. The isomer shift of site II being lower, they concluded that this can be explained by the existence of a five-fold or a four-fold coordinated sites. Finally they proposed a structural model for this low temperature phase.

The low temperature phase was also studied by Rodriguez et al. [9] by means of X-ray and electron diffraction methods. On the basis of the electron diffraction data, they found in fact a rhombohedral symmetry and gave the relationship between the 2H structure and the rhombohedral supercell. However, they did not specify the ordering of oxygen vacancies.

Rodriguez et al. [10] using neutron diffraction experiments confirmed the previous findings of phase transitions in $Sr_2Co_2O_5$ [7,8], the metastability of the brownmillerite - type structure and the existence of a cubic perovskite - type phase above 1155 K. They suggested in conclusion the following phenomena:

- the volume per unit formula is about 11% lower for the low temperature phase than for the brownmillerite - type one which confirms that the transition is related to a spin transition.

- above 1173 K only the perovskite - type phase exists. The vacancy positions would change so fast that it is not possible to maintain the typical brownmillerite

stacking sequence OT OT' OT OT'. Therefore the cubic symmetry is preserved at high temperature in a dynamic sense.

- The ordering of vacancies leading to the brownmillerite - type structure takes place in a very short time during the quenching.

A detailed study of the $SrCoO_{3-y}$ system was also published by Takeda et al. [11] who prepared a wide series of samples with a large oxygen nonstoichiometry ($0.71 \leq y \leq 0.20$). They observed the formation of the brownmillerite - type phase in the region of $0.58 \leq y \leq 0.48$. The perovskite - type phase was observed in two cases:

- firstly by annealing the brownmillerite - type compound under various high oxygen pressures at 573 K ($0.32 \leq y \leq 0.2$).

- secondly by fast quenching of the powder samples from temperatures above 1473 K. ($y \cong 0.71$). This phase corresponds to that mentioned by Rodriguez [11].

During the slow cooling, or annealing below 1073 K, the samples crystallized with the low temperature structure but they suggested that the hexagonal $Sr_2Co_2O_5$ does not maintain its initial stoichiometry. It would decompose into a phase whose composition is close to $SrCo_{0.9}O_x$ and Co_3O_4 or CoO.

They also studied the temperature dependence of the electrical conductivity in air from room temperature up to 1273 K and found a semiconducting - metallic transition at about 1173 K; in the perovskite region, a metallic behavior is observed.

The preparation and the study of the physical properties of the almost stoichiometric $SrCoO_3$ was reported by Shaplygin et al [12]. The preparation was based on the nitrate solid - liquid process with subsequent heat treatment under high oxygen pressure (6.5 GPa, 1273 K, $KClO_3$). They found the cubic perovskite structure with the Pm3m space group and the cell parameter a = 384 pm and a semiconductor behavior, which is contradictory to the observations of Taguchi [3] who found a metallic behavior for $SrCoO_{2.95}$.

The high and low temperature forms of $Sr_2Co_2O_5$ were studied by EXAFS spectroscopy by Battle et al. [13]. This study enabled to clarify the structure of the low temperature form of $Sr_2Co_2O_5$; short Co-Co distances (246 pm) were observed,

References page 91

strongly suggesting that the structure contains face sharing CoO_6 octahedra, in contrast to that of the high temperature phase where only corner-sharing polyhedra were found.

Zinkevich et al. [14] studied the electrical conductivity of the $SrCoO_{3-y}$ oxide and corroborated the structural transition to the high temperature perovskite - type phase associated with a metallic p-type behavior. They also pointed out that after quenching the high temperature phase to liquid nitrogen, the electrical conductivity found at room temperature was about 7-8 order smaller than that measured at high temperature. This was explained by the structural change which appears during the quenching (formation of the brownmillerite type phase), which is in agreement with previous observations of Grenier [7,8] and Takeda [11]. They confirmed the results of Takeda's work [11] concerned with the decomposition of the low temperature phase.

Finally Watanabe et al. [15] and Oda [16] prepared single crystals with the $SrCoO_{2.70}$ composition using the floating zone method with an infrared lamp image furnace. They found for these crystals a distorted tetragonal structure (I4/mcm). By annealing at 673 K under high oxygen pressures of 100 MPa and 1600 MPa the crystals became cubic. The (y) values of these samples being 0.16±0.04 and 0.03±0.03, respectively.

The magnetic measurements showed a ferromagnetic behavior. The magnetic moment of the almost stoichiometric sample was found to be 1.55 μ_B at 4.2 K under 8 kOe and the Curie temperature (T_C) close to 210 K.

II.2. The $Sr_2Co_2O_{5\pm x}$ compound

The literature overview shows clearly that the cobalt ions in $Sr_2Co_2O_5$ may adopt two different spin states:

- the high spin state exists at high temperature in the perovskite - type phase and in the brownmillerite - type compound which is formed during the fast quenching of the previous one.

- the low temperature structural phase seems to characterize a mixture of low and intermediate spin states of Co^{3+}. This material reveals a structure derived from the 2H $BaNiO_3$ - type.

It also results from the previous works that there is no general agreement about the nature and the stability of the different phases occurring in the studied system.

Therefore several questions may be addressed about these discrepancies in the conclusions of the various contributions relative to $Sr_2Co_2O_5$:

1) What is the composition range of the above mentioned phases of $Sr_2Co_2O_5$ (i.e. the oxygen stoichiometry) and what is their stability in relation to p_{O_2} and T ?

2) What are the conditions for preparing these phases, more especially with regards to the electrochemical purposes, where the useful electrode material is needed?

3) The brownmillerite - type structure is rather well known, but does it exist really at high temperature or is it formed only during the fast quenching?

4) What is the real structure of the low temperature phase?. Is the composition of this phase $Sr_2Co_2O_5$ or does it decompose into a Co substoichiometric oxide and Co_3O_4?

It was relevant to find clear answers for all above mentioned questions, especially with respect to the preparation of starting $Sr_2Co_2O_5$ materials for the electrochemical oxidation and their electrochemical behavior. In the following paragraph an attempt to find answers will be presented.

References page 91

II.2.1. Preparation of the powders of $Sr_2Co_2O_5$

II.2.1.1. Choice of the method for preparing the starting powder.

There exist several possibilities for preparing powders of double oxides. The choice of such a preparation method should be achieved according to the required properties and use of the final materials.

For example the materials used as electrodes in various electrochemical applications (e.g. electrocatalysts, electrode materials for solid oxide fuel cells) require to be homogeneous in composition as well as in the distribution of the particle size.

Therefore four different methods have been employed to prepare the starting $Sr_2Co_2O_5$ material.

Appropriate amounts of $SrCO_3$ and either $Co(NO_3)_2,6H_2O$ or Co_3O_4 powder were used for all preparations.

The first sample of $Sr_2Co_2O_5$ was prepared by heating finely ground mixture of $SrCO_3$ and Co_3O_4 in air at 1473 K for 48 h. After regrinding the powder was refired at 1273 K for 24 h.

For preparing the second sample stoichiometric amounts of $SrCO_3$ and $Co(NO_3)_2,6H_2O$ were diluted in nitric acid (HNO_3:H_2O, 1:1), then dried on a sand - bath. The dark rose precipitate was carefully decomposed in the flame (platinum crucible) until the weight did not change between two subsequent heatings. The black powder resulting from this treatment was slowly fired up to 1373 K for 24 h. Then it was finally annealed at 1273 K for 24 h before quenching in air.

The oxalate method was employed for preparing the third sample. Precipitates of strontium and cobalt oxalates were at first dried, then decomposed at 1123 K in air for 24 h.

The fourth sample was obtained using a coprecipitation method. Appropriate amounts of $SrCO_3$ and $Co(NO_3)_2,6H_2O$ were diluted in nitric acid (5% solution) in

order to give a 0.1 M solution. This solution was then immersed in a solution of 2 M KOH and 2 M K_2CO_3. Cobalt(II) hydroxide and strontium carbonate were precipitated under constant stirring. The precipitate was quickly recovered and centrifuged (5000 rpm). Then it was washed several times with distilled water and centrifuged. Finally the powder was dried at 400 K and then fired at 1223 K for 24 h.

All prepared powders were checked by the scanning electron microscopy and energy dispersive X-ray spectrometry. Only two powders gave satisfactory results.

The samples prepared by solid state reaction and especially by the oxalate process were inhomogeneous (Sr/Co ≠ 1 in some parts of samples).

On contrary powders prepared either by coprecipitation or by the nitrate way were homogeneous in composition. The particle size in "coprecipitate" samples and "nitrate" powder was about 1 μm and 1-3 μm respectively.

As it will be discussed later (cf. §.III.2.) the nitrate method appeared to be the most suitable preparation method for $Sr_2Co_2O_5$ with regards to the electrochemical treatment.

II.2.1.2. Preparation of phases of given composition.

However, the XRD analysis of the starting material showed that the as - prepared powders correspond to a mixture of the brownmillerite - type and the low temperature phase.

For preparing pure samples of each phase existing in the studied system it was necessary to perform a second heat treatment of the starting material. The procedures for obtaining these phases are summarized in Table I.

References page 91

Brownmillerite - type phase		**Low temperature phase**			
Atmosphere	air	Atmosphere	argon*	Atmosphere	air
ramp 1	↑ 200 K/h	ramp 1	↑ 200 K/h	ramp 1	↑ 200 K/h
level, dwell 1	1473 K, 2 h	level, dwell 1	1073 K, 24 h	level, dwell 1	1073 K, 24 h
ramp 2	↓ 100 K/h	ramp 2	↓ 10 K/h	ramp 2	↓ 1.2 K/h
level, dwell 2	1223 K, 24 h	level, dwell 2	300 K	level, dwell 2	300 K
quenching	liquid nitrogen				
Analysis	$Sr_2Co_2O_{4.96}$	Analysis	$Sr_2Co_2O_{5.06}$	Analysis	$Sr_2Co_2O_{5.20}$
XRD pattern	Fig 1. a	XRD pattern	Fig 1.b	XRD pattern	Fig 1. c

*) p_{O_2} = 10 Pa

Table I: Procedures for obtaining the $Sr_2Co_2O_{5\pm x}$ phases.

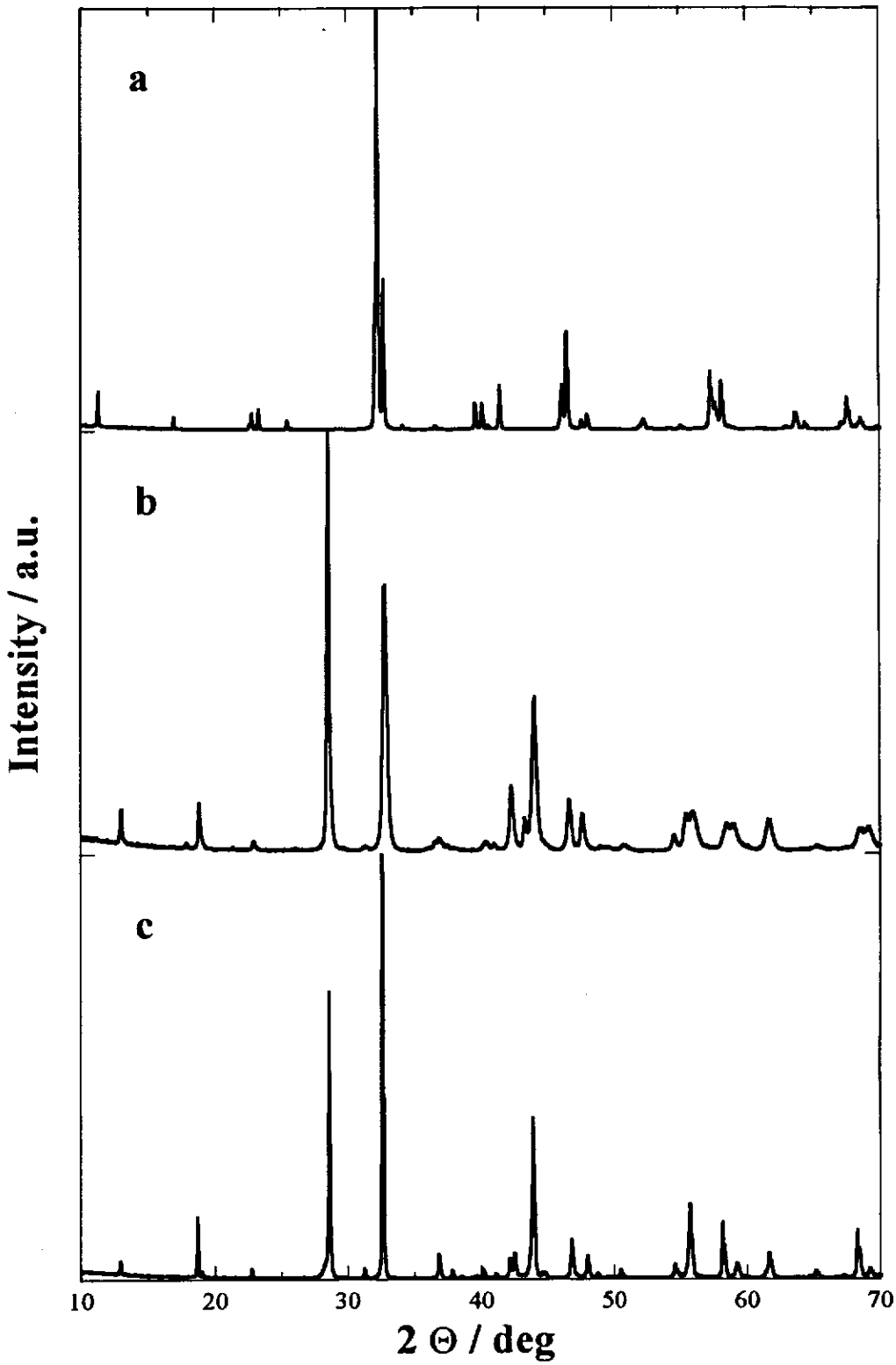

Fig. 1. XRD pattern of a) brownmillerite - type $Sr_2Co_2O_{4.96}$, b) low temperature $Sr_2Co_2O_{5.06}$, c) low temperature $Sr_2Co_2O_{5.20}$.

References page 91

Chemical analyses for $Co^{2+/3+}$ and $Co^{3+/4+}$ were carried out by bichromatometric analysis (with an excess of Mohr salt) as previously described [17].

In our experimental conditions, the cubic phase as quoted by Takeda [11] was never obtained.

II.2.2. Structural transitions in $Sr_2Co_2O_5$

II.2.2.1. High temperature X - ray powder diffraction

In the first stage, the thermal stability of the various phases was studied using the high temperature X - ray diffraction (HTXRD). Experiments were performed either in air ($p_{O_2} \cong 21$ kPa) or in purified nitrogen atmosphere ($p_{O_2} \cong 10$ Pa). But there were no significant differences in the results obtained in both atmospheres.

Fig 2 shows the results of the first series of experiments. The powder of the low temperature phase was heated on the platinum sample holder (the diffraction lines belonging to this sample holder are marked by arrows) placed in the diffractometer chamber filled by purified nitrogen. The results of these experiments are summarized in the following Table II.

Table II: Temperature dependence of the cell parameters for the low temperature $Sr_2Co_2O_5$ phase.

Temperature (K)	a (pm)	c (pm)	V/Z ($10^8 pm^3$)
300	942.6	1260.5	1.616
473	945.4	1262.0	1.628
673	949.0	1265.1	1.645
873	950.3	1267.1	1.652
1073	953.0	1271.6	1.667
1400	398.2	-	

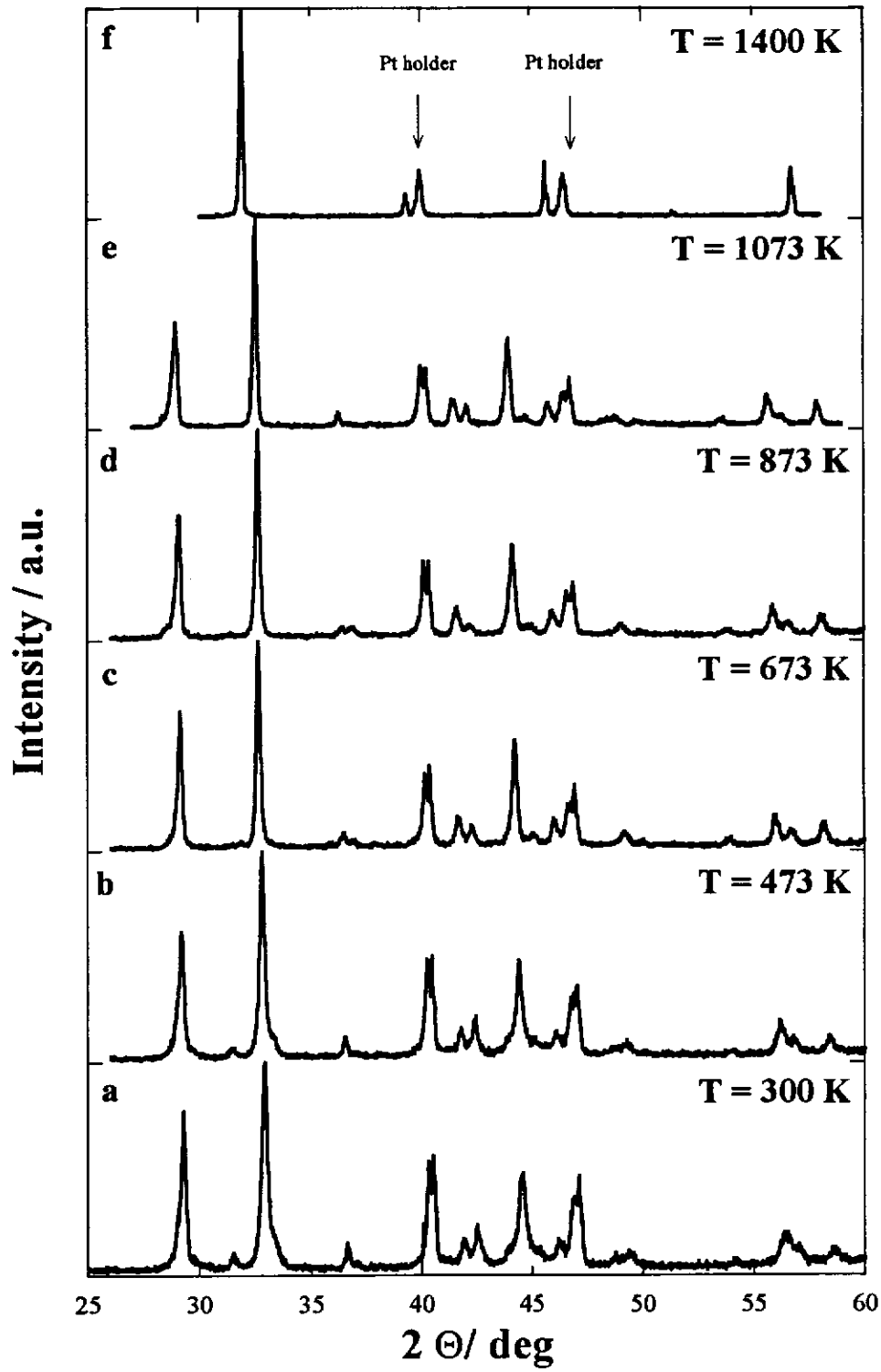

Fig. 2. Temperature dependence of the XRD pattern of $Sr_2Co_2O_5$ (low temperature phase).

References page 91

It is evident from this table that the low temperature phase undergoes a thermal expansion during the heating. Both a and c parameters change linearly with increasing temperature until the occurrence of a phase transition at about 1173 K.

Above this temperature, the X-ray diffraction pattern characterizes a cubic perovskite - type phase. One should point out that no XRD pattern corresponding to the brownmillerite phase can be seen during the heating. This result confirms the previous observations of Rodriguez et al. [10] who detected the same structural transition by means of neutron diffraction. The XRD pattern of the cubic phase (at 1473 K) is shown in Fig 2 f. The cell parameter of this sample at 1473 K is a = 398.3 pm.

When the metastable brownmillerite - type powder was heated in the diffractometer chamber up to 773 K, only the thermal expansion of the sample was detected (Fig 3). The results are summarized in Table III:

Table III: Temperature dependence of the cell parameters for the brownmillerite - type powder.

Temperature (K)	a (pm)	b (pm)	c (pm)	V/Z (10^8 pm^3)
300	556.6	1575.2	546.7	1.198
573	557.3	1590.6	546.8	1.212
673	557.1	1599.6	546.8	1.218
773	557.7	1601.5	547.4	1.222

In the case of the thermal expansion of the brownmillerite - type structure one can notice that the preferred direction of the thermal expansion is that of the b axis It may be evident from the mean linear thermal expansion coefficients, $\Delta a / a = 0.20\%$, $\Delta b / b = 1.65\%$ and $\Delta c / c = 0.13\%$ in the above mentioned temperature range (300 - 773 K).

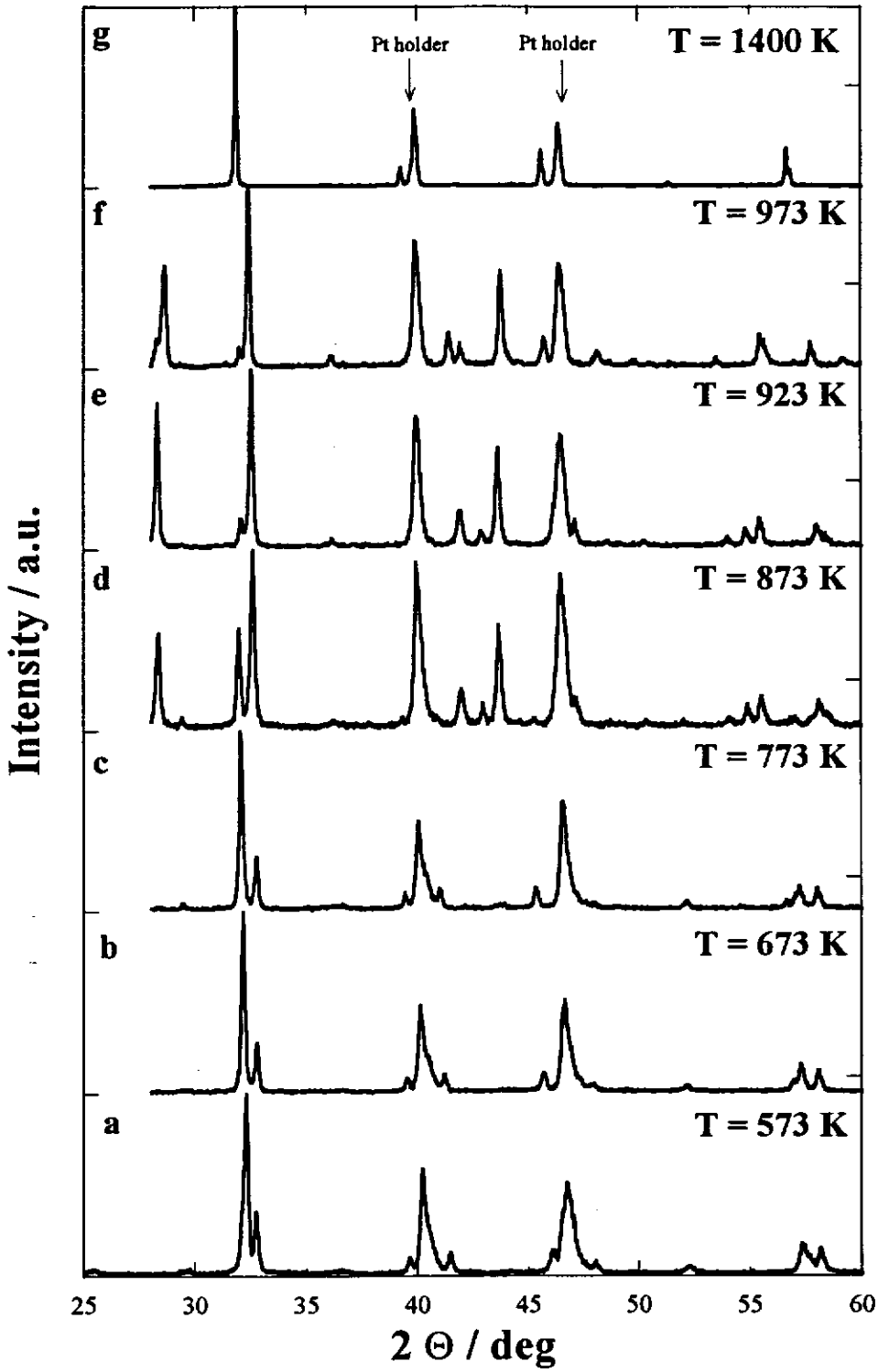

Fig. 3. Temperature dependence of the XRD pattern of the brownmillerite - type $Sr_2Co_2O_5$ phase.

References page 91

At temperature about 873 K the diffraction lines characterizing the low temperature phase appear. As shown in Fig 3 d-f the mixture of both phases is observed over an interval of 100 K (in the mentioned experimental conditions), and finally above 1173 K, in the same way that in the case of the low temperature variety, the sample undergoes the structural transition to the cubic phase with the cell parameter a = 398.2 pm.

These series of HTXRD experiments performed at different temperatures showed clearly that no brownmillerite - type structure is formed when $Sr_2Co_2O_5$ is heated up to 1473 K, which confirms the conclusions of Rodriguez et al. [10].

II.2.2.2. Thermal analyses

In the second stage the various structural transitions of $Sr_2Co_2O_5$ were studied using DTA and TGA in order to specify the transition temperatures.

II.2.2.2.1. Differential thermal analysis

The DTA curve (Fig. 4a, curve 1) concerned with the brownmillerite-type powder B shows several features. Three peaks appear on the $\Delta T=f(T)$ curve at increasing temperature. The first exothermic peak at T_S = 580 K, we will see below, corresponds to the Neel temperature, since the second exothermic one at T_S = 820 K characterizes the structural transition B $\rightarrow$ H. The third one at T_S = 1183 K is endothermic and occurs during the structural transition H $\rightarrow$ C. During the cooling (Fig 4b, curve 1) only one exothermic peak at T_S = 1092 K is observed. When the temperature of the sample is increased again from the room temperature up to 1400 K the first two peaks disappear and only the third one is found at the same temperature as on the first curve. This last behavior characterizes the low temperature phase behavior.

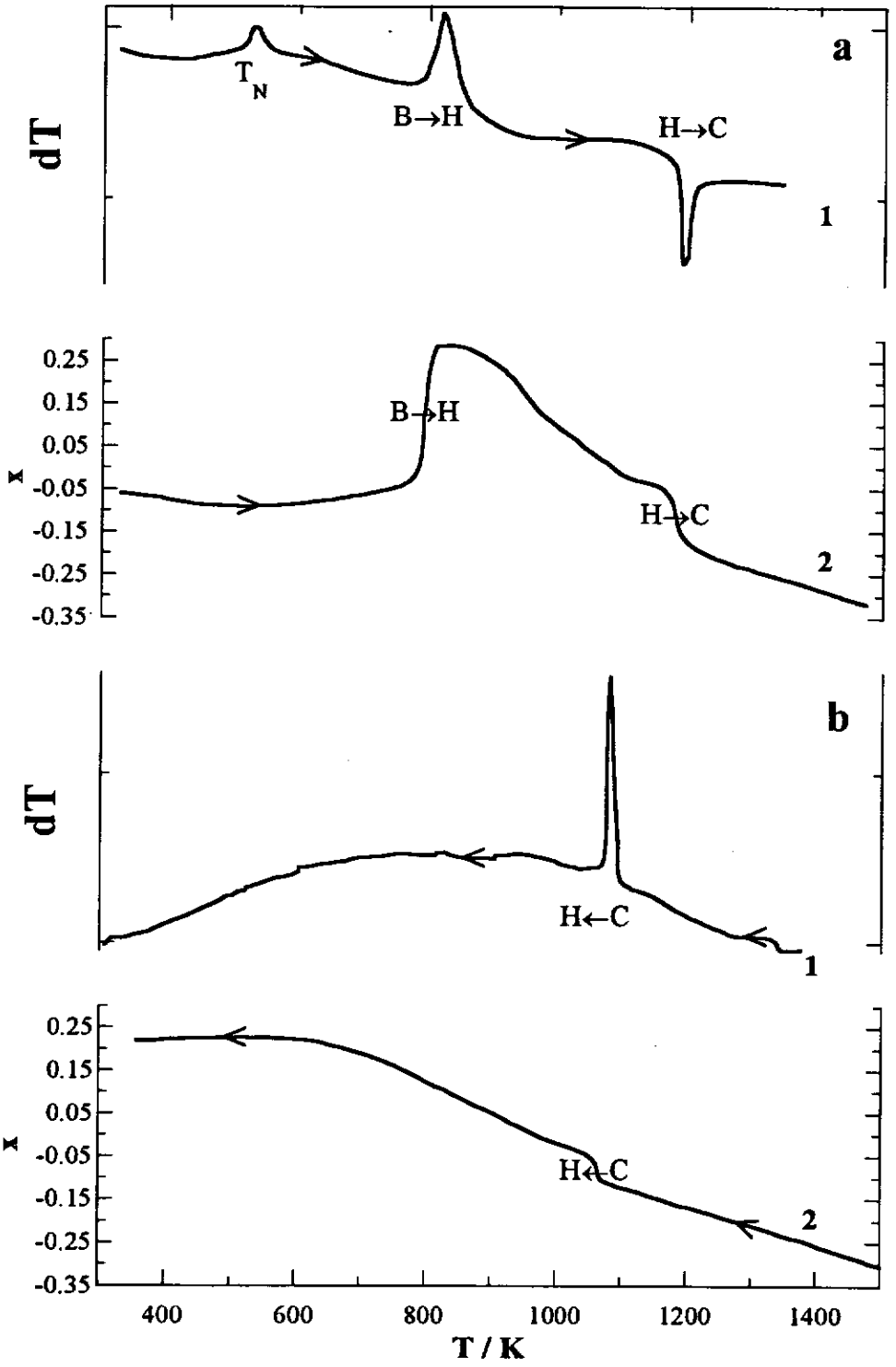

Fig. 4. DTA and TGA curves for the brownmillerite - type $Sr_2Co_2O_{4.96}$ phase.

References page 91

II.2.2.2.2. Thermogravimetric analysis.

TGA experiments to determine the thermal dependence of the oxygen stoichiometry of $Sr_2Co_2O_5$ were performed in air in the temperature range between room temperature and 1450 K. Figure 4a, curve 2 shows the results of such an experiment achieved with the powder B (the brownmillerite - type phase). The composition of the starting powder, determined by means of the bichromatometric titration, was found to be $Sr_2Co_2O_{4.94}$ (y = 0.53, according to the $SrCoO_{3-y}$ formulation).

It is interesting to note that important changes in the oxygen stoichiometry occur at temperatures similar to those determined by DTA. Then the first drastic increase of the oxygen content occurs at about 810 K where the sample reaches the composition $Sr_2Co_2O_{5.28}$ (y = 0.36) which seems to be the definite composition of the low temperature H phase when obtained by cooling slowly from high temperature in air. When the temperature increases the oxygen content starts to decrease again. Then a second break in the TGA curve is observed at about 1180 K corresponding to the second structural transformation from the low to the high temperature phase (H $\rightarrow$ C). This compound reveals a relatively large nonstoichiometry of oxygen and reaches the composition $Sr_2Co_2O_{4.68}$ (y = 0.66) at about 1450 K.

On the reverse step when the temperature decreases the oxygen content starts to increase again. Only one change in the TGA curve appears (Fig. 4 b curve 2), again connected with the structural transformation of the high temperature phase to the low temperature one (C $\rightarrow$ H) and the almost stoichiometric composition $Sr_2Co_2O_5$ is reached at this moment. In the domain of the low temperature phase when the sample is cooled down to 600 K the oxygen content increases up to the composition $Sr_2Co_2O_{5.24}$ (y = 0.38). And finally in the region between 600 K and room temperature this composition remains constant.

The results of the TGA measurements show clearly that the structural changes of $Sr_2Co_2O_5$ are accompanied by changes in the oxygen stoichiometry when the thermal treatment is performed in air. The values of the compositions in the temperature range of 1000 - 1400 K correspond to those found by Grenier [7] who analyzed the oxygen content after quenching as a function of the annealing temperature.

II.2.2.3. Magnetic susceptibility measurements

Fig. 5 shows the thermal dependence of the inverse of the molar susceptibility of $Sr_2Co_2O_5$. Clearly, several magnetic transitions are observed:

- At 570 K, the minimum of $1/\chi_m$ indicates the Neel temperature of the brownmillerite - phase confirming the previous neutron study [10]. The values of the magnetic susceptibility as well as the Néel temperature obviously characterize the high spin state for the trivalent cobalt.

- At increasing temperature, a first change in the thermal variation of the susceptibility is observed around 730 K. Then at about 850 K, a sharp transition occurs involving a large decrease of the magnetic susceptibility.

- At highest temperature, another transition is observed around 1150 K coupled with an increase of the magnetic susceptibility.

The values of the temperatures of the transitions well agree with those determined by DTA and HTXRD. One can conclude that the high spin state of Co^{3+} characterize the brownmillerite and the cubic phases since a lower spin state can be associated with the low temperature phase.

At decreasing temperature, the transition from the cubic to the hexagonal structure related again to the spin transition occurs at about 1080 K.

References page 91

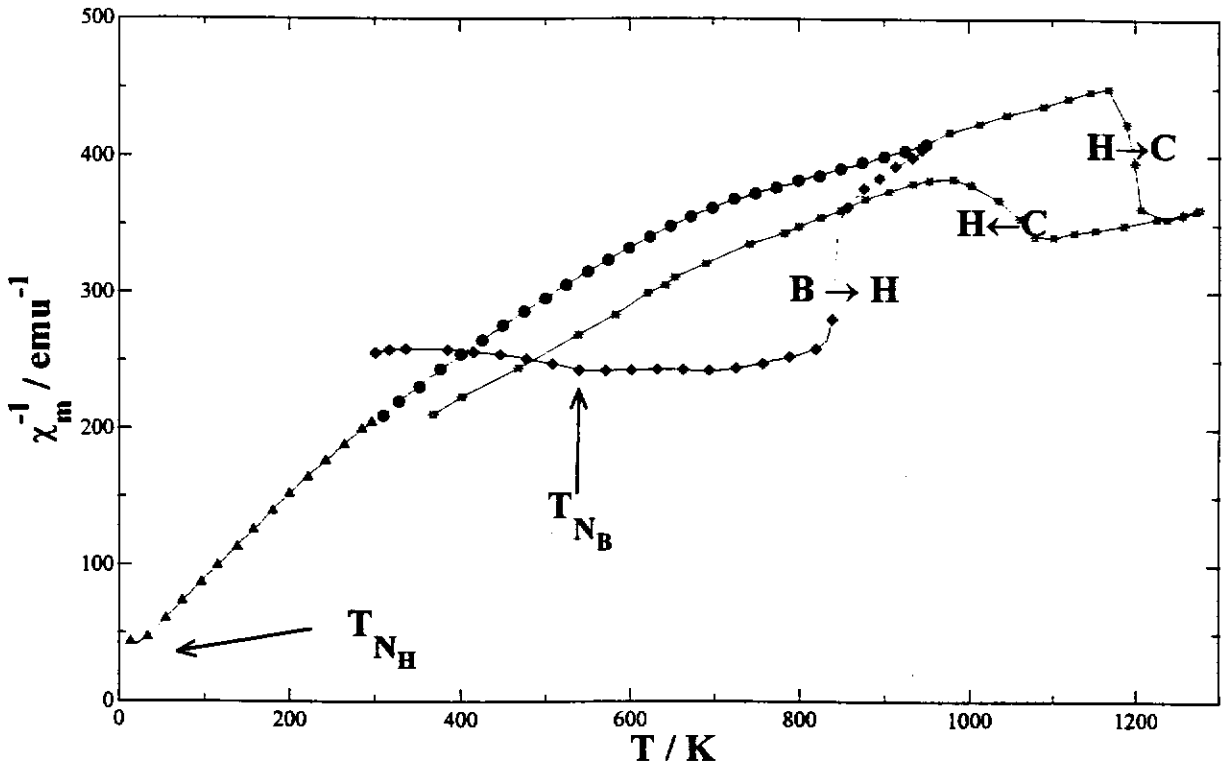

Fig. 5. Thermal variation of the inverse of the molar susceptibility of $Sr_2Co_2O_{5\pm x}$.

●●◆◆▲▲ this work

✱✱✲✲ Grenier et al. [7]

II.2.3. Conclusions

On the basis of above mentioned experiments the following conclusions can be drawn:

- Three main structural types exist for $Sr_2Co_2O_{5\pm x}$
  - the low temperature phase with the structure deriving from the 2H $BaNiO_3$ - type phase
  - the high temperature cubic phase above ≈1173 K.
  - the metastable brownmillerite - type phase formed during the relatively fast quenching of the cubic phase
- The structural transformation H ↔ C is caused by the change in the electronic configuration of cobalt ion (low spin ↔ high spin state transition).
- The oxygen content of $Sr_2Co_2O_5$ may vary from $Sr_2Co_2O_{4.60}$ up to $Sr_2Co_2O_{5.30}$. The overstoichiometry characterizes the H phase and the substoichiometry the B or C phases.

In the following part each phase will be described in detail.

II.2.4. The brownmillerite - type phase

The orthorhombic brownmillerite - type $Sr_2Co_2O_{5\pm x}$ phase was found to be metastable. It can be prepared only during fast quenching from temperatures above 1223 K and appears in fact as the ordered structural variety of the cubic high temperature phase.

According to the TGA data this phase exhibits always an oxygen substoichiometry above this temperature. Table IV shows the results of a series of experiments where the brownmillerite - type phase was prepared after annealing at various temperatures followed by quenching down to liquid nitrogen. The cubic phase

References page 91

was never stabilized under these experimental conditions, the quenching being too slow.

Table IV: Dependence of the cell parameters and composition of the brownmillerite - type $Sr_2Co_2O_{5-x}$ powder on the quenching temperature.

Temperature (K)	x	a (pm)	b (pm)	c (pm)	V/Z ($10^8 pm^3$)
1273	0.14	557.31	1573.18	547.59	1.200
1323	0.24	557.97	1575.58	547.08	1.202
1353	0.32	557.67	1574.47	547.24	1.201
1413	0.34	557.34	1577.22	546.55	1.201
1473	0.38	557.59	1578.22	546.55	1.202
1553	0.42	558.69	1580.77	545.78	1.205

The chemical analysis of all quenched samples confirmed the results of TGA. It can be noticed that no significant oxidation occurs during quenching down to liquid nitrogen. The slight difference in the values of the oxygen content of the quenched samples and those of TGA can be explained by the accuracy limits of both analytical methods and also by the fact, that TGA is operated under dynamic conditions. On the contrary the samples prepared by quenching were equilibrated for 24 hours at each temperature before quenching.

It is interesting to note that when the temperature from which the brownmillerite phase is quenched increases, the b parameter increases similarly as in the case of the thermal expansion observed during the heating of the phase in the HTXRD experiment. This will be explained later on the basis of the structural data.

It can be also concluded that contrary to the results of Takeda's work [11], the existence domain of the brownmillerite-type structure for $Sr_2Co_2O_{5-x}$ is extended up to x= 0.42.

II.2.4.1. Crystal structure of the brownmillerite $Sr_2Co_2O_5$ phase.

Since the crystal structure of $Sr_2Co_2O_5$ has not been known yet and only preliminary refinements of this structure [6] have suggested the space group to be Icmm, attempts to determine the space group were done using high resolution transmission electron microscopy (HRTEM).

II.2.4.2. High Resolution Transmission Electron Microscopy of the Brownmillerite - type phase

The main objective of this study was to determine the Bravais type of the crystal lattice of the brownmillerite - type $Sr_2Co_2O_5$ phase.

Several microcrystallites of $Sr_2Co_2O_{4.96}$ were studied by means of the high resolution transmission microscopy (HRTEM). Typical electron diffraction patterns observed in this study are shown in Figures 6 a-c. They can be indexed on the basis of the orthorhombic symmetry of the brownmillerite - type cell.

According to previous structural studies concerned with compounds having this structure, three space groups (Pcmn, Icmm and Ibm2) are possible. The reflection conditions in these space groups are summarized in the following Table V.

References page 91

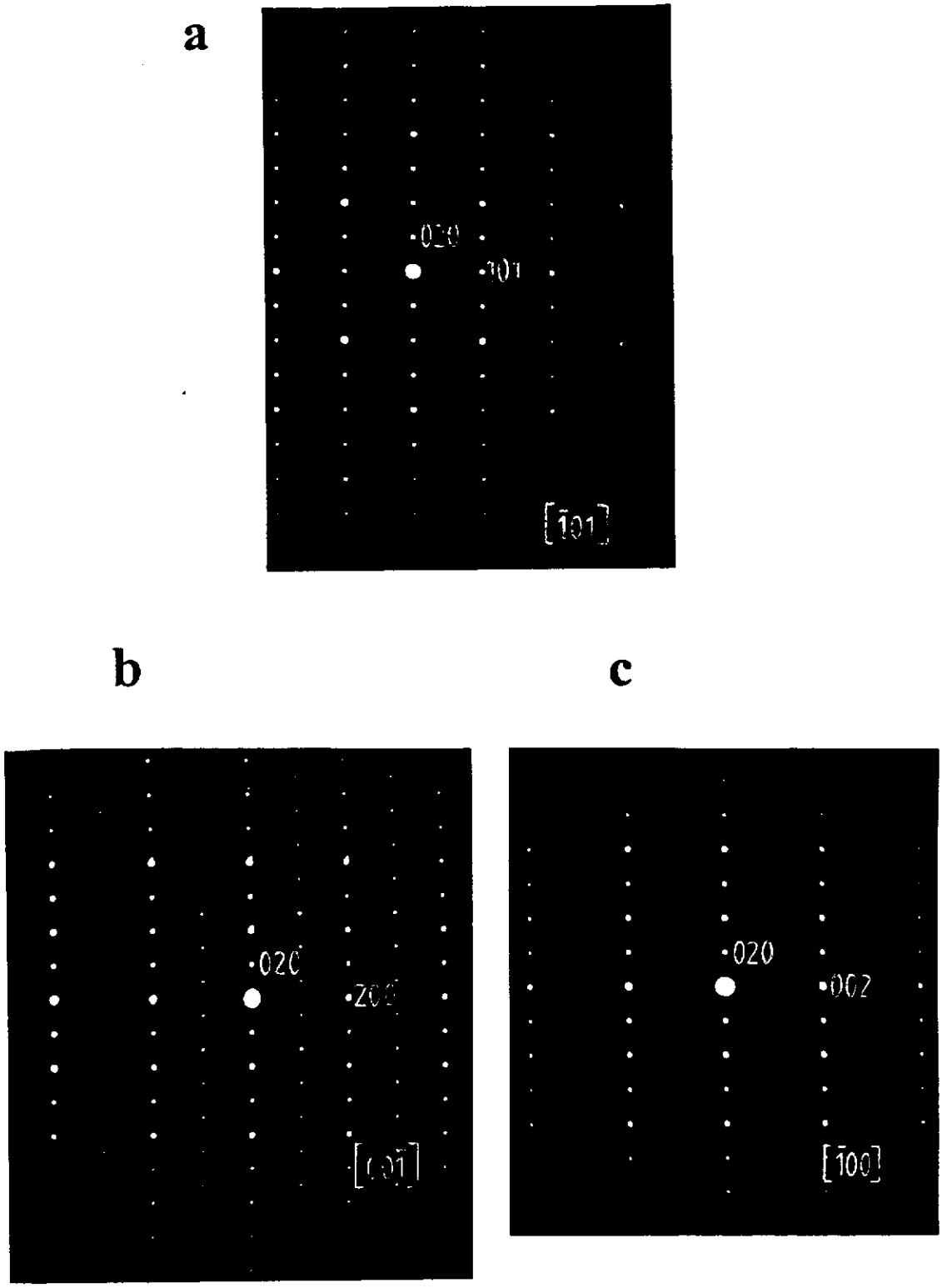

Fig. 6. Electron diffraction patterns of brownmillerite - type $Sr_2Co_2O_{4.96}$ along a) $[\bar{1}01]$, B) $[00\bar{1}]$, C) $[\bar{1}00]$ zone axes.

Table V: Reflection conditions for the mentioned space groups.

Pcmn	Icmm	Ibm2
	hkl: h+k+l=2n	hkl: h+k+l=2n
hk0: h+k=2n	(hk0: h+k=2n)	(hk0: h+k=2n)
0kl: l=2n	0kl: k,l=2n	0kl: k,l=2n
(00l: l=2n)	(00l: l=2n)	(00l: l=2n)
(0k0: k=2n)	(0k0: k=2n)	(0k0: k=2n)
(h00: h=2n)	(h00: h=2n)	(h00: h=2n)
	(h0l: h+l=2n)	(h0l: h+l=2n)

The main difference between the primitive Pcmn and the body centred I type groups is marked in the table by shading.

Based on these assumptions the electron diffraction patterns of the brownmillerite - type $Sr_2Co_2O_5$ compound were clearly indexed using the body centred orthorhombic space group. The difference between the P type and I type can be seen from the Fig. 7. This figure correspond to the pattern shown in Fig 6 a, and represents the $[\bar{1}01]_O$ zone axis electron diffraction pattern. The spots plotted with asterisks which do not appear in the observed pattern correspond to those which should be observed for the Pcmn space group ((h,k,l): no conditions, 0k0: k=2n).

A typical pattern along this zone axis is given in Fig. 8 for $Ca_2Fe_2O_5$ [18]. No systematic absences corresponding to h+k+l = 2n+1 can be observed. It determines a primitive Bravais lattice for $Ca_2Fe_2O_5$ and as a consequence a body centred (I Bravais lattice) space group for $Sr_2Co_2O_5$.

The majority of the electron diffraction patterns and subsequent images revealed the ordering of the structure as described in paragraph I.1.5., i.e. the OTOT' sequence along the b axis.

However, during the observations some additional phenomena were observed. The metastability of this brownmillerite - type $Sr_2Co_2O_5$ was "confirmed". When the crystallites are exposed to the electron beam (with an accelerating voltage of 200 kV in

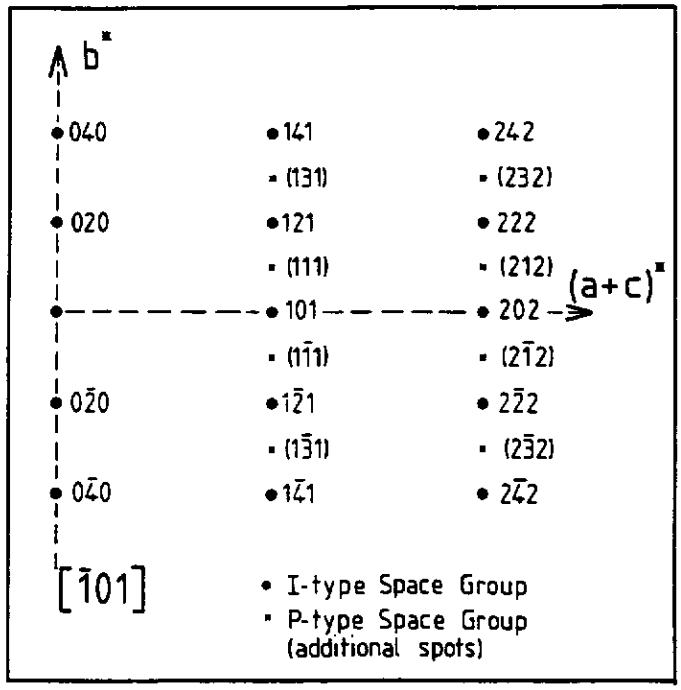

Fig 7. Difference between the E.D. patterns for I - type and P - type Bravais lattices of the brownmillerite - type structure along the [$\bar{1}$ 01] zone axis.

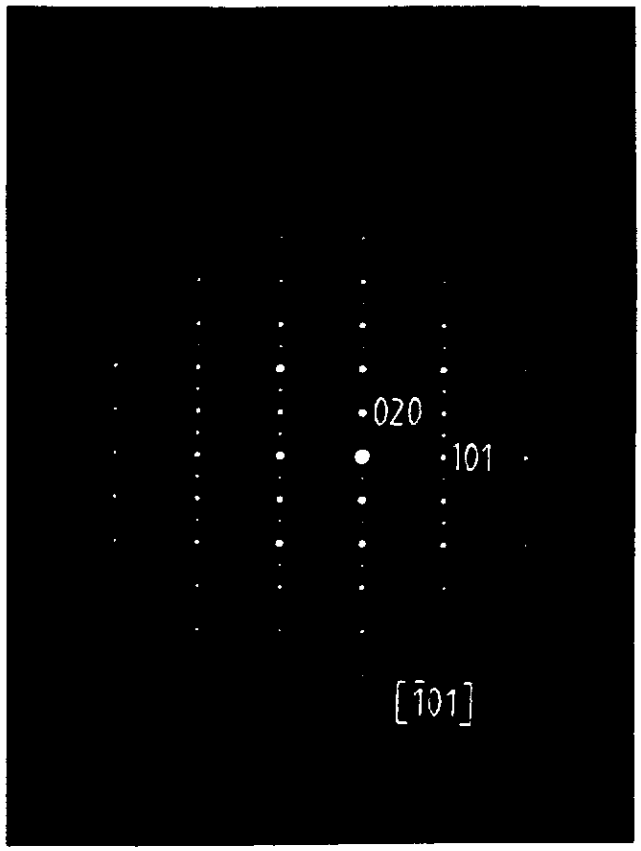

Fig. 8. Electron diffraction pattern of $Ca_2Fe_2O_5$ along the [$\bar{1}$ 01] zone axis.

the vacuum of 10^{-5} Pa) some instability was observed; it is caused by local heating and irradiation which leads to changes in the crystalline structure.

This is evidenced in Figures 9 a,b. Some additional diffraction spots appear in the electron diffraction pattern (Fig 9 a.) The hk0 reflections with h+k=2n+1, not allowed in the I space groups, appear.

The changes in the crystalline structure are also visible in the image displayed in Fig. 9 b.

In addition the presence of large domains as shown in Fig. 10 a was also rather frequently observed in these materials. The electron diffraction pattern corresponds in fact to the presence of twins having perpendicular b axes. These twins are clearly visible in the HRTEM image shown in Fig. 10 b.

II.2.4.3. The crystal structure refinement using the Rietveld method

The refinement calculations were achieved with the experimental data based on the stepwise XRD acquisition ($10° \leq 2\theta \leq 120°$,$\Delta 2\theta = 0.02°$,t = 40s). The Fullprof, multipurpose profile fitting program, version 2.2Dec92, written by Rodriguez [20] was used for these calculations.

The results of the previous HRTEM study ruled out the Pcmn space group and confirmed that the body - centered space groups Ibm2 or Icmm should be used for the description of the brownmillerite - type structure of $Sr_2Co_2O_5$. Both space groups require identical systematic absences and therefore were considered for the structure refinement.

The refinements performed with the models based on both space groups gave almost the same results concerning the atomic coordinates and the reliability factors.

The results of the refinement using Ibm2 and Icmm space groups are summarized in Tables VI and VII respectively.

References page 91

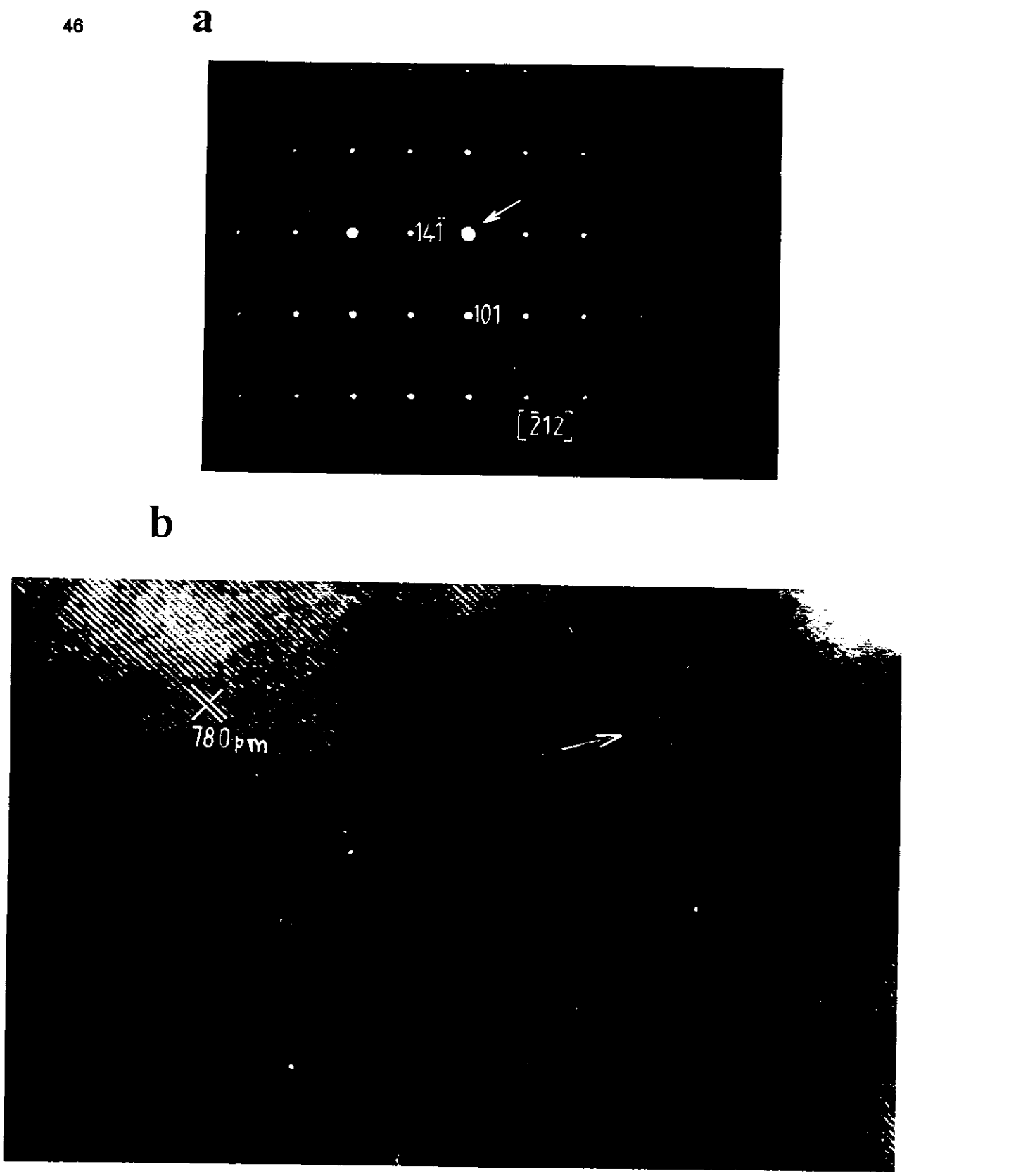

Fig. 9. a) Electron diffraction pattern of the brownmillerite - type $Sr_2Co_2O_{4.96}$ phase along the [$\bar{2}$ 12] zone axis damaged by electron beam irradiation; b) HRTEM image of this damaged region.

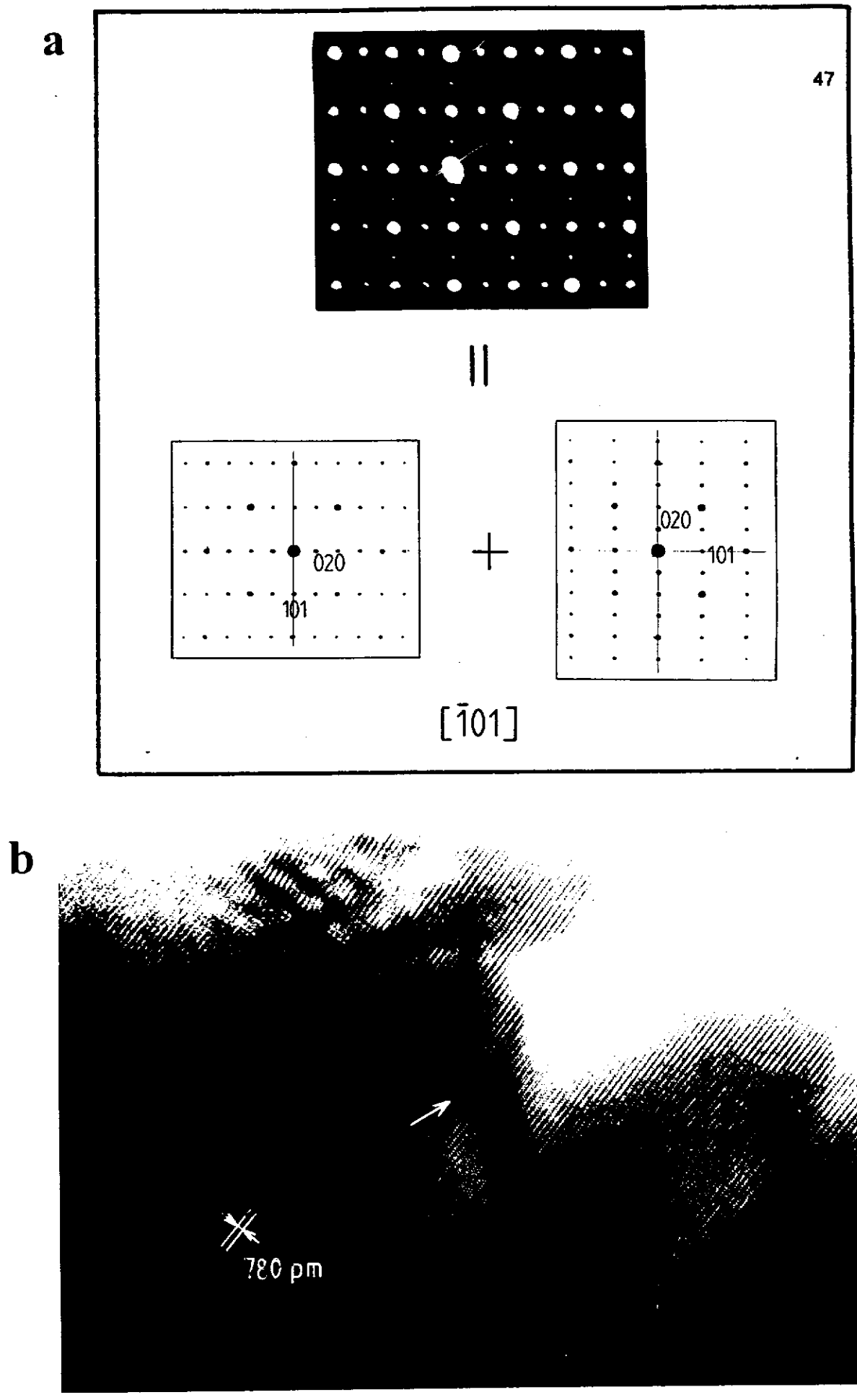

Fig. 10. a) Electron diffraction pattern of brownmillerite - type $Sr_2Co_2O_{4.96}$ characterizing twins having perpendicular b - axes. b) HRTEM image of these twins.

References page 91

Table VI: Results of the Rietveld refinement of the structure of $Sr_2Co_2O_{4.96}$ with the Ibm2 space group.

$Sr_2Co_2O_5$ Brownmillerite Ibm2					
No. of fitted parameters:	34				
ATOM PARAMETERS:					
Name	x	y	z	B	occ.
Sr, 8(c)	0.51007(3)	0.61128(6)	0.00329(2)	0.449(3)	1.000
Co1, 4(a)	0.00000	0.00000	0.00000	0.314(6)	1.000
Co2, 4(b)	0.55818(5)	0.25000	0.47948(2)	0.126(9)	1.000
O1, 8(c)	0.26728(3)	0.99586(6)	0.27750(3)	0.072(2)	1.000)
O2, 8(c)	0.03742(2)	0.14587(3)	0.02794(3)	0.072(2)	1.000
O3, 4(b)	0.65245(2)	0.25000	0.11693(3)	0.072(2)	1.000
Cell parameters					
a		b		c	
557.632(9)		1574.430(3)		547.217(9)	
RELIABILITY FACTORS:					
R_p		R_{wp}		R_{exp}	
8.63		11.2		5.64	
R_I		R_f			
5.52		4.15			

Table VII: Results of the Rietveld refinement of the structure of $Sr_2Co_2O_{4.96}$ with the Icmm space group.

$Sr_2Co_2O_5$ Brownmillerite Icmm					
No. of fitted parameters:	30				
ATOM PARAMETERS:					
Name	x	y	z	B	occ.
Sr, 8(h)	0.51105(3)	0.61134(5)	0.00000	0.415(3)	1.000
Co1, 4(a)	0.00000	0.00000	0.00000	0.115(5)	1.000
Co2, 8(i)	0.56046(5)	0.25000	0.46877(2)	0.115(5)	0.500
O1, 8(h)	0.25000	0.99535(6)	0.25000	0.470(1)	1.000
O2, 8(h)	0.03456(2)	0.14679(3)	0.00000	0.470(1)	1.000
O3, 8(i)	0.63512(2)	0.25000	0.12611(2)	0.470(1)	0.500
Cell parameters					
a		b		c	
557.628(9)		1574.407(3)		547.216(8)	
RELIABILITY FACTORS:					
R_p		R_{wp}		R_{exp}	
8.50		10.9		5.65	
R_I		R_f			
5.42		4.16			

The main differences between the Ibm2 and Icmm space groups are those listed:

For the Ibm2 space group:

- The non - centrosymmetric space group.
- The positions of the Co(2) and O(3) atoms i.e. 4(b) are fully occupied.
- The number of refined parameters is 34.

For the Icmm space group:

- The centrosymmetric space group
- The O(1) atom has the fixed x and z coordinates to be 0.25
- The z coordinates of Sr and O(2) atoms are fixed at 0.
- The special positions 8(i) for Co(2) and O(3) atoms are only half occupied.
- The disorder in y = 0.25 and y = 0.75 following from the statistic occupancy of the 8(i) positions exists for the Icmm space group.
- The number of the refined parameters is 30.

The combination of XRD and electron diffraction techniques demonstrates clearly that $Sr_2Co_2O_{4.96}$ has body-centred symmetry but leaves open the question whether structural model describes better the structure of the studied material.

Nevertheless the Icmm space group can be finally chosen for the description of the structure of $Sr_2Co_2O_{4.96}$ because of following reasons:

- This space group reveals higher symmetry
- The smaller number of refined parameters is required to achieve the almost same result.
- When the structure is described by means of this space group, smaller distorsion of polyhedra occurs
- The disorder onto the 8(i) sites is identical to the structure reported by Greaves [20] for $Sr_2Fe_2O_5$. In the brownmillerite structure the relative orientation of the equivalent tetrahedra alternate along b axis , but an incorrect stacking sequence could occur at intervals along y which would be seen in the diffraction data as a positional disorder of

References page 91

the tetrahedral sites. It may be supported by the occurrence of twins, observed by means of HRTEM. This would also explain the observation [21] of a different space group for single crystal $Sr_2Fe_2O_5$ where better crystallinity could result in fewer faults in the stacking sequence. On the contrary in our case, the single crystals having the brownmillerite structure cannot be probably prepared because of the metastability of this phase and therefore this phenomenon cannot be verified.

The observed, calculated, and difference profiles are drawn in Fig 11. It is evident that all diffraction lines are indexed using the Icmm space group. The structure of the brownmillerite-type $Sr_2Co_2O_5$ oxide is shown in Fig 12.

The interatomic distances are presented in Table VIII

Table VIII: Interatomic distances (pm) in $Sr_2Co_2O_5$ brownmillerite - type phase

Sr polyhedron		Co(1) octahedron		Co(2) polyhedron	
Sr-O(1)	261.0	Co(1)-O(1)	195.5	Co(2)-O(2)	171.8
Sr-O(1)	261.0	Co(1)-O(1)	195.5	Co(2)-O(2)	171.8
Sr-O(1)	264.2	Co(1)-O(1)	195.5	Co(2)-O(3)	190.4
Sr-O(1)	264.2	Co(1)-O(1)	195.5	Co(2)-O(3)	192.1
Sr-O(2)	259.4	Co(1)-O(2)	231.9	mean	181.5
Sr-O(2)	279.5	Co(1)-O(2)	231.9		
Sr-O(2)	279.5	mean	207.6		
Sr-O(3)	243.1				
mean	264.0				

As follows from this table, the mean distance of 264 pm between Sr and Oxygen atoms agrees well with the value expected on the basis of the ionic radii given by Shannon and Prewit [22] (i.e. $r_{Sr^{2+}}$=132 pm, $r_{O^{2-}}$=140 pm). The mean value of the Co(1) - O in the octahedral sites implies that the Co atoms should be in the high spin state in these sites ($r_{Co^{3+}}$=62 pm). The Co(2) - O bond distances in tetrahedral sites are

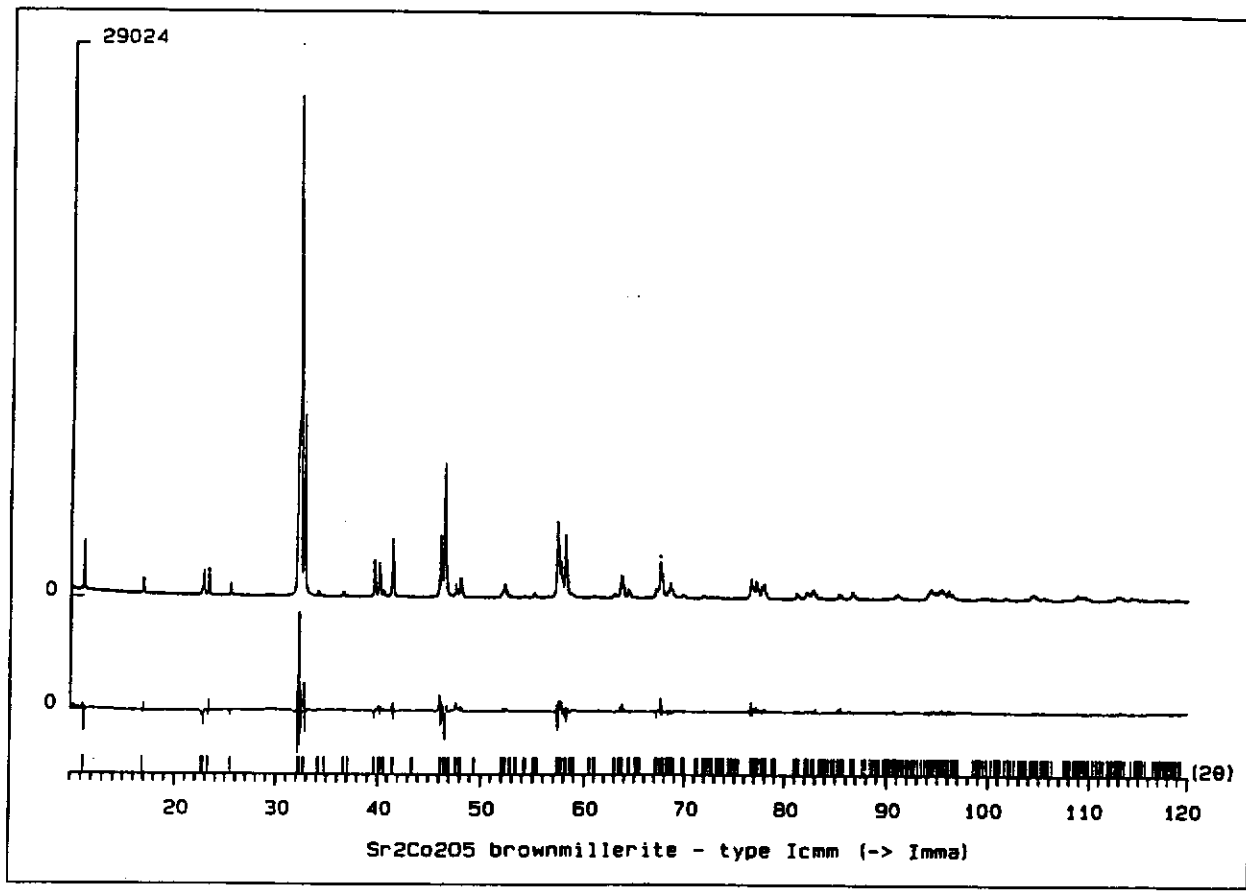

Fig. 11. Observed, calculated and difference profiles for brownmillerite - type $Sr_2Co_2O_{4.96}$.

References page 91

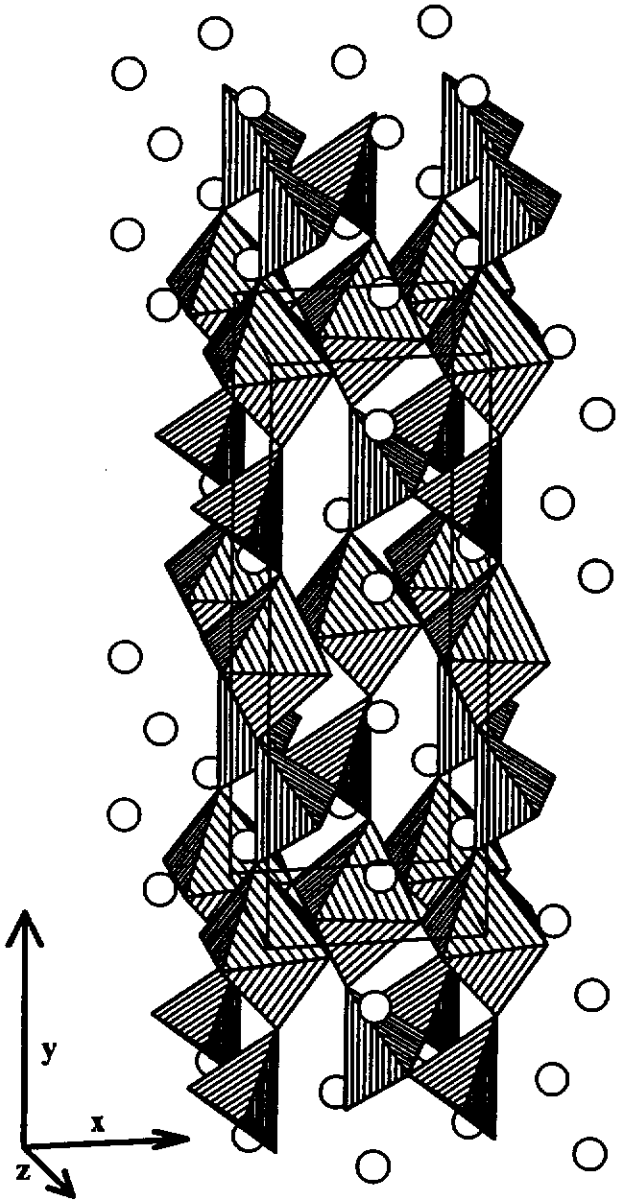

Fig. 12. Refined structure of the brownmillerite - type $Sr_2Co_2O_{4.96}$ phase.

smaller than those of the octahedral sites ($r_{Co^{3+}}$=42 pm). This value, rather small, can be compared to that of $r_{Fe^{3+}}$ in the tetrahedral site in the structure of $Sr_2Fe_2O_5$ ($r_{Fe^{3+}}$ = 47 pm [20]). The ionic radius of the Co^{3+} cation should be inferior to that of Fe^{3+}. Finally the character of bonds in the tetrahedral sites is usually much more covalent than that of octahedral sites.

The rather long distance between the apical oxygen in the octahedra and subsequent lower overlap of the appropriate orbitals may explain the easier thermal expansion of the crystal lattice along the b axis.

Finally the results of the experimental and calculated data are presented in Table IX

References page 91

Table IX: Observed and calculated intensities for $Sr_2Co_2O_{4.96}$.

H	K	L	d_{obs}	d_{calc}	I_{obs}	I_{calc}
0	2	0	7.837	7.872	285	235
1	1	0	5.242	5.256	31	54
0	4	0	3.928	3.936	24	40
1	0	1	3.897	3.906	91	126
1	3	0	3.811	3.822	117	116
1	2	1	3.491	3.499	64	71
2	0	0	2.786	2.788	925	943
1	4	1	2.769	2.772	3048	2880
1	5	0	2.749	2.742	57	55
0	0	2	2.733	2.736	1064	1059
2	2	0	2.623	2.628	1	1
0	6	0	2.620	2.624	32	24
0	2	2	2.583	2.584	8	7
2	1	1	2.452	2.4538	50	36
1	1	2	2.425	2.4269	9	12
2	4	0	2.274	2.2751	240	244
0	4	2	2.246	2.2465	221	226
2	3	1	2.242	2.2454	5	5
1	3	2	2.224	2.2246	37	37
1	6	1	2.177	2.1781	396	381
1	7	0	2.086	2.0858	3	3
0	8	0	1.966	1.9679	473	440
2	0	2	1.952	1.9528	930	963
2	5	1	1.950	1.9503	18	18
1	5	2	1.935	1.9367	16	18
2	6	0	1.911	1.9108	78	57
2	2	2	1.894	1.8954	86	79
0	6	2	1.889	1.8938	75	69
3	1	0	1.846	1.8459	1	4
3	0	1	1.761	1.7599	25	28
1	8	1	1.756	1.7574	11	11
3	3	0	1.753	1.7520	62	60
2	4	2	1.748	1.7493	63	62
1	0	3	1.733	1.7336	14	13
3	2	1	1.719	1.7175	3	6
1	2	3	1.693	1.6930	12	20
1	9	0	1.668	1.6691	5	5
2	7	1	1.665	1.6673	31	29
1	7	2	1.658	1.6587	3	4
2	8	0	1.615	1.6078	215	216
3	4	1	1.606	1.6066	486	492
3	5	0	1.602	1.6007	37	33
0	8	2	1.596	1.5976	271	254
1	4	3	1.585	1.5865	549	568
0	10	0	1.573	1.5744	32	32
2	6	2	1.567	1.5666	12	10
3	1	2	1.531	1.5302	2	5
2	1	3	1.519	1.5192	19	20
3	3	2	1.475	1.4754	42	49
2	3	3	1.471	1.4656	6	6
3	6	1	1.461	1.4616	113	104
1	10	1	1.455	1.4602	163	152

II.2.5. The high temperature cubic phase.

As it was described before, when the $Sr_2Co_2O_{5\pm x}$ material is heated above 1223 K, it transforms into the cubic phase (cf. § II.2.2.). The existence of this phase was previously reported by Takeda et al. [11] who claimed this cubic phase by quenching from above 1473 K. They also determined the composition of this material to be $Sr_2Co_2O_{4.58}$. This cubic phase was also observed by Rodriguez et al. [6,10] by means of high temperature neutron diffraction. These authors concluded in their study that the brownmillerite - type phase is always formed when the cubic phase is quenched down to room temperature.

The ambiguity concerning the possible stabilisation of this phase at room temperature and the fact that there are no data about the structure and more especially the microstructure of this material, led us to study more in detail the thermal behavior and the resulting structure of the high temperature phase of $Sr_2Co_2O_{5-x}$.

We also observed in situ the existence of this phase when we performed the high temperature XRD study. However, attempts to quench this phase down to room temperature were quite unsuccessful. As it was pointed out above, the brownmillerite - type phase was always found when $Sr_2Co_2O_{5-x}$ was quenched in the range from 1223 K to 1550 K down to liquid nitrogen , the mass of the quenched product being about 0.6 g.

Therefore an attempt to quench as fast as possible was carried out: only a few milligrams of finely dispersed powder were placed on a platinum plate and heated up to 1523 K for 3 hours. Then it was quickly quenched down to 300 K. However, even in such a way, only the mixture of the cubic and brownmillerite - type phases (with an excess of the B - type phase) was prepared . The XRD pattern of this sample as well as the HTXRD pattern recorded at 1523 K are shown in Fig. 13 for comparison.

References page 91

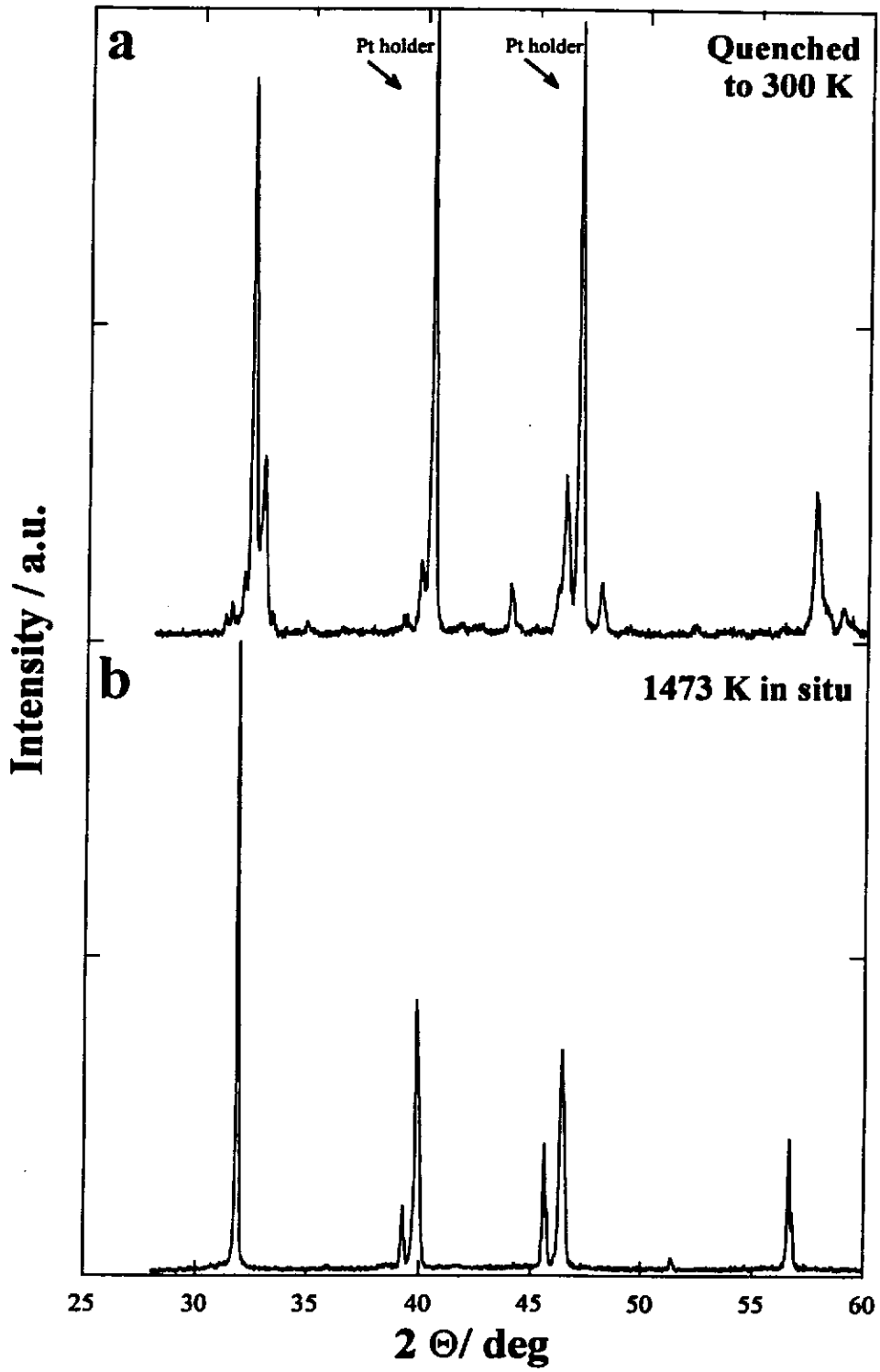

Fig. 13. High temperature XRD patterns for the $Sr_2Co_2O_{5-x}$ phase.

II.2.5.1. The HRTEM study of the high temperature phase

The HRTEM study of the as - prepared powder confirmed the result of the XRD experiments. Several observations of microcrystallites were achieved. Most electron diffraction patterns were found to belong to the brownmillerite - type phase. They were indexed with the body centred orthorhombic crystal lattice analogously to those of the $Sr_2Co_2O_{4.96}$ powder (cf. § II.2.4.2.). These patterns characterize the presence of twins having perpendicular b axes as previously observed in the brownmillerite - type phase (Fig. 14). However, the main difference may be the size of the corresponding domains. If they were found to be large in the case of the "classical" brownmillerite, in this case their size appears smaller.

In few cases, within the same crystallites, the electron diffraction patterns reported in Fig. 15, were observed in two different adjacent regions. They can be interpreted as the presence of the brownmillerite - type domains corresponding to the $[\bar{1}00]_o \equiv [10\bar{1}]_c$ and $[\bar{2}\bar{1}2]_o^* \equiv [01\bar{1}]_c^*$ zone axes respectively. In this case, these domains form an angle of 60^o and are situated along equivalent $[110]_c$ directions of the cubic perovskite subcell.

Probably, this kind of crystals leads to the XRD diagram of the brownmillerite - type.

Otherwise, more complex electron diffraction patterns were observed. A typical example is given in Fig. 16. It can be indexed on the basis of a double cubic perovskite cell (a ≐ 793.2 pm) at least in two directions of the space.

The image obtained along this zone axis shows the presence of very small microdomains whose size is typically a few nanometers (3 - 7 nm). The structure of each microdomain seems to be that of the brownmillerite according to the interfringe spacing (≅ 780 pm).

However, some discrepancy exists between this image and the electron diffraction pattern. If we assume that the reciprocal space is composed of 3 sets of

References page 91

a

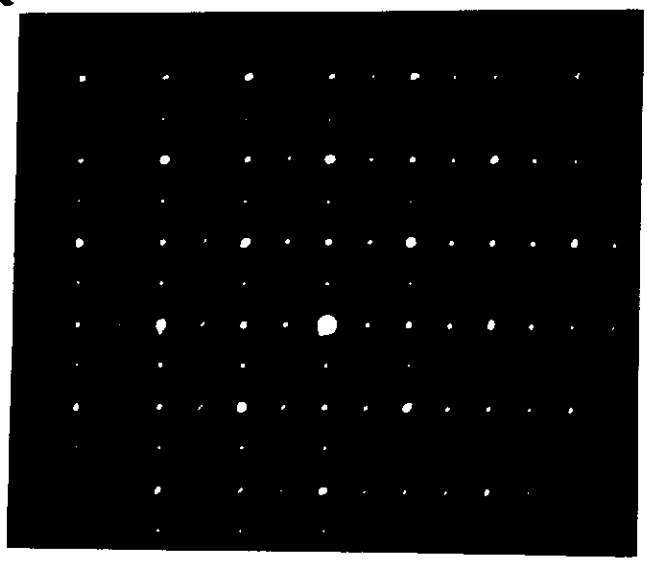

b

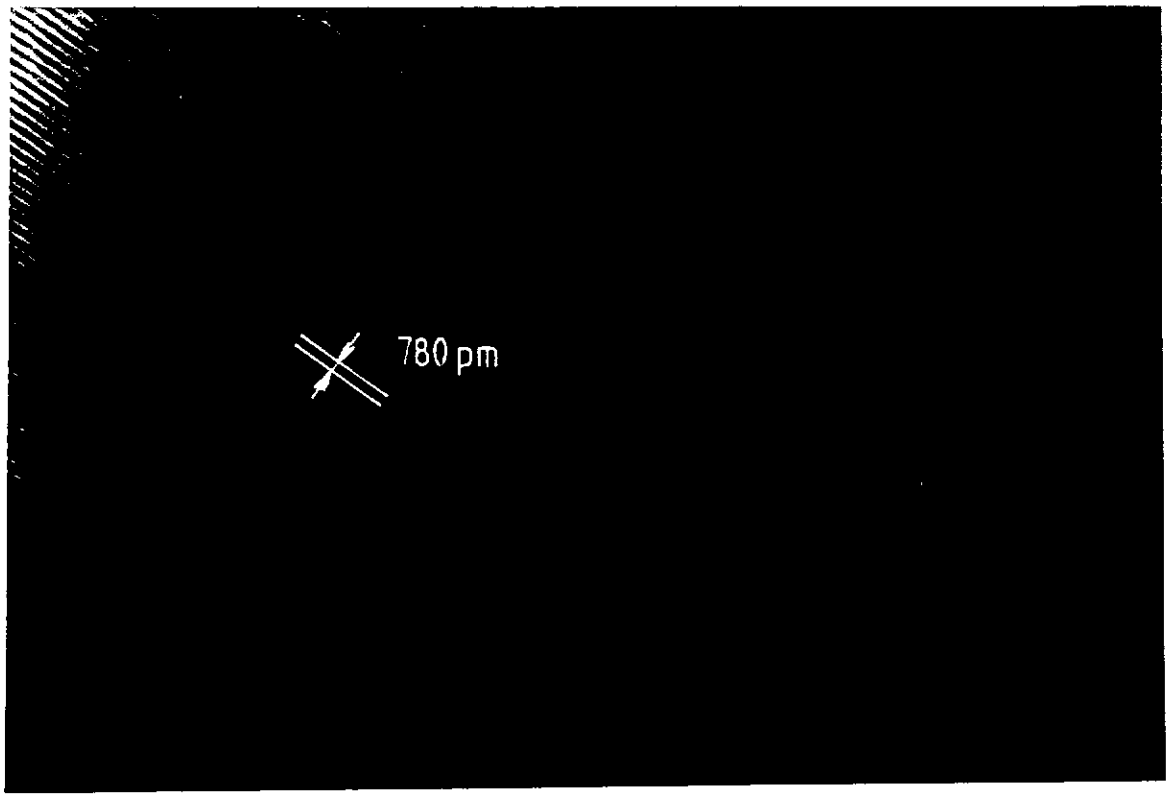

Fig 14. a) Electron diffraction pattern of the high temperature $Sr_2Co_2O_{5-x}$ phase having perpendicular b axes. b) subsequent HRTEM image.

a

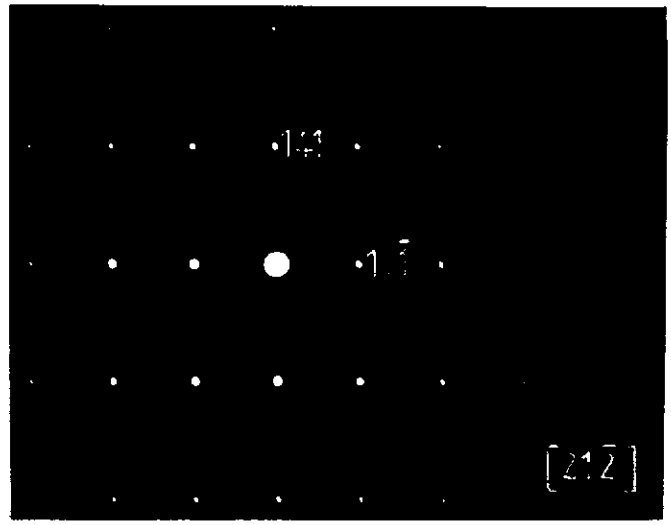

b

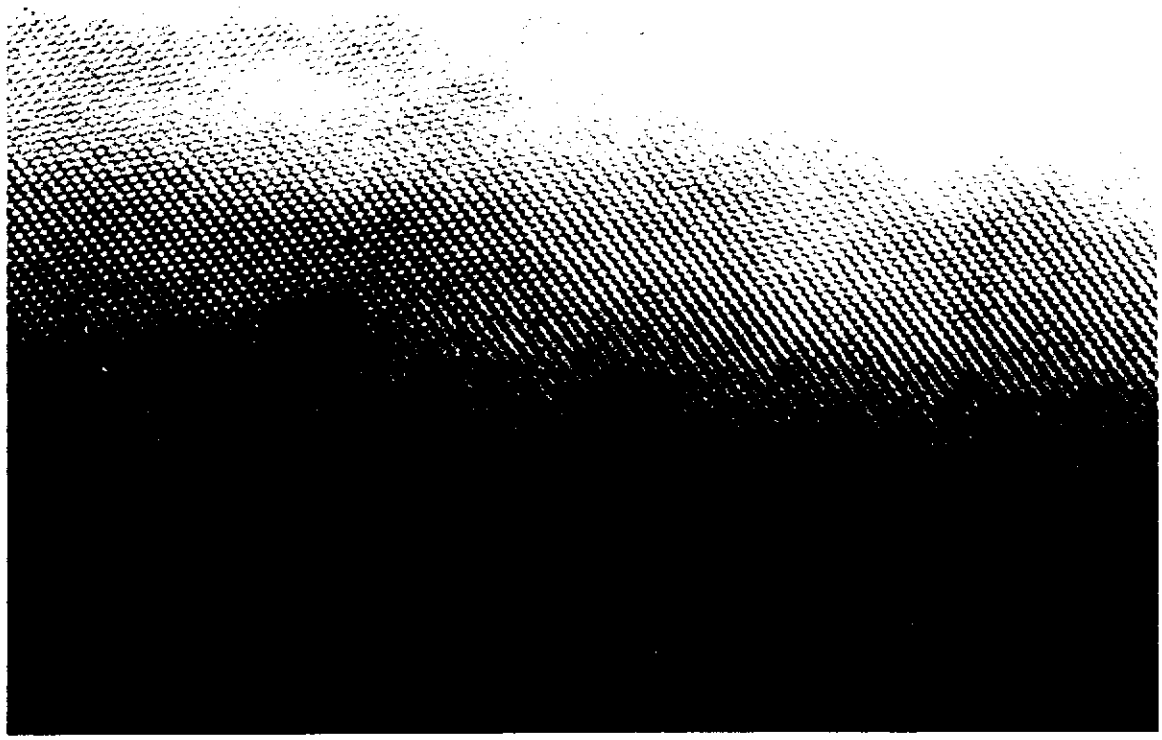

Fig. 15. a) Electron diffraction pattern of the high temperature $Sr_2Co_2O_{5-x}$ phase along the $[\bar{1}00]_o \equiv [10\bar{1}]_c$ and $[\bar{2}\,\bar{1}\,2]_o \equiv [01\bar{1}]_c$ zone axes b) subsequent HRTEM image.

References page 91

a

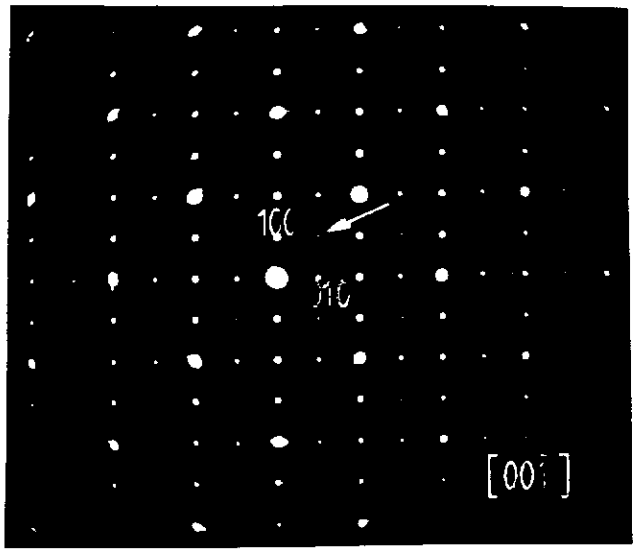

b

Fig. 16. a) Electron diffraction pattern of the high temperature $Sr_2Co_2O_{5-x}$ phase indexed on the basis of a double cubic perovskite cell. b) subsequent HRTEM image showing very small brownmillerite - type microdomains.

brownmillerite - type domains having perpendicular directions in the space (Fig. 16), the resulting reciprocal lattice does not lead to a double cubic perovskite cell, more particularly the spot marked by an arrow should not be present.

However, one should point out that the intensity of this spot seems to be related to the size of the microdomains; the more intense the spot, the smaller size of the domain.

The HRTEM experiments performed with this high temperature phase confirmed that the cubic phase existing at the high temperature above 1223 K is not stabilized at room temperature at least under our experimental conditions. Only a mixture of a cubic and of the brownmillerite - type phases is prepared, which confirms that this phase would exist only when the sample is heated above 1223 K. Nevertheless, a very fast quenching may stabilize this cubic phase.

The results of our study can be summarized as follows:

1) at high temperature, the composition was found to be close to $Sr_2Co_2O_{4.60}$, which leads to the occurrence of additional oxygen vacancies with respect to the composition of the brownmillerite - type phase ($Sr_2Co_2O_5$).

2) the metallic behavior [14] as well as the cubic symmetry of this phase would imply a high disorder of the oxygen vacancies and may be a high oxygen mobility.

3) according to the quenching rate, the phase observed at room temperature show a more or less ordered structure. In the best case ("normal quenching"), the macroscopic oxygen ordering occurs leading to the brownmillerite - type structure with the presence of twins. In the worst case ("fast quenching"), the cubic phase exhibits a microstructure made of very small domains in which oxygen vacancies would be ordered in the same way as in the basic unit of the brownmillerite (i.e. O-T-O-T' sequence).

The observed double cubic cell would result either from this particular microstructure or from ordering of the additional oxygen vacancies.

Such microdomain textures were previously observed in the oxygen deficient perovskites ABO_{3-y} ($y \leq 0.50$) and were evidenced for the first time by Alario-Franco

References page 91

et al. in $Ca_2LaFe_3O_{8+x}$ [23], and later on more generally in the Ca-La-Fe-O [24], in the Ba-Fe-O [25] or in the Sr-Fe-O systems [26] which were studied in the laboratory since 1975.

However it is the first time that microdomains are observed for compounds having the brownmillerite - type structure corresponding to $y > 0.50$.

Images of higher resolution are highly desirable to clarify this oxygen ordering.

II.2.6. The low temperature - rhombohedral phase

As it was mentioned above, the low temperature phase is formed during the slow cooling of the cubic phase from above 1223 K or heat treatment of the metastable brownmillerite-type compound above the temperature of 850 K and subsequent slow cooling down to room temperature. According to the used atmosphere the oxygen content and therefore the oxidation state of cobalt may significantly vary from the ideal composition of $Sr_2Co_2O_5$ (cf. § II.2.1.2.).

More or less similar XRD patterns are obtained for materials of composition $Sr_2Co_2O_{5.00}$ - $Sr_2Co_2O_{5.20}$ (see Fig. 1 b,c).

Table X: XRD data for the low temperature phase according to ref. [7]

H	K	L	d_{obs}	d_{calc}	I_{obs}
			6.87		3
1	0	0	4.72	4.71	12
			4.69		11
1	0	1	3.115	3.15	100
1	1	0	2.718	2.72	63
2	0	0	2.427	2.36	7
			2.126		11
0	0	2	2.122	2.122	6
2	0	1	2.078	2.060	4
			2.047		50
			2.043		14
1	0	2	1.932	1.935	32
			1.899		13
1	1	2	1.676	1.673	1
			1.650		15
1	2	1	1.638	1.642	7
			1.580		2
			1.576		1
3	0	0	1.570	1.570	1
			1.559		3
			1.557		2

In a first time Grenier et al. [7] proposed to index those patterns on the basis of the 2H $BaNiO_3$ - type cell, but found some additional diffraction lines (see Table X) which were assigned to the presence and ordering of oxygen vacancies in $Sr_2Co_2O_5$ with regard to the stoichiometric "$Sr_2Co_2O_6$" compound.

Later on Rodriguez et al. [9] confirmed this result and obtained some additional data using HRTEM. More especially, on the basis of the E.D. observations, they proposed a rhombohedral unit cell (superstructure of the 2H basic cell) and according to the systematic absences of diffractions, the $R\bar{3}m$ space group. Finally Takeda et al. [11] proposed a solution slightly different from the previous ones, pointing out that in fact the stoichiometric $Sr_2Co_2O_5$ does not exist. They attributed some of the additional diffraction lines to Co_3O_4. Finally they concluded that $Sr_2Co_2O_5$ undergoes a decomposition during the phase transition at 1092 K, forming a compound with the composition close to $SrCo_{0.9}O_x$ and Co_3O_4. This fact was supported in the disappearing of the diffraction lines assigned to Co_3O_4, when they prepared the phase with composition of $SrCo_{0.9}O_x$.

References page 91

Therefore investigations on the structure of the low temperature phase were led to clarify this problem concerned with the vacancy ordering in this compound and/or the possible partial decomposition.

In this way we tried:

- to check the crystal lattice symmetry using HRTEM
- to refine the structure on the basis of our XRD data and neutron diffraction data of the low temperature phase obtained in inert atmosphere by transformation from the brownmillerite - type phase, that J. Rodriguez-Carvajal kindly afforded us [27].

II.2.6.1. The HRTEM study of the low temperature phase.

In the previous paragraph we discussed that the XRD pattern of the $Sr_2Co_2O_{5+x}$ low temperature phase cannot be indexed with the primitive hexagonal crystal lattice (2H $BaNiO_3$ - type, $P6_3/mmc$), several diffraction lines remaining unindexed.

Both powders ($Sr_2Co_2O_{5.06}$ and $Sr_2Co_2O_{5.20}$ respectively) were studied by means of HRTEM. They exhibited basically the same electron diffraction patterns (Fig. 17 a-e).

In the first stage we tried once again to index these patterns using the 2H unit cell (a = 544 pm c = 424 pm, $P6_3/mmc$ space group). Indeed, this pattern well agrees with the 2H hexagonal space group (Fig. 17 a) and apparently no superstructure spots at least in the $(a,b)^*$ plane are observed. But as shown in Fig. 17 b, superstructure spots that cannot be indexed with the 2H hexagonal cell are clearly seen as for instance along the c^*_{2H}. Therefore it should be used either a primitive hexagonal space group having no systematic absences or a supercell with a multiple c parameter.

Next E.D. pattern (Fig. 17 c) also exhibits superstructure spots along for instance $[1\bar{2}2]$ (equivalent to [112]) direction which appears tripled.

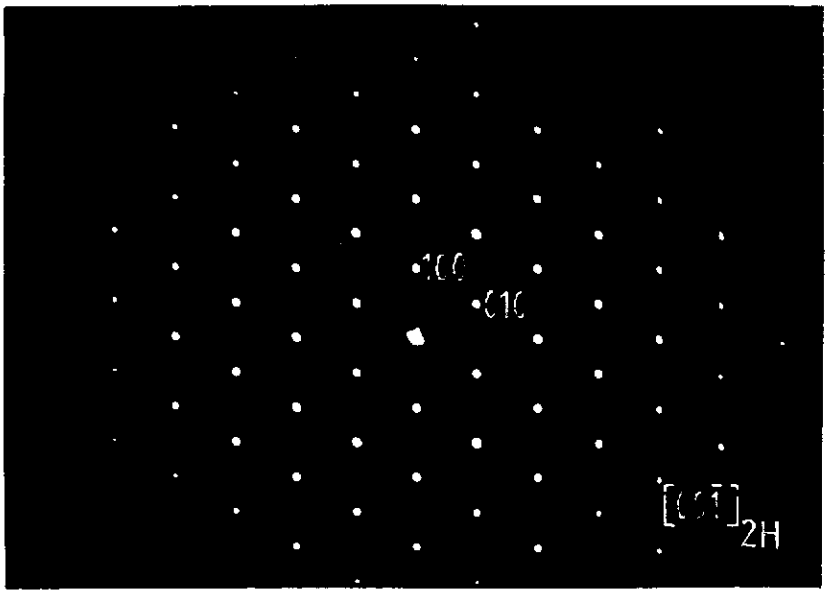

a

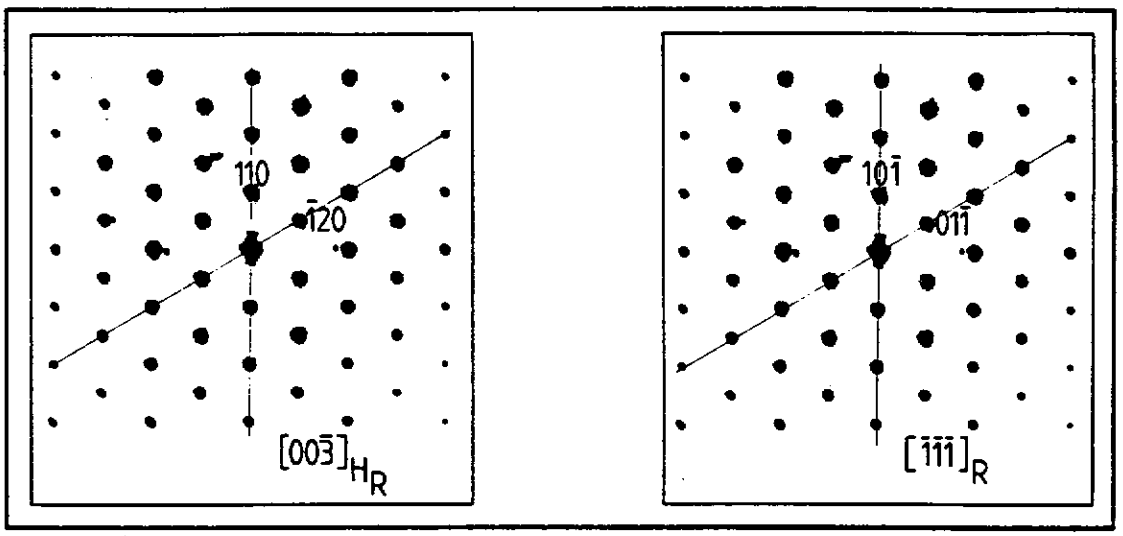

Fig. 17. Electron diffraction patterns of the low temperature $Sr_2Co_2O_{5+x}$ phase.

References page 91

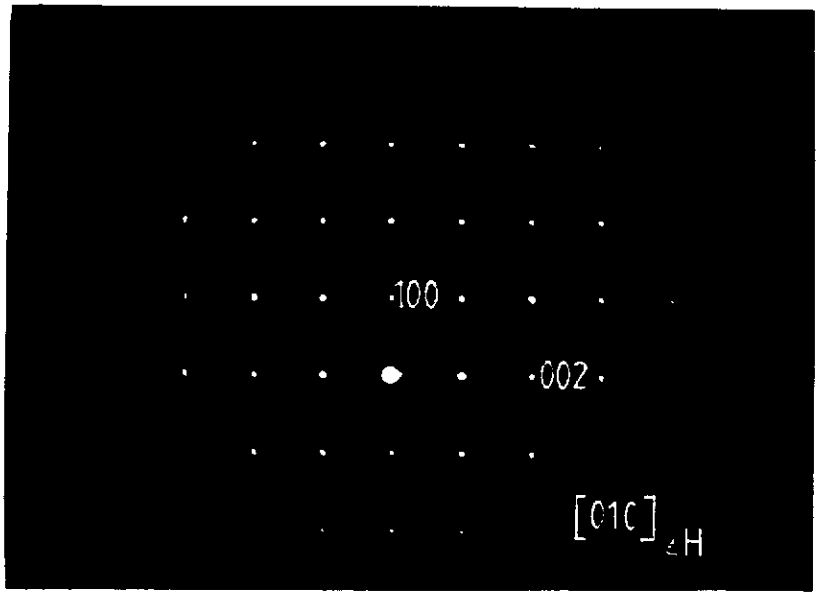

b

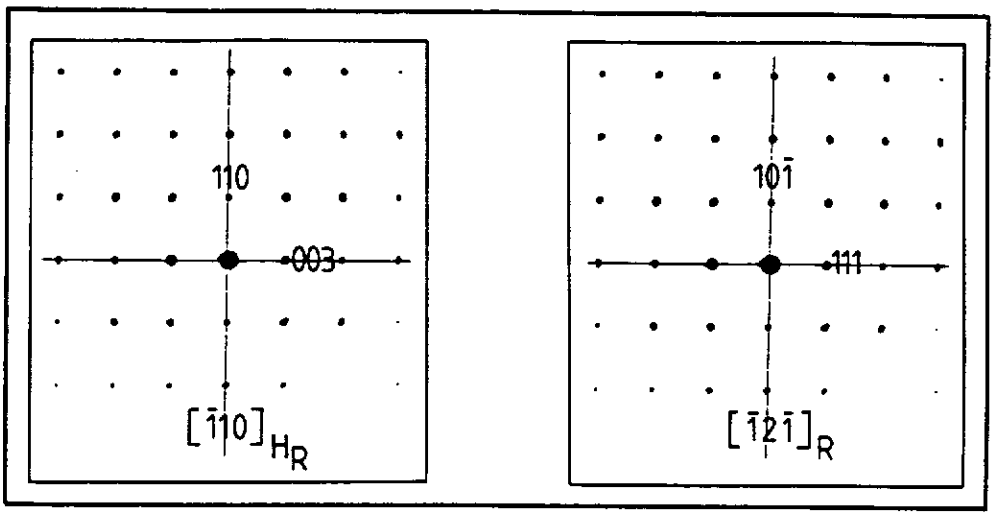

Fig. 17. Electron diffraction patterns of the low temperature $Sr_2Co_2O_{5+x}$ phase.

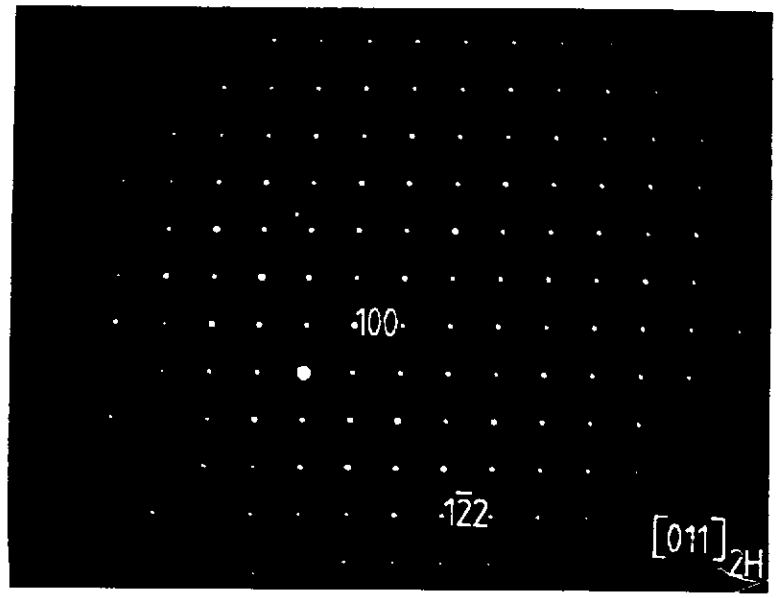

c

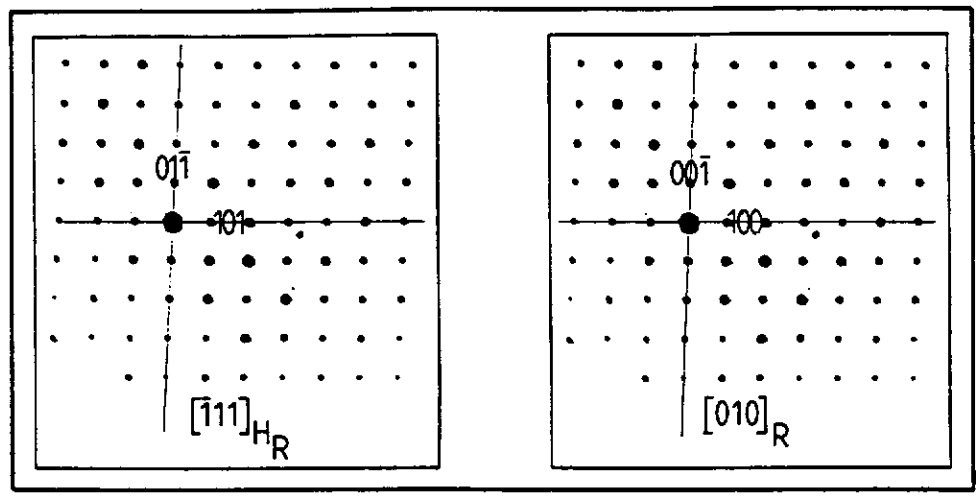

Fig. 17. Electron diffraction patterns of the low temperature $Sr_2Co_2O_{5+x}$ phase.

References page 91

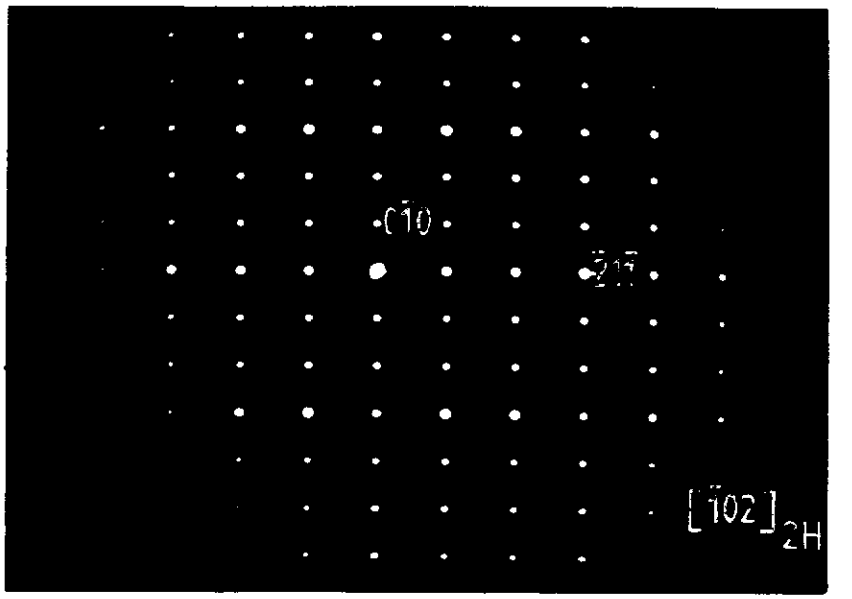

d

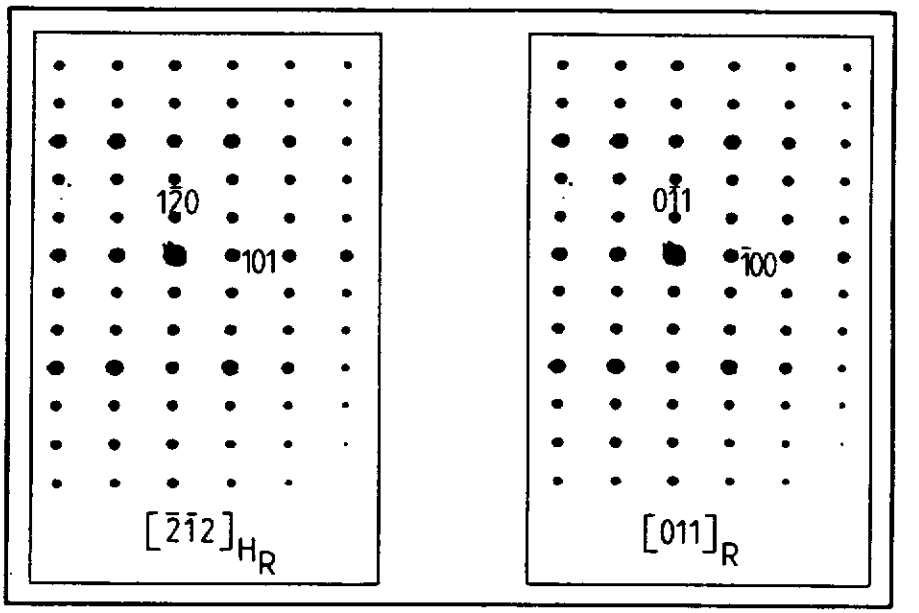

Fig. 17. Electron diffraction patterns of the low temperature $Sr_2Co_2O_{5+x}$ phase.

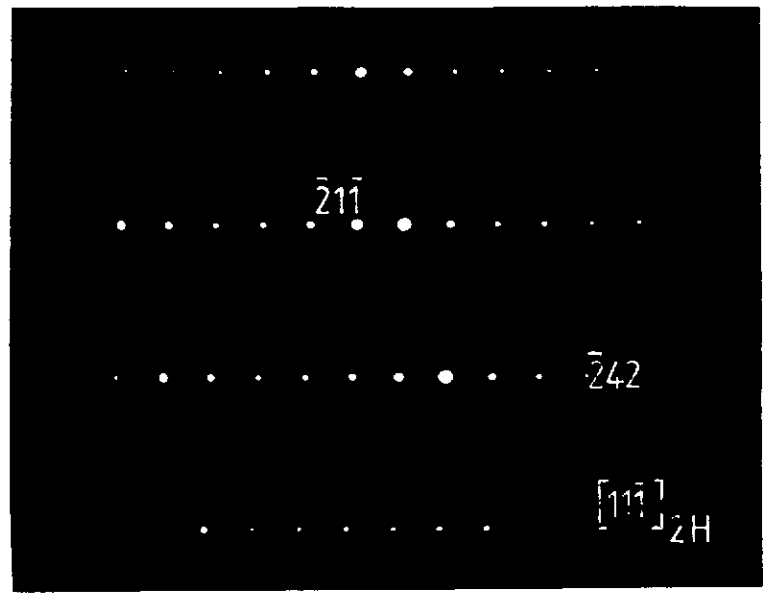

e

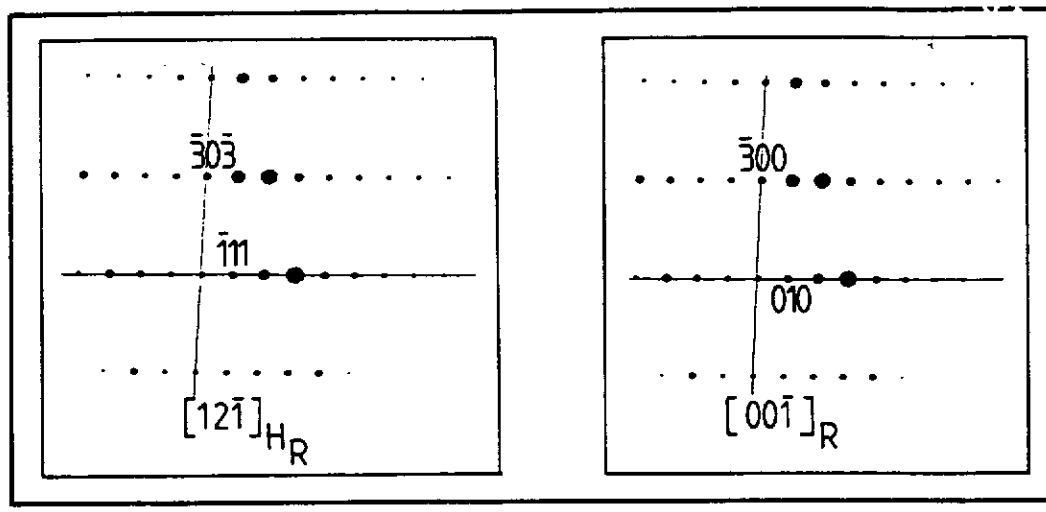

Fig. 17. Electron diffraction patterns of the low temperature $Sr_2Co_2O_{5+x}$ phase.

References page 91

Then assuming a H-type triple hexagonal cell, as described for example in the International Tables for Crystallography [28], having in addition a triple c parameter, all spots can be indexed (Figs. 17 a-e).

The observed reflection conditions (Table XI) lead to a trigonal symmetry. Therefore, the possible space group describing the structure of the low temperature phase of $Sr_2Co_2O_{5-x}$ has to belong to $\bar{3}$ or $\bar{3}m$ Laue classes.

Table XI: The reflection conditions for $P6_3/mmc$ and trigonal $\bar{3}$, $\bar{3}m$ space groups respectively.

$P6_3/mmc$	$\bar{3}$, $\bar{3}m$ Laue classes
	hkl: -h + k+ l = 3 n
	($h\bar{h}0l$: h + l = 3 n)
$hh\bar{2}\bar{h}l$: l = 2 n	($hh\bar{2}\bar{h}l$: l = 3 n)
000l: l = 2 n	(000l: l = 3 n)

Finally the following relationship describing the transformation from the primitive 2H - type hexagonal cell to the 9 times bigger hexagonal H_R cell may be expressed as follows:

$$\begin{pmatrix} a^*_{H_R} \\ b^*_{H_R} \\ c^*_{H_R} \end{pmatrix} = \underbrace{\begin{pmatrix} \frac{2}{3} & \frac{\bar{1}}{3} & 0 \\ \frac{1}{3} & \frac{1}{3} & 0 \\ 0 & 0 & \frac{1}{3} \end{pmatrix}}_{Q} \cdot \begin{pmatrix} a^*_{2H} \\ b^*_{2H} \\ c^*_{2H} \end{pmatrix} \qquad (a_{H_R}, b_{H_R}, c_{H_R}) = (a_{2H}, b_{2H}, c_{2H}) \cdot \underbrace{\begin{pmatrix} 1 & 1 & 0 \\ \bar{1} & 2 & 0 \\ 0 & 0 & 3 \end{pmatrix}}_{P}$$

where the matrix P is related to Q by $P = Q^{-1}$.

And the new cell parameters will be related to the old ones by:

$$a_{H_R} = a_{2H} \cdot \sqrt{3} \qquad c_{H_R} = 3 \cdot c_{2H} \qquad V_{H_R} = 9 \cdot V_{2H}$$

which leads to the estimated cell parameters of a = 943.6 pm and c = 1251.8 pm.

The transformation between the hexagonal axes notation and the rhombohedral axes notation is described using the following transformation matrices

$$\begin{pmatrix} a^*_{H_R} \\ b^*_{H_R} \\ c^*_{H_R} \end{pmatrix} = \underbrace{\begin{pmatrix} \frac{2}{3} & \frac{\bar{1}}{3} & \frac{\bar{1}}{3} \\ \frac{1}{3} & \frac{1}{3} & \frac{\bar{2}}{3} \\ \frac{1}{3} & \frac{1}{3} & \frac{1}{3} \end{pmatrix}}_{Q} \cdot \begin{pmatrix} a^*_R \\ b^*_R \\ c^*_R \end{pmatrix} \qquad (a_{H_R}, b_{H_R}, c_{H_R}) = (a_R, b_R, c_R) \cdot \underbrace{\begin{pmatrix} 1 & 0 & 1 \\ \bar{1} & 1 & 1 \\ 0 & \bar{1} & 1 \end{pmatrix}}_{P}$$

II.2.6.1.1. Indexation of the XRD patterns

Based on the results of the HRTEM - E.D. study the XRD patterns of both materials ($Sr_2Co_2O_{5.06}$ - $Sr_2Co_2O_{5.20}$) were correctly indexed using a trigonal space group with a rhombohedral Bravais lattice. This indexation is shown in the Table XII. As indicated in the Table XII, some weak diffraction lines remained unindexed, addressing the question of possible impurities (e.g. CoO or Co_3O_4) in the sample. The chemical analysis of the studied powder did not reveal significant changes in the ratio between Sr and Co (Sr:Co=1.00±0.01). It was finally supposed that the $Sr_2Co_2O_{5+x}$ phase may decompose into the Co substoichiometric one as observed by Takeda et al. [11].

The nature of this phenomenon will be explained later.

References page 91

Table XII: Indexation of the XRD patterns of $Sr_2Co_2O_{5.06}$.

Indexation of the XRD patterns of $Sr_2Co_2O_{5.06}$ using the R - type unit cell							
h_{H_R}	k_{H_R}	l_{H_R}	h_R	k_R	l_R	d_{obs}	d_{calc}
1	0	1	1	0	0	6.83	6.858
0	1	2	1	1	0	4.97	4.976
1	1	0	1	$\bar{1}$	0	4.72	4.732
						4.66	
0	0	3	1	1	1	4.16	4.174
0	2	1	1	1	$\bar{1}$	3.88	3.895
2	0	2	2	0	0	3.42	3.429
1	1	3	2	1	0	3.13	3.131
2	1	1	2	$\bar{1}$	0	3.01	3.007
1	0	4	2	1	1	2.93	2.925
						2.85	
1	2	2	2	1	1	2.77	2.776
3	0	0	2	$\bar{1}$	$\bar{1}$	2.73	2.732
0	2	4	2	2	0	2.49	2.4880
						2.459	
						2.437	
0	1	5	2	2	1	2.397	2.3955
2	2	0	2	0	$\bar{2}$	2.369	2.3661
1	3	1	2	$\bar{2}$	1	2.235	2.2367
2	1	4	3	1	0	2.203	2.2022
2	0	5	3	1	1	2.136	2.1373
0	0	6	2	2	2	2.089	2.0874
2	2	3	3	1	$\bar{1}$	2.058	2.0585
4	0	1	3	$\bar{1}$	$\bar{1}$	2.027	2.0222
1	2	5	3	2	0	1.948	1.9478
0	4	2	2	2	$\bar{2}$	1.948	1.9475
1	1	6	3	2	1	1.910	1.9098
3	2	1	3	0	$\bar{2}$	1.859	1.8595
1	3	4	3	2	$\bar{1}$	1.826	1.8396
1	4	0	2	1	$\bar{3}$	1.790	1.7886
3	1	5	4	1	0	1.682	1.6834
3	0	6	4	1	1	1.657	1.6587
1	4	3	3	2	$\bar{2}$	1.644	1.6441
0	5	1	2	2	$\bar{3}$	1.627	1.6254
0	4	5	3	3	$\bar{1}$	1.587	1.586
5	0	2	4	$\bar{1}$	$\bar{1}$	1.587	1.5859
3	3	0	3	0	$\bar{3}$	1.578	1.5774
2	2	6	4	2	0	1.565	1.5653
2	1	7	4	2	1	1.550	1.5493
0	1	8	3	3	2	1.540	1.5377
2	4	1	3	1	$\bar{3}$	1.540	1.5373
2	3	5	4	2	$\bar{1}$	1.505	1.5038
4	2	2	4	0	$\bar{2}$	1.505	1.5037

II.2.6.2. Relations between the 2H and R structural types in the real space

The relation between the 2H and R structural types will be now described using the hypothetical "$SrCoO_3$" hexagonal 2H structure and in the next step with the transformation to the R structural type, which is in fact caused by the vacancy ordering in the above mentioned "$SrCoO_3$" structure.

II.2.6.2.1 Description of the 2H-type structure

The hypothetical "$SrCoO_3$" can be theoretically described similarly to the $BaNiO_3$ or $BaCoO_3$ 2H - type oxides.

The structure of $BaNiO_3$ has been previously reported by three authors [29-31]. It is worthwhile to point out at this place, that the atomic position of Ba^{2+} cations given by Krischner [29] and Lander [30] was wrong, i.e. the 2(b) position (1/3, 2/3, 1/4) of the $P6_3mc$ space group . When constructing the structure of $BaNiO_3$ using these coordinates, the Ba-O bond lengths are about 160 pm, which is obviously too short with respect to the atomic radii ($r_{Ba^{2+}}$=127 pm, $r_{O^{2-}}$=140 pm) (Fig 18 a).

Only Takeda's description is correct [31]. He proposed on the basis of monocrystal investigations the $P6_3/mmc$ space group with the position 2(d) for Ba (1/3, 2/3, 3/4). This position leads to correct interatomic distances, d(Ba-O) about 260 pm (Fig 18 b).

The hypothetical hexagonal "$SrCoO_3$" can be therefore described according to Takeda [31] as follows (cf. Table XIII):

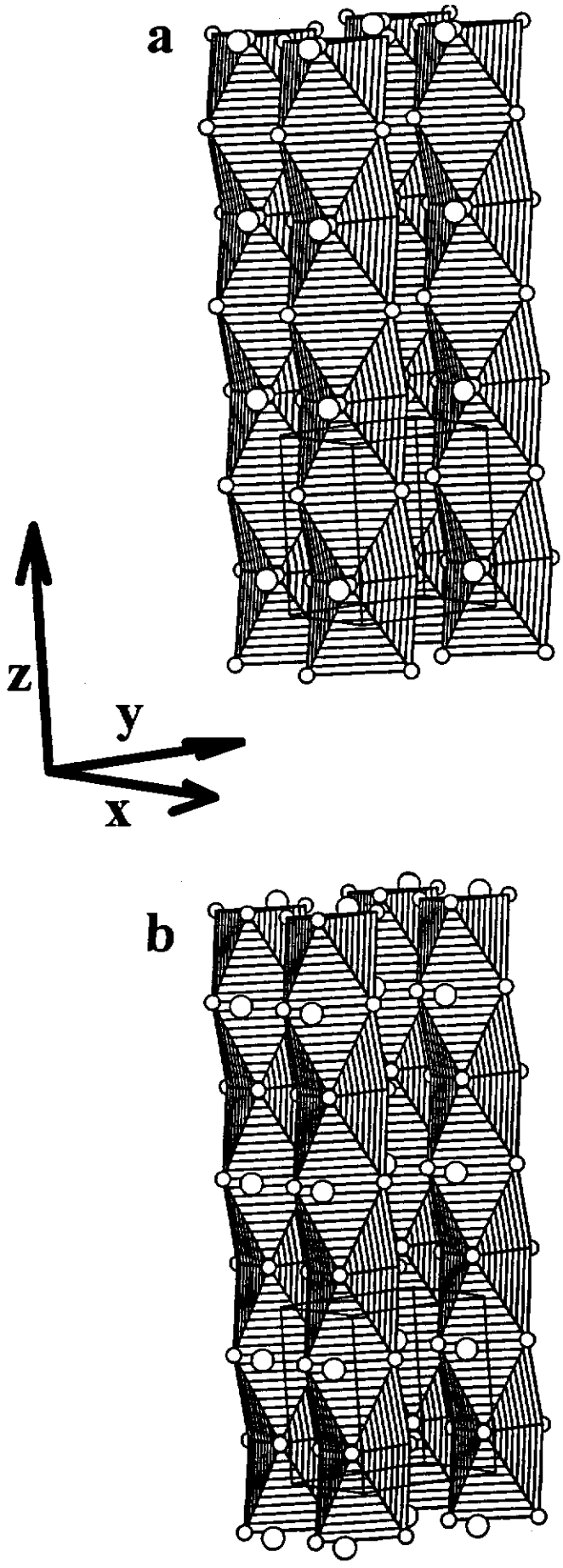

Fig. 18. Structure of $BaNiO_3$ a) according to Krischner [29] and Lander [30], the Sr position is not correct, b) according to Takeda [31], with the correct Sr position.

Table XIII: Atomic positions for "$SrCoO_3$" in the $P6_3/mmc$ space group.

"$SrCoO_3$" :- $P6_3/mmc$ space group				
Sr^{2+}	2(d)	1/3	2/3	3/4
Co^{4+}	2(a)	0	0	0
O^{2-}	6(h)	1/6	-1/6	1/4

II.2.6.2.2. Transformation of the primitive hexagonal cell into a multiple hexagonal cell having the rhombohedral unit cell.

It is clear that only the structure of this stoichiometric $SrCoO_3$ can be described with this primitive hexagonal cell. Supposing the occurrence of the oxygen vacancy ordering, it obviously involves a multiple cell deriving from the 2H - type cell. This new cell (H_R), found by HRTEM observations, is sketched in Figure 19. The multiplication factor of the unit cell parameter a ($a_H = a_{2H}*\sqrt{3}$) and the existence of the "hexagonal centring points" [28] lead to a so called triple H cell ($a_H = a_{2H}*\sqrt{3}$, $c_H = c_{2H}$, Fig. 19). This intermediate unit cell has a volume three times bigger that the primitive 2H unit cell.

Finally, the hexagonal H_R cell describing the rhombohedral cell is obtained by the multiplication of the c parameter $c_{H_R} = 3*c_{2H}$ (as follows from the value estimated by HRTEM). It implies that the H_R type unit cell is 9 times bigger than the primitive hexagonal 2H cell. It leads to the following formula - $Sr_{18}Co_{18}O_{54}$ for the stoichiometric compound involving 18 equivalent positions for Co and 18 equivalent positions for Sr atoms per unit cell.

References page 91

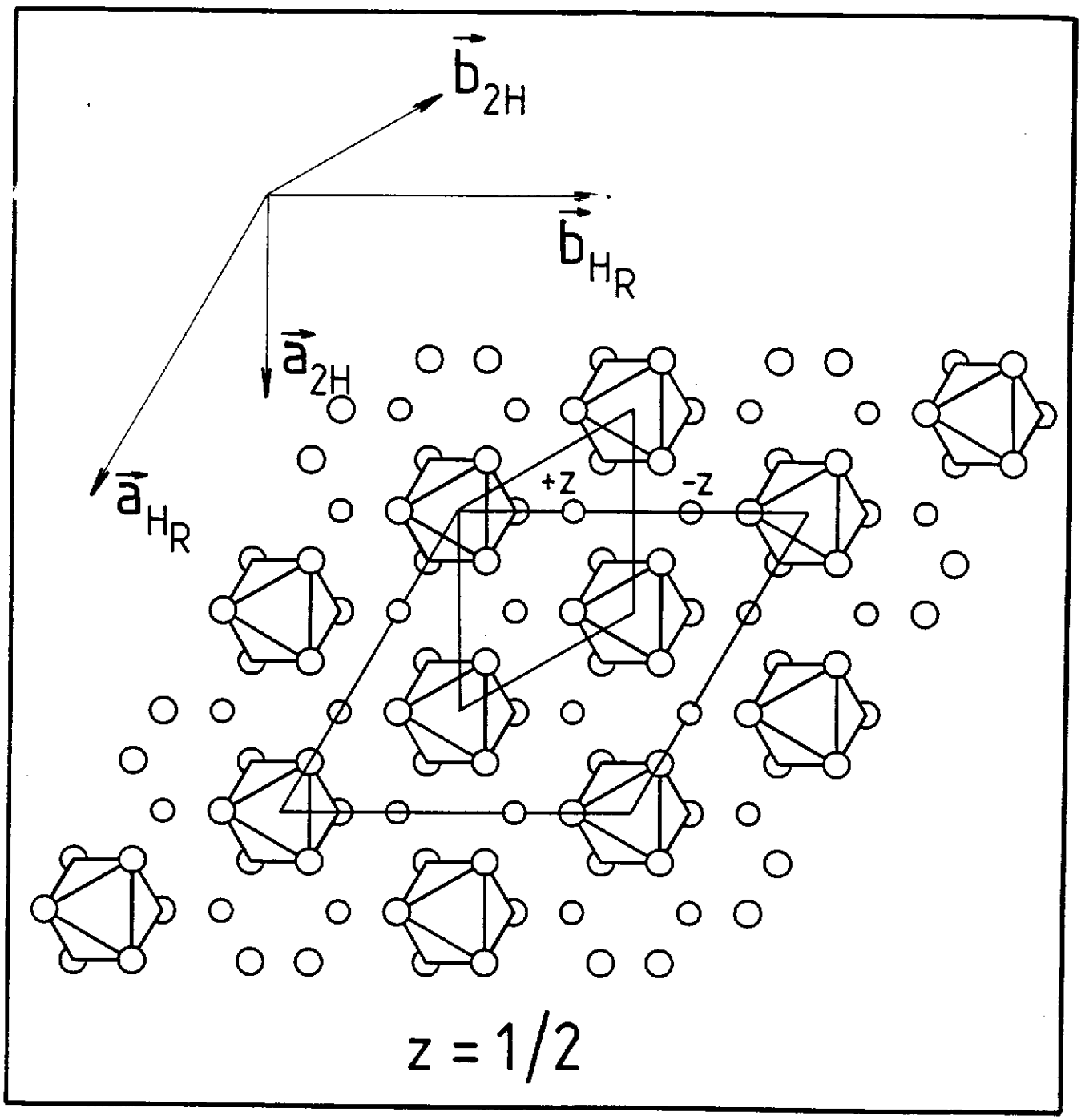

Fig. 19. Passage from the 2H - type cell to a multiple H_R cell.

II.2.6.2.3. Determination of a possible rhombohedral space group.

The HRTEM study led, according to the reflection conditions, to the $\bar{3}$ and $\bar{3}$m Laue classes. These classes involve 5 space groups: R$\bar{3}$m, R3m, R$\bar{3}$, R3 and R32. Therefore it seems to be adequate to analyse more carefully which space group can be used to describe the structure of the studied material.

Cobalt atoms are placed in all above mentioned R type groups in special positions (0, 0, z) with z=0, 1/6, 1/3, 1/2, 2/3 and 5/6. These special positions are common for all the five R space groups.

Regarding the tables of the mentioned groups, strontium atoms should be always placed in the general position (x, y, z, x = 0, y = 1/3, z = 1/4, equivalent to x =2/3, y = 0, z = -1/12, deduced from the 2H position). This fact may be taken as a criterion for the most suitable space group.

The R$\bar{3}$m group has the general position 36(i) which implies that it generates twice the necessary number of Sr atoms per unit cell (see Fig 20 a) and even an occupancy factor of 50 % does not lead to the correct position of Sr expected from a multiple 2H - type cell.

The R3m and R32 space groups have the general position with 18 equivalents (18(c) and 18(f) respectively), but the symmetry required by these space groups does not correspond again to the expected position of the strontium atoms (see Fig. 20 b,c).

Only the R$\bar{3}$ and R3 space groups allow to describe the studied structure having basically the 2H - type position of the strontium and cobalt atoms. (see Fig. 20 d). So R$\bar{3}$ and R3 space groups were used, as it will be seen below, for the refinement of the structure of rhombohedral $Sr_2Co_2O_{5+x}$.

References page 91

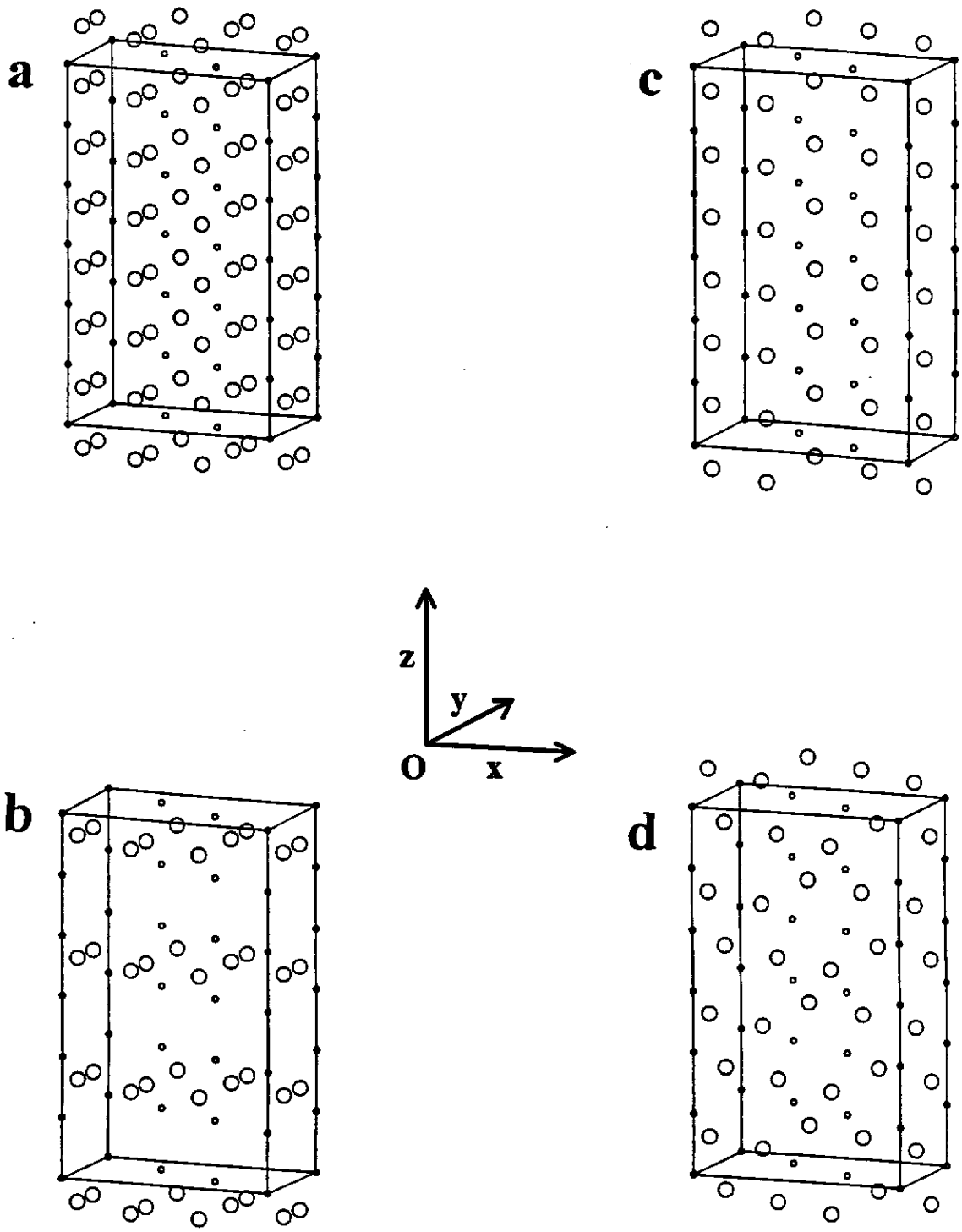

Fig. 20. Atomic positions of cobalt and strontium in a) $R\bar{3}m$, b) R3m, c) R32 and d) $R\bar{3}$ or R3 space groups, respectively.

II.2.6.3. Structure refinement by neutron diffraction at 300 K using the $R\bar{3}$ space group

We started our refinements on the basis of the atomic positions of atoms in the $R\bar{3}$ space group deduced from the positions in 2H structure as mentioned above for Sr and Co as well as for the oxygen atoms; they are reported in the Table XIV and Fig. 21 a.

Table XIV: Atomic positions for $Sr_2Co_2O_{5+x}$ in $R\bar{3}$ space group.

Atomic positions in the $R\bar{3}$ space group				
Atom	Wyckoff symb.	x	y	z
Co 1	3(a)	0.00	0.00	0.00
Co 2	6(c)	0.00	0.00	1/6
Co 3	6(c)	0.00	0.00	1/3
Co 4	3(b)	0.00	0.00	1/2
Sr 1	18(f)	2/3	0.00	-1/12
O 1	18(f)	1/6	0.00	-1/12
O 2	18(f)	1/6	0.00	1/4
O 3	18(f)	1/6	0.00	-5/12

The result of this refinement showed that the majority of the diffraction lines is indexed using this space group. But as shown in Fig. 21 b substantial discrepancies remain between the observed and the calculated intensity of most lines. In addition, some lines are still not indexed. These diffraction lines, corresponding to those remaining unindexed in Table XII are assigned as supposed by Takeda [11] to the presence of cobalt oxides in both neutron and X-ray diffractograms. It was finally concluded that the presence of cobalt oxides can be explained only assuming that the $Sr_2Co_2O_{5+x}$ phase decomposes during the structural transitions to the low

References page 91

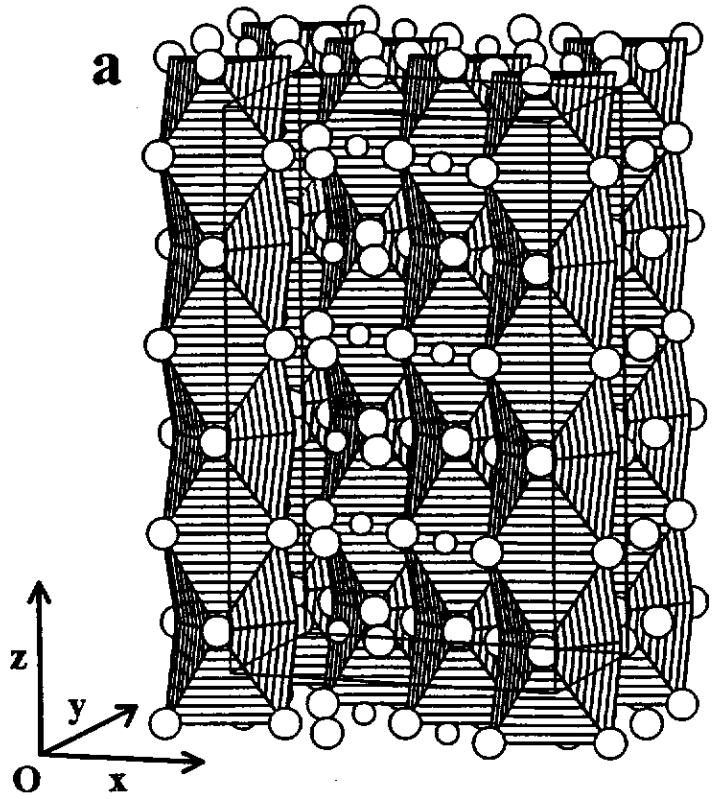

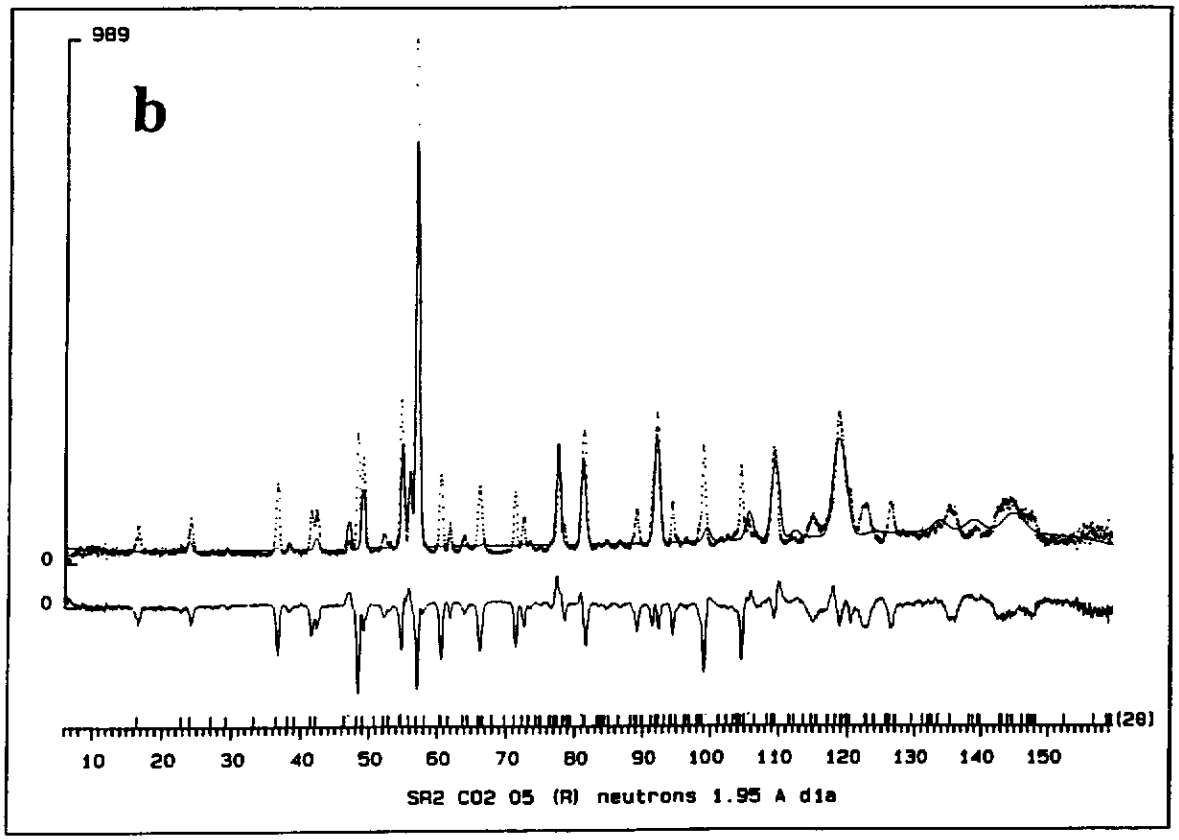

Fig. 21. a) Structure of the hypotetical rhombohedral "$SrCoO_3$" as described with the $R\bar{3}$ space group. b) The observed, calculated and difference profiles for $Sr_2Co_2O_{5.06}$ using this model.

temperature rhombohedral phase, forming a nonstoichiometric oxide with B cation deficiency.

II.2.6.4. The models based on the B site nonstoichiometry.

The perovskite compounds in which B-site vacancies occur are seldom. There are only few examples of such nonstoichiometric oxides such as $Ba_3Re_2O_9$ [32], $Ba_3Ta_2O_9$ [33] or $Ba_3W_2O_9$ [34,35]. These oxides adopt the 2H - type structure with face sharing octahedra, described in terms of hexagonal closest packing of BaO_3 layers with pairs of B ions alternating with vacancies (Fig. 22 a). The B ions (or vacancies) are ordered between columns such that two thirds of all octahedral sites between all layers are filled. This leads to minimize intrachain electrostatic repulsions between highly charged B ions so that local charge balance is reached. A typical example [36] of this type of oxides is shown in Fig 22 a.

Supposing such a model is valid for Co deficient $Sr_2Co_2O_{5+x}$ it is necessary to estimate a number of vacant B sites per chain.

In the h.c. packing the distance between two parallel AO_3 layers of atoms is 242 pm leading to the size of the octahedral holes to be $0.41.r_{O^{2-}} \cong 57$ pm. Supposing the ionic radius of Co^{3+} ion in the low spin configuration in O_h site to be 52.5 pm, the cobalt ion can perfectly fit this octahedral site. Considering the c parameter close to 1250 pm, it follows that obviously only five cobalt atoms can fit along the c-axis.

It well agrees with the observations of Takeda et al. [11] who supposed the composition of $SrCo_{0.9}O_x$ (Sr/Co = 1.12) for this oxide, which is in fact close to the ratio of 6Sr/5Co = 1.2.

The model based on only one sixth of cobalt vacancies for describing the structure of the low temperature compound is shown in Fig 22 b. It corresponds to the hypothetical formulation "$Sr_6Co_5O_{18}$" with the atomic positions (R3 space group) as indicated in the Table XV.

References page 91

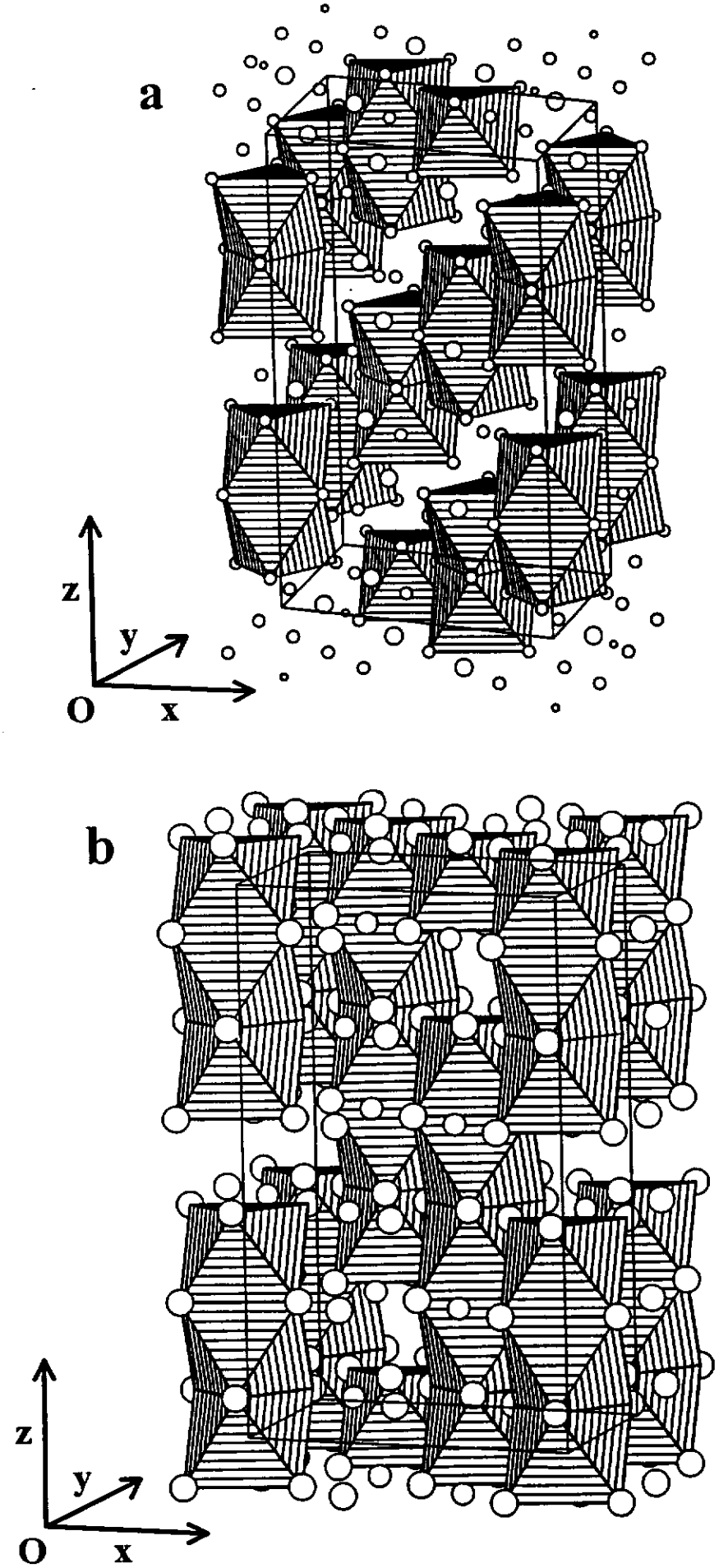

Fig. 22. a) Structure of $Ba_3W_2O_9$ [35], b) Model of the hypothetical "$Sr_6Co_5O_{18}$" structure based on the B - site nonstoichiometry.

Table XV: Atomic positions of $Sr_{18}Co_{15}O_{54}$ in R3 space group.

Atomic positions using R3 space group for $Sr_{18}Co_{15}O_{54}$				
Atom	Wyckoff symb.	x	y	z
Co1	3(a)	0.00	0.00	0.00
Co2.	3(a)	0.00	0.00	1/6
Co3	3(a)	0.00	0.00	-1/6
Co4	3(a)	0.00	0.00	1/3
Co5	3(a)	0.00	0.00	-1/3
Sr1	9(b)	2/3	0.00	-1/12
Sr2	9(b)	-2/3	0.00	1/12
O 1	9(b)	1/6	0.00	-1/12
O 2	9(b)	-1/6	0.00	1/12
O 3	9(b)	1/6	0.00	1/4
O 4	9(b)	-1/6	0.00	-1/4
O 5	9(b)	1/6	0.00	-5/12
O 6	9(b)	-1/6	0.00	5/12

Preliminary refinements assuming a mixture of $Sr_6Co_5O_{18}$ with CoO were not still satisfactory; the Bragg R factor remained rather high (12.3 %) and also the R_p and R_{wp} factors revealed insufficient agreement between the observed and calculated spectra. But the main result clearly shows that all diffraction lines are finally indexed. In addition the z coordinates and especially occupancy factors of the O(5) and O(6) atoms indicate the possible coalescence of those positions into only one with z coordinate of 1/2. Moreover, the values of the occupancy factors for these oxygen atoms are close to 50 %, which leads to a composition close to $Sr_6Co_5O_{15}$ corresponding to that obtained by chemical analysis $Sr_6Co_5O_{14.2}$.

Assuming one missing cobalt atom and one position for O(5) and O(6) positions, a new model can be represented theoretically in the following notation (Table XVI):

References page 91

Table XVI: Model for the $Sr_{18}Co_{15}O_{45-y}$ structure refinement.

Atomic positions using R3 space group for $Sr_6Co_5O_{15-y}$				
Atom	Wyckoff symb.	x	y	z
Co1	3(a)	0.00	0.00	0.00
Co2	3(a)	0.00	0.00	0.20
Co3	3(a)	0.00	0.00	-0.20
Co4	3(a)	0.00	0.00	0.40
Co5	3(a)	0.00	0.00	-0.40
Sr1	9(b)	2/3	0.00	-0.10
Sr2	9(b)	-2/3	0.00	0.10
O 1	9(b)	1/6	0.00	-0.10
O 2	9(b)	-1/6	0.00	0.10
O 3	9(b)	1/6	0.00	0.30
O 4	9(b)	-1/6	0.00	-0.30
O 5	9(b)	-1/6	0.00	0.50

The refinements based on this model (or in its corresponding centrosymmetric group $R\bar{3}$) were finally satisfactory enough. The final differences between the observed and calculated profiles are mainly due to anisotropic broadening of the Bragg peaks due to microstrains. The modelling of which is beyond the scope of this work. The results of this refinement carried out with the neutron diffraction data and the mixture of $Sr_6Co_5O_{15-y}$ with CoO are represented in Table XVII.

Table XVII: Results of the structure refinement using the $Sr_6Co_5O_{15-y}$ R3 space group.

$Sr_{18}Co_{15}O_{45-y}$ (R3)					
No. of fitted parameters:	30				
ATOM PARAMETERS:					
Name	x	y	z	B	occ.
Sr1, 9(b)	0.66636(7)	-0.02148(6)	-0.08037(7)	1.096(8)	1.000
Sr2, 9(b)	-0.66636(7)	0.02148(6)	0.08037(7)	1.096(8)	1.000
Co1, 3(a)	0.00000	0.00000	0.00000	1.498(2)	1.000
Co2, 3(a)	0.00000	0.00000	0.19054(3)	1.498(2)	1.000
Co3, 3(a)	0.00000	0.00000	-0.19054(3)	1.498(2)	1.000
Co4, 3(a)	0.00000	0.00000	0.38483(3)	1.498(2)	1.000
Co5, 3(a)	0.00000)	0.00000	-0.38483(3)	1.498(2)	1.000
O1, 9(b)	0.16179(9)	0.00724(2)	-0.09440(6)	0.230(7)	1.000
O2, 9(b)	-0.16179(9)	-0.00724(2)	0.09440(6)	0.230(7)	1.000
O3, 9(b)	0.15156(9)	-0.00681(1)	0.28599(4)	0.230(7)	1.000
O4, 9(b)	-0.15156(9)	0.00681(1)	-0.28599(4)	0.230(7)	1.000
O5, 9(b)	0.05638(2)	-0.08845(2)	0.50000	0.230(7)	0.680
Cell parameters					
a		c		γ	
942.219(5)		1251.52(8)		120	
RELIABILITY FACTORS:					
Bragg R-factor		Rf-factor			
4.97		3.43			
CoO (Fm3m)					
ATOM PARAMETERS:					
Name	x	y	z	B	occ.
Co	0.00000	0.00000	0.00000	0.520	1.000
O	0.50000	0.50000	0.50000	0.860	1.000
Cell parameters					
a		a		a	
42.5778(6)		42.5778(6)		42.5778(6)	
RELIABILITY FACTORS:					
Bragg R-factor		Rf-factor			
3.43		2.30			
GLOBAL RELIABILITY FACTORS:					
Rp		Rwp		Rexp	
7.83		10.5		4.11	

References page 91

The observed, calculated, and difference profiles are drawn in Fig. 23. Then the interatomic distances are presented in Table XX.

Table XX: Interatomic distances (pm) in $Sr_6Co_5O_{14.04}$ rhombohedral phase.

Co(1) atom		Co(2), Co(3) atoms		Co(4), Co(5) atoms		Sr(1), Sr(2) atoms	
O(1)	190.3	O(2)(1)	191.6	O(3)(4)	191.5	O(1)	261.8
O(1)	190.3	O(2)(1)	191.6	O(3)(4)	191.5	O(1)	267.2
O(1)	190.3	O(2)(1)	191.6	O(3)(4)	191.5	O(2)	252.7
O(2)	190.3	O(3)(4)	188.7	O(5) 2/3	187.0	O(2)	268.5
O(2)	190.3	O(3)(4)	188.7	O(5) 2/3	187.0	O(3)	264.1
O(2)	190.3	O(3)(4)	188.7	O(5) 2/3	187.0	O(3)	269.5
mean	190.3	mean	190.2	mean	189.3	O(4)	246.9
						O(4)	302.9
						O(5)	253.2
						mean	265.2

As it follows from the table the mean distance Co - O is 190 pm which implies the $r_{Co^{3+}}$ = 50 pm. This value agrees well with those given by Shannon et al. [22] for the Co^{3+} with the low spin state configuration in octahedral sites. The same agreement was found for strontium atoms. The mean Sr - O distance is 265.2 pm and therefore the $r_{Sr^{2+}}$ = 125 pm.

This refined structure is also drawn in Fig 24. It can be clearly seen that the sequence $O_hO_hC_{4v}C_{4v}O_hO_h$ (with the translations t(2/3,1/3,1/3) and t(1/3,2/3,2/3)) along the z axis in fact causes the existence of the rhombohedral symmetry for the $Sr_{18}Co_{15}O_{45-y}$ compound. It is also evident that this structure is much denser in comparison to the brownmillerite - type structure. There is also no particular crystallographic direction, especially due to the statistical ordering of vacancies in the O(5) site, in which the "chains" of oxygen vacancies may be formed.

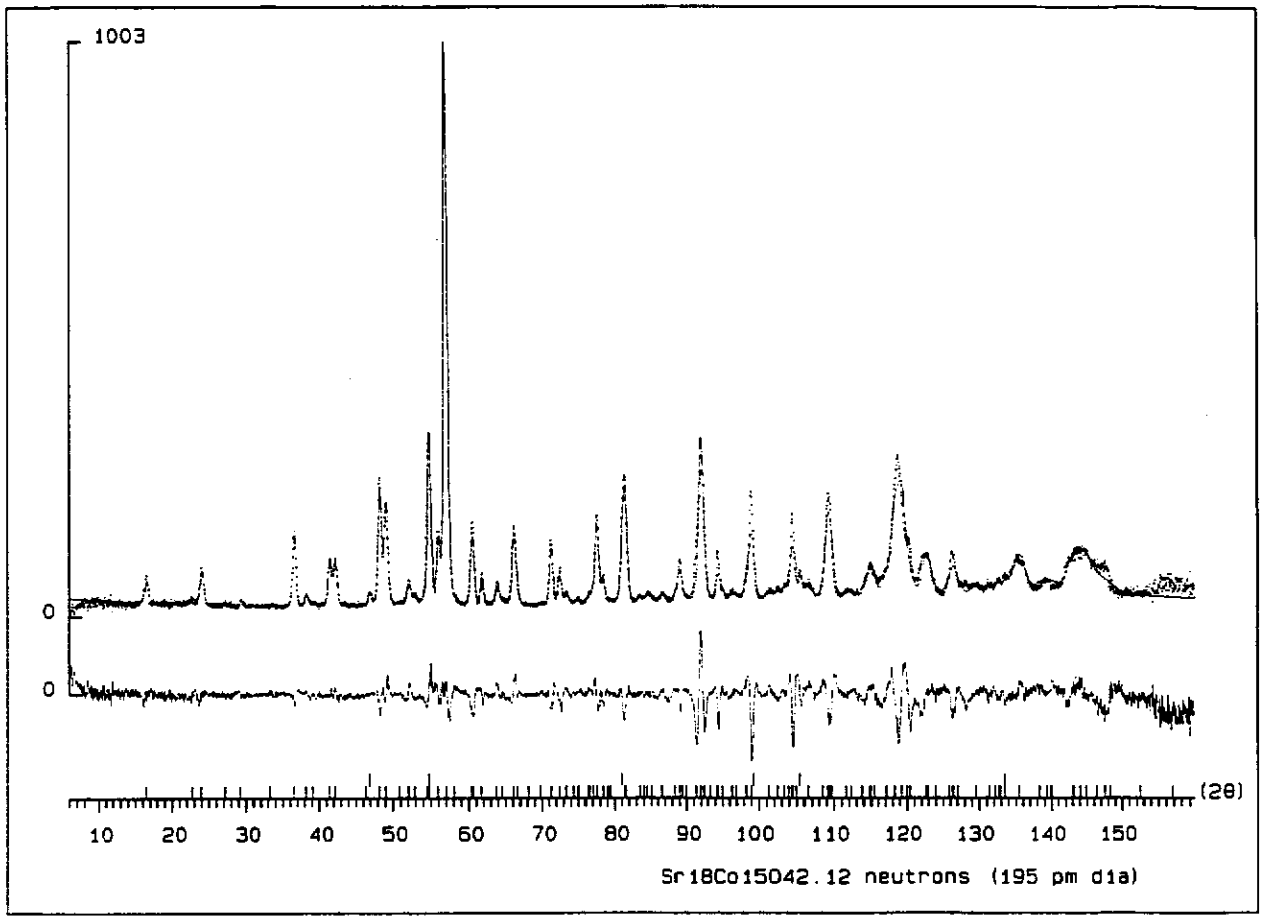

Fig. 23. Observed, calculated and difference profiles for $Sr_6Co_5O_{14.04}$.

References page 91

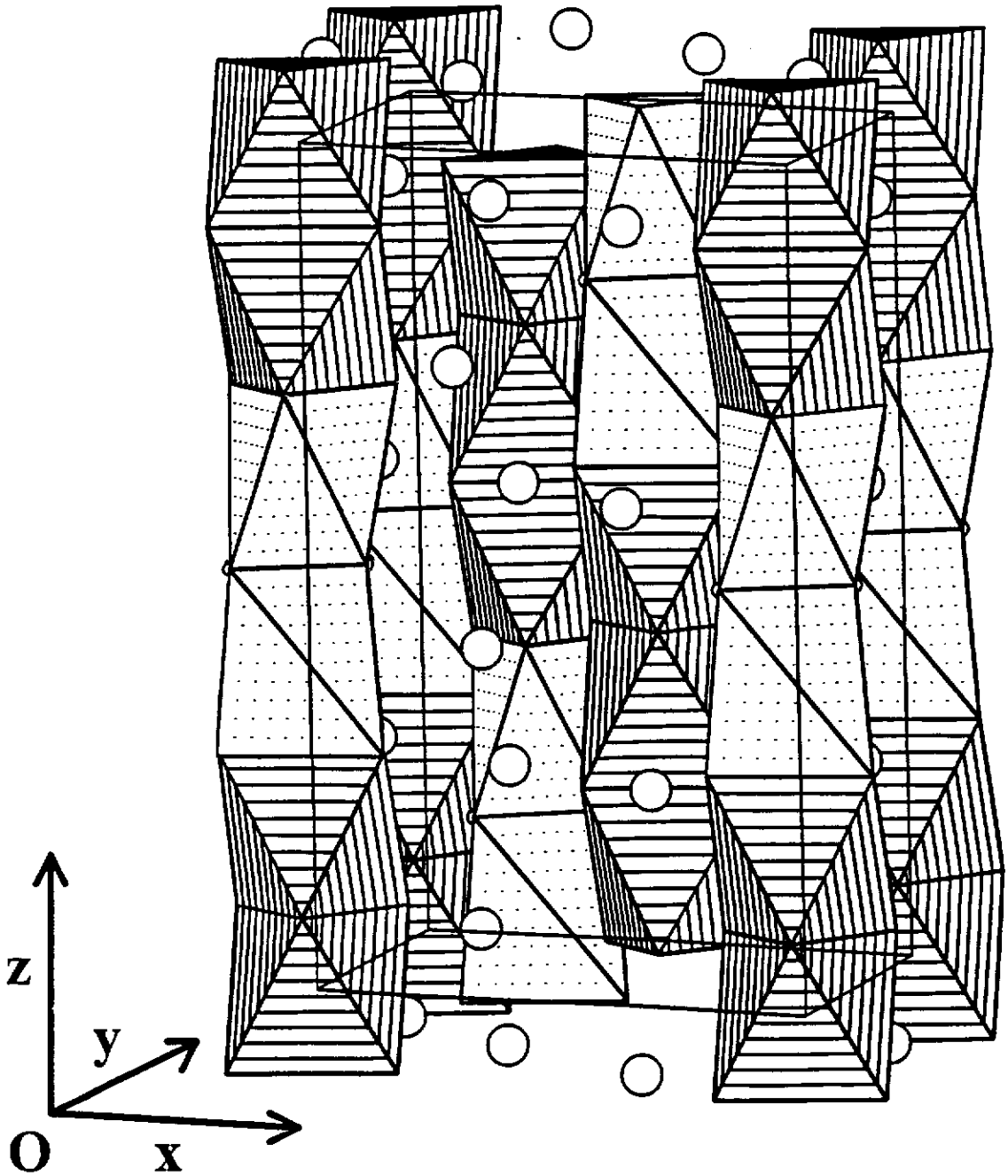

Fig. 24. Refined structure of $Sr_6Co_5O_{14.04}$

II.3. Conclusions

Before studying the electrochemical behavior of the $Sr_2Co_2O_5$, some preliminary conclusions can be drawn.

The brownmillerite - type $Sr_2Co_2O_{5\pm x}$ phase was found to be metastable. It was prepared in air during the quenching in liquid nitrogen from temperatures above 1223 K. The nonstoichiometry amount (x) strongly depends on the quenching temperature. In general the brownmillerite - type phase reveals always some oxygen nonstoichiometry.

The crystal structure of the $Sr_2Co_2O_{4.96}$ brownmillerite - type compound was refined using the Rietveld method. The Icmm space group was finally chosen for description of the structure of this compound.

The results of the HRTEM study confirms the orthorhombic body - centred crystal lattice. The E.D. patterns and subsequent HRTEM images evidence the presence of twins characterising domains having perpendicular b- axes. In addition, the metastability of this phase was "confirmed" by the instability of the material under the electron beam.

The high temperature cubic phase could not be prepared in the pure state, at least in our experimental conditions. Only the mixture of the cubic and brownmillerite - type phases was prepared. This phase was only observed by in situ XRD at temperatures above 1300 K.

The HRTEM revealed the large presence of the brownmillerite - type domains whose size is typically a few nanometers. It is the first time that this microstructure texture was observed for compounds having the brownmillerite - type structure corresponding to $y > 0.50$.

The low temperature $Sr_2Co_2O_{5+x}$ phase, prepared either by slow cooling of the cubic phase or by a heat treatment of the brownmillerite - type phase was studied by means of HRTEM, XRD and neutron diffraction. The E.D. patterns were indexed with the trigonal symmetry, the Bravais lattice being a rhombohedral type.

References page 91

The passage from the initial 2H - type hexagonal unit cell to the multiple R3 one was depicted.

The Rietveld refinements of the neutron diffraction patterns based on this R3 multiple cell were carried out; they demonstrated the existence of a Co substoichiometric compound $Sr_6Co_5O_{15-y}$. The resulting crystal structure determination leads to the interatomic distances fully compatible with the Co atoms with a low spin state configuration.

However, the results are promising, it should be pointed out that the additional work is necessary to elucidate fully this structure.

Moreover, this part of experimental work was carried out simultaneously with the electrochemical experiments. Therefore for convenience in the following chapter (Chapter III, The Electrochemical Oxidation) the notation "$Sr_2Co_2O_5$" will be used for the low temperature phase.

II.4. References Chapter II

1) Watanabe H., J. Phys. Soc. Japan, **12**, 515, 1957.

2) Watanabe H., Takeda T., Proc. Int. Conf. Ferrites, July 1970, p.588, Univ. Park Press, Baltimore 1971.

3) Taguchi H., Shimada M., Koizumi M., Mat. Res. Bull., **15**, 165, 1980.

4) Raccah P.M., Goodenough J.B., J. Appl. Phys., **39**, 1209, 1968

5) Takeda T., Yamaguchi Y., Watanabe H., J. Phys. Soc. Japan, **33**, 970, 1972

6) Rodriguez J., *PhD Thesis, University of Barcelona, 1984*, (unpublished).

7) Grenier J.C., Ghodbane S., Demazeau G., Pouchard M., Hagenmuller P., Mat. Res. Bull. **14**, 831, 1979.

8) Grenier J.C., Fournès L., Pouchard M., Hagenmuller P., Mat. Res. Bull. **21**, 441, 1986.

9) Rodriguez J., Gonzalez-Calbet J.M., Mat. Res. Bull. **21**, 429, 1986.

10) Rodriguez J., Gonzalez-Calbet J.M., Grenier J.C., Pannetier J., Anne M., Solid State Commun., **62**, 231, 1987.

11) Takeda Y., Kanno R., Takada T., Yamamoto O., Z. Anorg. Allg. Chem., **540 / 541**, 259, 1986

12) Shaplygin I.S., Lazarev V.B., Zh. Neorg. Khim., **30**, 3214, 1985

13) Battle P.D., Gibb T.C., Steel A.T., J. Chem. Soc. Dalton Trans., 2359, 1987

14) Zinkevich M.V., Vashchuk V.V., Neorg. Mater., **28**, 816, 1992

15) Watanabe H., Yamaguchi Y., Oda H., Takei H., Proc. ICM, Munchen, 1979

16) Oda H., Yamaguchi Y., Yamaguchi H., Takei H., Watanabe H., Proc ICM, Munchen, 1979

17) Wattiaux A, PhD Thesis, University of Bordeaux I, 1985.

18) Zhou F., private communication.

19) Rodriguez-Carvajal J., Fullprof, version 2.2.1, dec. 1992, private communication

20) Greaves C., Jacobson A.J., Tofield B.C., Fender B.E.F., Acta Cryst., **B31**, 641, 1975

21) Von Harder M., Müller-Buschbaum Hk., Z. Anorg. Allg. Chem., **464**, 169, 1980

22) Shannon R.D., Prewitt C.T., Acta Cryst., **B25**, 925, 1969.

23) Alario-Franco M.A., Henche M.J.R., Regi M.V., Calbet J.M.G., Grenier J.C., Wattiaux A., Hagenmuller P., J. Solid State Chem., **46**, 23, 1983.

24) Alario- Franco M.A., Calbet J.M.G., Regi M.V., Grenier J.C., J. Solid State Chem., **49**, 219, 1983.

25) Parras M., Regi M.V., Calbet J.M.G., Alario-Franco M.A., Grenier J.C., Hagenmuller P., Mat. Res. Bull., **22**, 1413, 1987.

26) Grenier J.C., Ea N., Pouchard M., Hagenmuller P., J. Solid State Chem., **58**, 243, 1985.

27) Rodriguez-Carvajal J., private communication.

28) Hahn T., ed., *International Tables for Crystallography*, Volume A, second edition, Kluwer Academic Press, Dordrecht, 1989, p. 69.

29) Krischner H., Torkar K., Kolbesen B.O., J. Solid State Chem. **3**, 349, 1971

30) Lander J.J., Acta Cryst. **4**, 148, 1951

31) Takeda Y., Kanamaru F., Shimada M., Koizumi M., Acta Cryst. **B32**, 2464, 1976.

32) Calvo C., Ng H. N., Chamberland B.L., Inorg. Chem., **17**, 79, 1978.

33) Jacobson A.J., Scanlon J.C., Poeppelmeier K.R., Longo J.M., Cox D.E., Mat. Res. Bull., **16**, 359, 1981

34) Poeppelmeier K.R., Jacobson A.J., Longo J., Mat. Res. Bull., **15**, 339, 1980.

35) Von Kemmler-Sack S., Treiber U., Z. Anorg. Allg. Chem., **455**, 65, 1979.

Chapter III

Electrochemical oxidation of $Sr_2Co_2O_5$

III.1. A literature overview

The mixed oxides of non - noble metals studied as electrocatalysts for oxygen evolution generally belonged to two main groups, namely spinels [1-3] and perovskites [4-7]. In most works, the studied materials were described as very promising electrocatalysts for oxygen evolution.

Among them, perovskite - type anode catalysts with the composition of $La_{1-x}Sr_xCoO_{3-y}$, and substitutional variants, have been studied more extensively than the other mixed oxides.

Thus Meadowcroft [8] was one of the first who has found good electrocatalytic properties of $La_{1-x}Sr_xCoO_{3-y}$,. Tseung et al. [5] reported reversible behavior of $La_{0.5}Sr_{0.5}CoO_{3-y}$ as an oxygen electrode.

At low current densities in 45 % KOH an overvoltage minimum was found at about $x = 0.75$, while $x \cong 0.15$ produced an overvoltage maximum [9].

Kudo et al. [10,11] obtained the most active material with 20 % of La substituted by alkaline earth element. Moreover, they observed easy reduction of the material, which limits the range of potentials which may be applied. The reduction corresponds the formation of vacancies of oxygen sublattice.

An extensive study of the $La_{1-x}A_xCoO_{3-y}$ (A = Sr, Ba) was done by van Buren et al. [12-14]. By the coulometric method they determined the nonstoichiometry ratio within the range of $0.03 \leq y \leq 0.194$. They determined the diffusion coefficient of oxygen species in the lattice of $La_{0.5}Sr_{0.5}CoO_{3-y}$ at 350 K to be $1.55.10^{-13}$ cm^2s^{-1} by using a three-dimensional equation [13,14]. The value determined at 300 K was of the order of 10^{-15} cm^2s^{-1}, which is in rough accord with the value reported by Kudo et al. for $Nd_{0.5}Sr_{0.5}CoO_3$ ($7.6.10^{-14}$ cm^2s^{-1}) [14].

Kobussen et al. [15-20] investigated the mechanism of the oxygen evolution reaction on $La_{0.5}Ba_{0.5}CoO_{3-y}$ by recording polarization curves and AC impedance

techniques. From the Tafel slope (b = 50 mV) they concluded that the rate determining step is that of the presence of adsorbed intermediates (OH_{ads} or O_{ads}) on the surface of the electrode.

The same authors [20] studied also the passivation processes of $La_{0.5}Ba_{0.5}CoO_{3-y}$ during the oxygen evolution reaction. They concluded that the metastable surface complexes, rich in cobalt, are formed during the electrolysis. The role of these complexes in the oxygen evolution reaction was not clarified.

The "surface metallization" of the ceramic electrode materials was observed at the first time some years ago by Bockris and Otagawa [21], when they studied the electrocatalytic properties of the perovskite oxides.

Wattiaux et al. [22,23] studied the oxygen evolution on ceramic electrodes made of $La_{1-x}Sr_xFe_{1-z}Co_zO_{3-y}$. They observed that the rate determining step is that of the following reaction :

$$OH_{ads} + OH^- \longleftrightarrow O^-_{ads} + H_2O$$

at the small overvoltages. They also confirmed the metallization of the surface of the electrode material, observed previously by Bockris. In fact their conclusion predicted the possibility to oxidize not only the surface, but also the bulk of these materials thanks to side effects during the evolution reaction [23].

Thus the electrochemical oxidation of transition metal oxides has been developed as an alternative processing method for preparing interesting materials such as high T_c superconductors or possible electrocatalysts, in fact in all cases perovskite - related oxides.

Thus using the anodic oxidation in alkaline solutions, the superconducting phases $La_2CuO_{4+\delta}$ (δ = 0.09) [24] and $La_{2-x}Nd_xCuO_{4+\delta}$ (δ = 0.08) [25] have been prepared. The $SrFeO_3$ oxide has been obtained starting from $Sr_2Fe_2O_5$ [26]. XRD

References page 133

and Mössbauer resonance data showed clearly that this electrochemical oxidation is a bulk treatment leading to a fully oxidized material.

Finally the oxygen overstoichiometry in $La_2NiO_{4+\delta}$ was extended up to $\delta = 0.25$ in a similar way [27].

In all mentioned cases these materials have been prepared using constant potential electrolysis.

The synthesis of bulk superconducting $La_2CuO_{4+\delta}$ using the constant potential electrolysis in nonaqueous solutions of 0.0025 M H_2SO_4 in methanol was announced by Bennet et al. [28]. They demonstrated that the oxidation reaction occurs also in nonaqueous medium and the intercalation - deintercalation of oxygen species is reversible.

The constant current anodic polarization was used for preparation of the $La_2CuO_{4+\delta}$ superconductor by Rudolf et al. [29]. Chou et al. [30] studied the reversibility of the oxygen intercalation and deintercalation reaction by means of constant current electrolysis with subsequent open circuit voltage measurements. They concluded that this reaction, controversially to the results of Lagueyte or Bennet, is irreversible.

Up to now no cobalt containing oxide was undergone to the electrochemical oxidation. It was therefore interesting to study the electrochemical oxidation of $Sr_2Co_2O_{5\pm x}$, more especially with regards to the existence of two different allotropic phases. The results of this study are described below.

III.2. Preparation of the starting electrode material

The commonly used method for preparing ceramic electrodes of the starting materials is that previously proposed by Wattiaux et al. [22]. This method gave reliable results in the case of $La_{1-x}Sr_xFe_{1-y}Co_yO_{3-\delta}$ [23], La_2CuO_4 [24], $La_{2-x}Nd_xCuO_4$ [25] or La_2NiO_4 [27], which led us to adopt it.

Powders prepared by nitrate way (cf. § I.3.1.) were used for the preparation of pellets of the starting material. The starting powder was pressed into pellets for 2 min using an uniaxial pressure of 2 MPa (∅ 8 mm, e≅ 2 mm, m ≅ 0.4 g). The pressed pellets were sintered in air at 1473 K for 2 h, then annealed in air at 1223 K for 24 h and finally cooled in argon down to room temperature (cooling rate 10 $K.h^{-1}$) as shown in the scheme of Fig 1.

By such a way, the pellets of the rhombohedral phase were prepared, with the density of 80%. (The density of the ceramic material is given as a percentage of the theoretical density). According to previous observations [22,24], this density seems to be optimal density for electrochemical oxidation of ceramic materials.

The brownmillerite - type $Sr_2Co_2O_{5-x}$ phase was found to be metastable (cf. § I.3.2.): this fact brings a severe complication in the preparation method, the necessity to quench the final sintered material. As it is well known, ceramic materials have a bad thermal conductivity and therefore the pellets should be quenched in liquid nitrogen with a special care from temperatures which should be higher than those for powders.

Therefore the thermal treatment shown in Fig 2 was found to be the most suitable to obtain pellets having the brownmillerite - type structure.

The as - prepared pellets showed indeed the brownmillerite - type structure and revealed a density of about 80 - 85 % Moreover, they exhibited many imperfections which influence in fact the electrochemical process. Among them, the most important are cracks which are caused by thermal strains during the quenching and are of course

References page 133

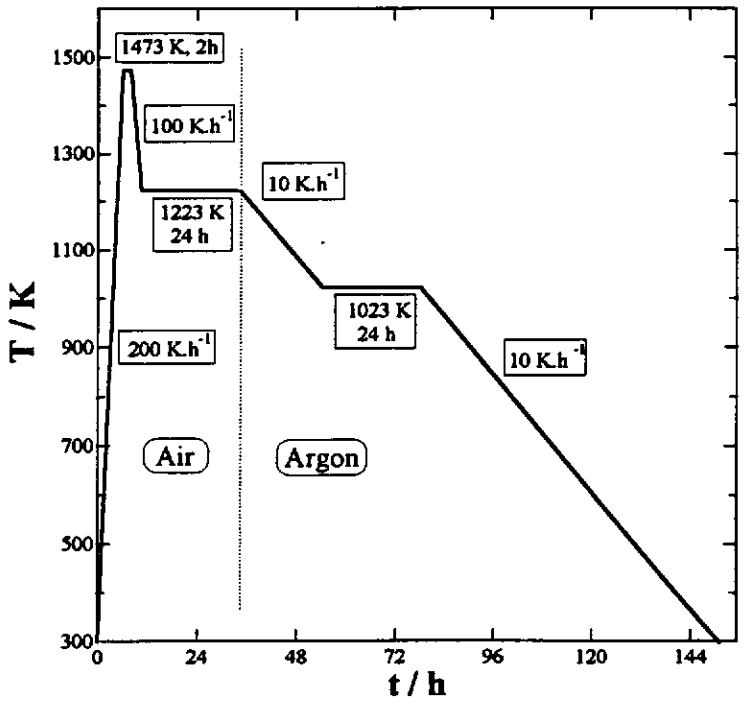

Fig. 1. Heating scheme for preparing the pellets of the rhombohedral phase.

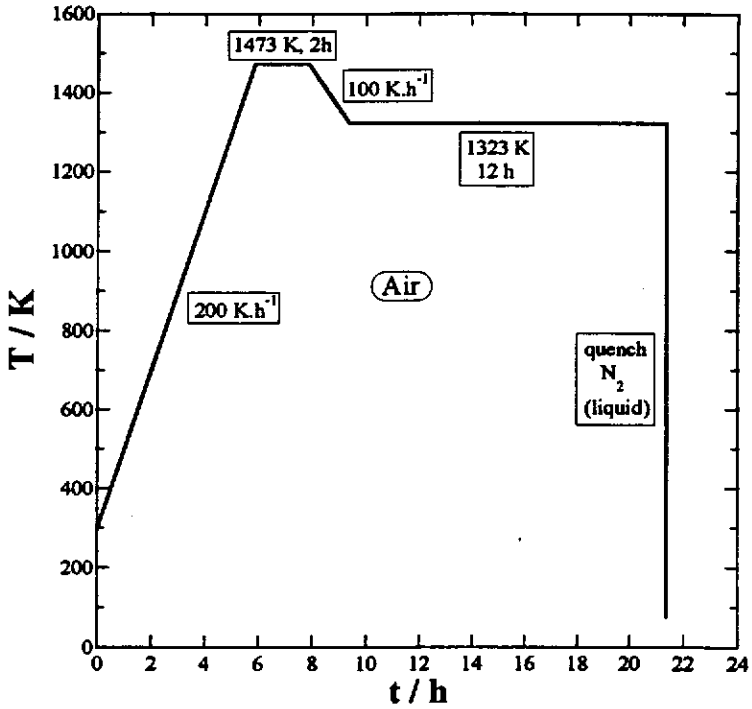

Fig. 2. Heating scheme for preparing the pellets of the brownmillerite - type phase.

impossible to avoid (Fig. 3). These cracks have harmful effects due to drastic increase of the porosity of the ceramic.

III.3. Electrochemical behavior of the brownmillerite - type phase.

III.3.1. The study of the stability of the starting material

The basic condition of electrochemical experiments carried out with electrodes made of ceramic materials is the stability of such an electrode in the used electrolyte. Obviously, it should be studied at first.

Therefore, the initial brownmillerite - type powder was placed into solutions of KOH and NaOH (each hydroxide in concentrations of 6.1 M, 1 M, 0.1 M and 0.01 M), in air. After 1 week the powders were recovered from these solutions, quickly washed with distilled water, alcohol and ether. The XRD patterns were recorded on each sample. In all cases the presence of very small peaks assigned to $SrCO_3$ was detected in this XRD patterns, which can be explained by the chemical corrosion having two different causes according to the $[OH^-]$ concentration. Regarding the domains of stability of cations which form the mentioned oxide (Pourbaix diagrams [31] , Fig 4 a-c), it is evident that at pH less than 14, strontium ions preferably exist as the soluble Sr^{2+} species. They may leave the surface of the oxide and react with CO_3^{2-} ions formed in hydroxide solutions by the dissolution of gaseous CO_2 of the ambient atmosphere. The formed $SrCO_3$ may precipitate back to the surface of the oxide (according to so called dissolution - precipitation mechanism).

When the pH becomes higher than 13, another mechanism of corrosion takes place. In these conditions the cobalt ion exists preferably in the form of the rather soluble $HCoO_2^-$ anion. It means that in this case the material is attacked on Co sites and the Sr^{2+} ions fix CO_3^{2-} ions (as in the previous case) and the presence of $SrCO_3$ can be detected.

References page 133

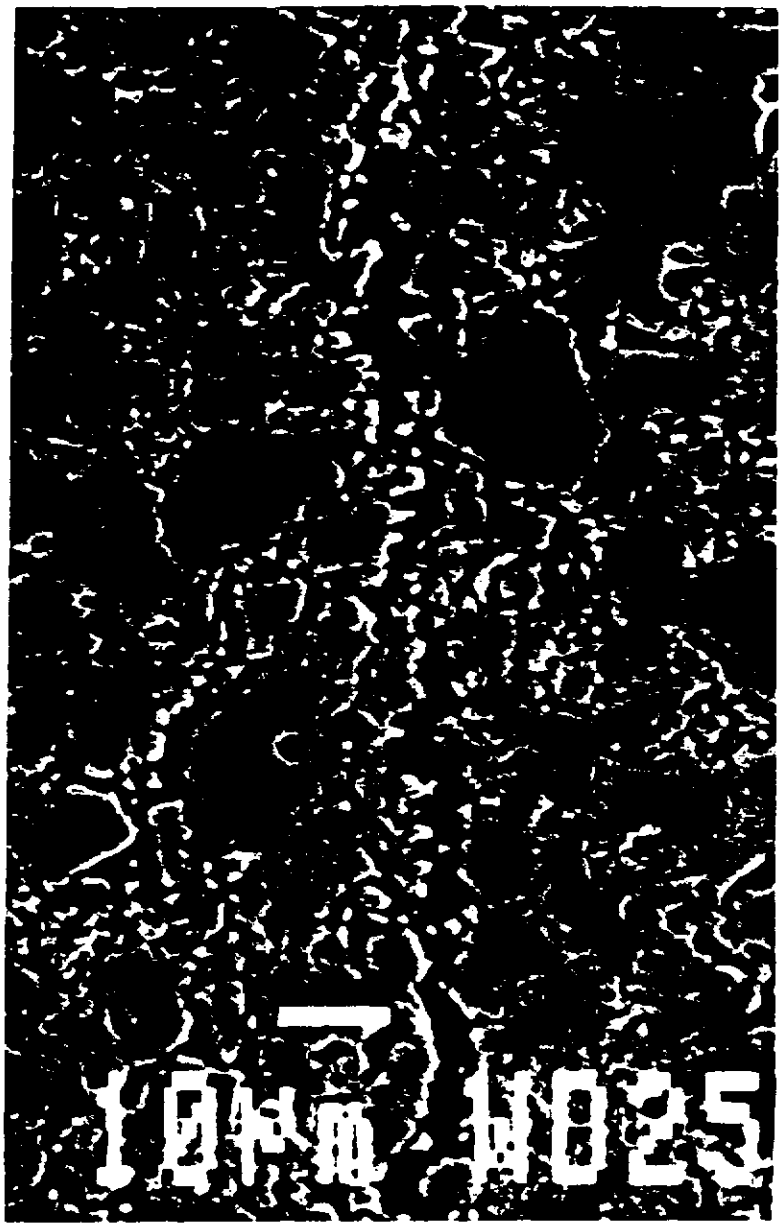

Fig. 3. SEM photograph of the surface of the brownmillerite - type pellet revealing cracks caused by thermal stresses during quenching.

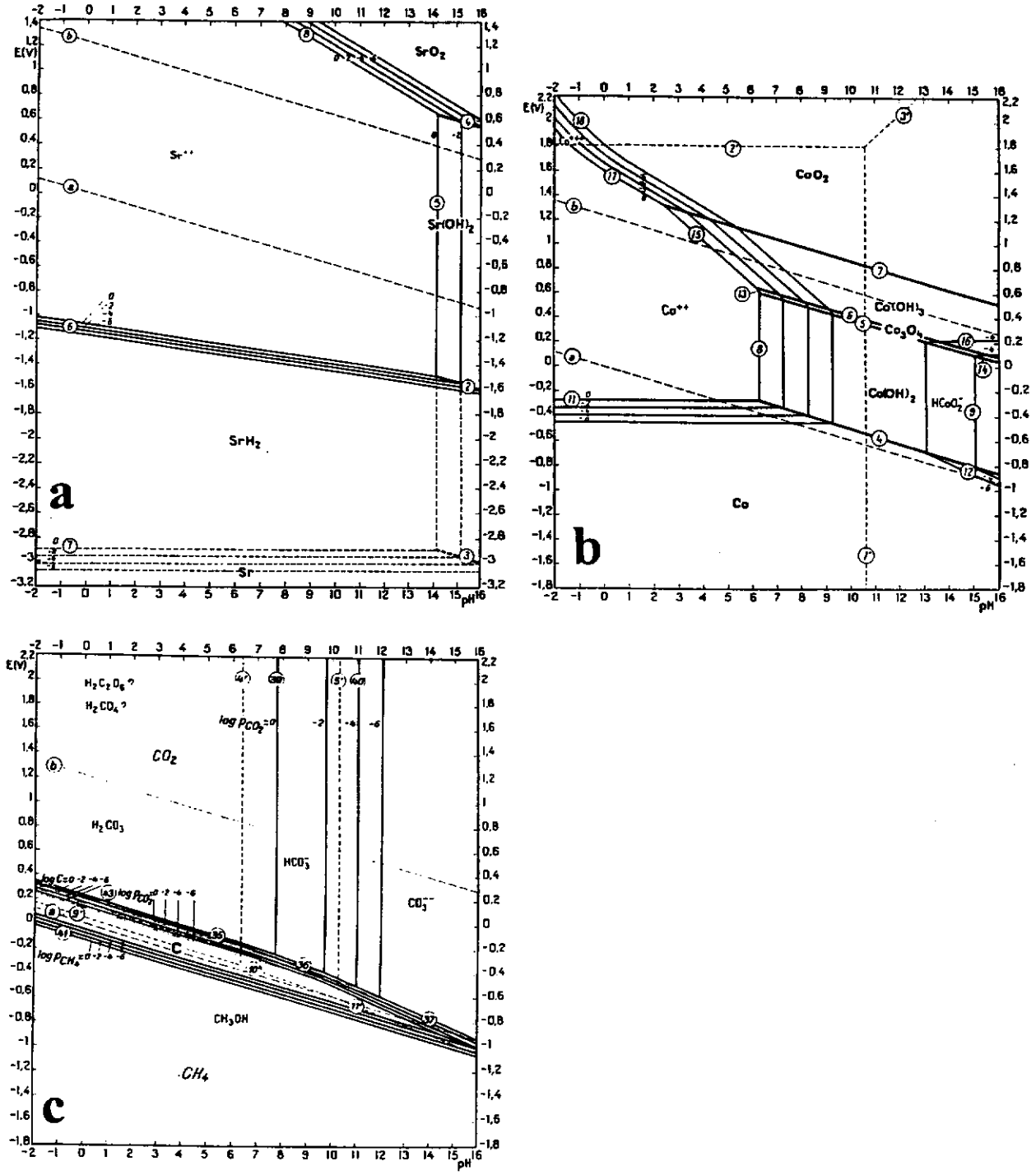

Fig. 4. Predominance area diagram (Pourbaix diagram [31]) for: a) strontium in aqueous solution, b) cobalt in aqueous solution and c) carbon in aqueous solution.

References page 133

It was found that the alkaline metal cation does not influence the corrosion process. Therefore the commonly known fact that NaOH solutions contain usually less of carbonate impurities [32] influenced the choice of NaOH as the electrolyte for the present study.

In all studied cases, the analysis of strontium and cobalt content in hydroxide solutions after the powders had been removed, was performed. We found that the amounts of Sr and Co were close to the detection limits (ICP AES, Co = 3 $ng.ml^{-1}$, Sr = 3.10^{-3} ng.ml) and therefore we can conclude that all corrosion products precipitated back onto the surface of the powders.

In any case the amounts of corrosion products, partially amorphous, represent very small part of the total quantity of studied materials, the intensity of the lines being on the limits of the instrumental resolution ($\cong$ 2-3 wt.%). Therefore they do not influence substantially the studied phenomena on $Sr_2Co_2O_{5\pm x}$ ceramic electrodes as well as the results of chemical analyses of the oxidized materials.

The presence of chemical corrosion of $Sr_2Co_2O_{5\pm x}$ in alkaline solutions corroborates previous observations of Kobussen et al.[20] and Matsumoto et al.[33] who studied the degradation processes of $La_{1-x}Sr_xCoO_3$ electrode material during the anodic polarization. For instance, Kobussen et al. [20] observed the formation of cobalt rich oxide multilayers on the surface of the electrodes after electrolysis. However, they did not fully explained the origin of these layers.

III.3.2. Voltammetric experiments

Several series of voltammetric experiments with electrodes made of the brownmillerite - type $Sr_2Co_2O_5$ material were done to determine all phenomena appearing during the polarization of these electrodes. The measurements were done using rather high scan rates (typically 150 $mV.min^{-1}$) or low scan rates ($\approx$ 1.2 $mV.min^{-1}$).

The figure 5 a shows a typical I-E curve measured on the $Sr_2Co_2O_5$ brownmillerite - type electrode between 0.0 V and 0.80 V (E_{ini} = 0.15 V, v = 0.15 $V.min^{-1}$, T=298 K, p_{O_2}=21 kPa, rotation speed 2000 rpm, in 1M NaOH).

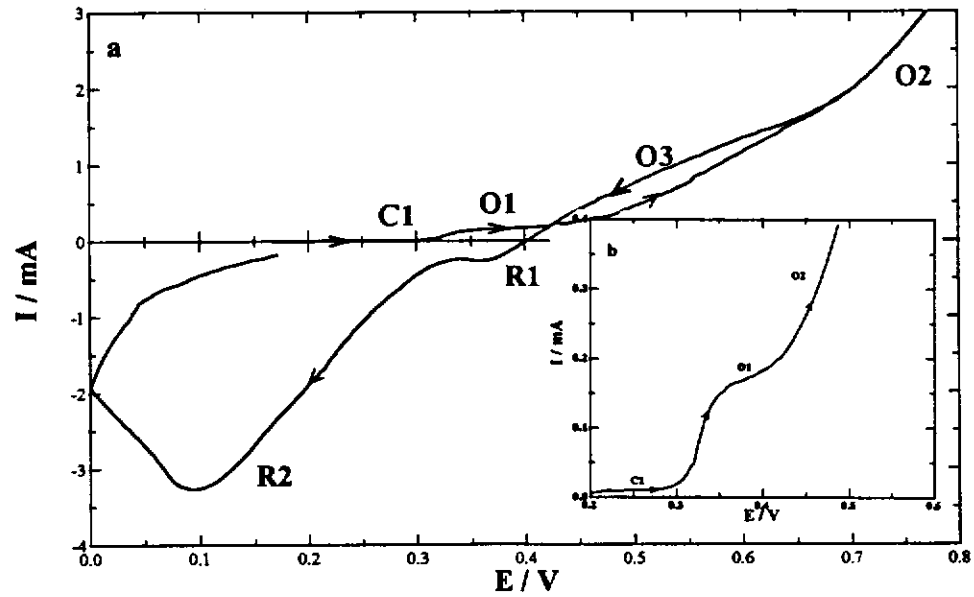

Fig. 5. a) Voltammetric curve of a brownmillerite - type $Sr_2Co_2O_5$ electrode in a 1M NaOH solution (RDE 2000 rpm, sweep rate v=150 $mV.min^{-1}$, T=300 K, air.)
b) Anodic part of this voltammetric curve.

There are three regions in the anodic part of the curve. The current starts to rise linearly immediately after the polarization begins (C_1, E < 0.3 V). This part is assigned to the charging of the double layer on the interface between the electrolyte and the electrode surface following from the works of Bockris et al.[34] or Carapuca et al. [35].

The second - a wave shape part (O_1, E = 0.30 - 0.50 V) with the half - wave potential about $E_{1/2}$ = 0.33 V. This wave can be ascribed to the oxidation of the electrode material according to following reaction:

$$Sr_2Co_2O_5 + 2\,x\,OH^- \Longleftrightarrow Sr_2Co_2O_{5+x} + x\,H_2O + 2\,x\,e^-$$

At potentials higher than 0.50 V, the current increases again and the evolution of gaseous oxygen takes place in the third region (O_2, E > 0.5 V) according to the reaction:

$$4\,OH^- \Longleftrightarrow O_2\,(g) + 2\,H_2O + 4\,e^- \qquad E^\circ_{th} = 303\ mV\ /\ (HgO/Hg,\ 1M)$$

However, comparing the I-E curve measured on $Sr_2Co_2O_5$ with those obtained on other ceramic materials [22-27], this oxidation plateau (O_1) is not well distinguished from the third part (O_2) - the gaseous oxygen evolution (Fig 5 b). It may be explained on the basis of mixed phenomena. The global current of the pseudo - plateau O_1 likely covers the contributions of both electrochemical reactions - the $Co^{3+} \rightarrow Co^{4+}$ oxidation reaction and that of the oxygen evolution reaction which could be considered to be small in this region. .

On the reverse sweep there are also three typical regions. The part marked as O_3, (E = 0.4 - 0.65 V) may be explained by the fact that the material is still oxidized during this part of the reverse sweep. The main characteristic for such a phenomenon is that the current on the reverse sweep is more positive than the current of the forward part. It is due to the decreased resistivity of the electrode material resulting from the prolonged oxidation and subsequent decrease of the oxygen overvoltage.

The peak (R_1, E = 0.35 V) can be attributed to the oxygen reduction step. The last intense peak (R_2) corresponds to the reduction of the electrode material. It has been ascertained by Kudo et al [11] that in this part the opposite reaction of the oxidation reaction takes place.

$$Sr_2Co_2O_{5+x} + x\,H_2O + 2\,x\,e^- \Longleftrightarrow Sr_2Co_2O_5 + 2\,x\,OH^-$$

The decomposition of the perovskite material was observed at more negative potentials in the region where the hydrogen evolution reaction appears (E < -0.80 V).

One can also plot the log I vs. potential for the anodic part of this voltammetric curve (Fig. 6). The Tafel slope for the wave (O_1) determined from this plot is about 30 $mV.dec^{-1}$. Taking into account the mechanism for the oxygen evolution reaction in

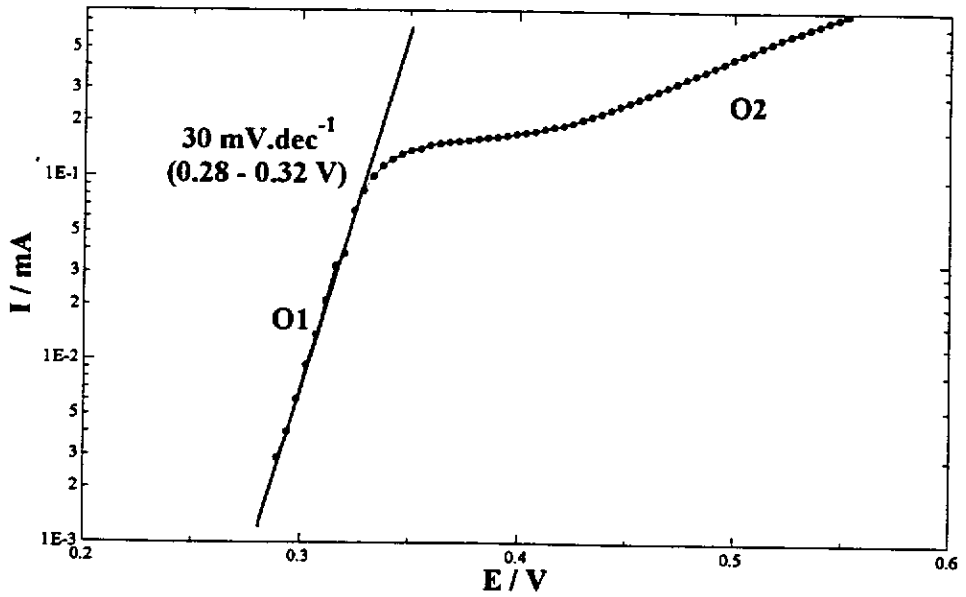

Fig. 6. log I vs. potential plot of the anodic part of the voltammetric curve shown in Fig. 5b.

alkaline media proposed by Wattiaux et al. [22] (Table I), this value implies the fourth reaction to be the rate determining step.

Table I: Mechanism of the oxygen evolution as proposed by Wattiaux [22].

Rate-determining step	$\partial\eta/\partial I$ *	b ($mV.dec^{-1}$)
$M + OH^- \rightarrow M(OH^-)_{ads}$		
$M(OH^-)_{ads} \rightarrow M(OH)_{ads} + e^-$	2RT/F	116
$M(OH)_{ads} + OH^- \rightarrow M(O^-)_{ads} + H_2O$	RT/F	58
$M(O^-)_{ads} \rightarrow M(O)_{ads} + e^-$	2RT/3F	38
$2\,M(O)_{ads} \rightarrow 2\,M + O_2$	RT/4F	14.5

(* $\alpha = 0.5$, charge transfer coefficient)

References page 133

The experiments carried out at low sweep rates , i.e. 1.2 $mV.min^{-1}$, in fact quite near to the steady state, show similar behavior. A typical curve recorded in such conditions is shown in Fig. 7a; it is very similar to the previous one (Fig 5a). The figure 7b shows the IR compensated polarization curve during the anodic sweep, allowing to

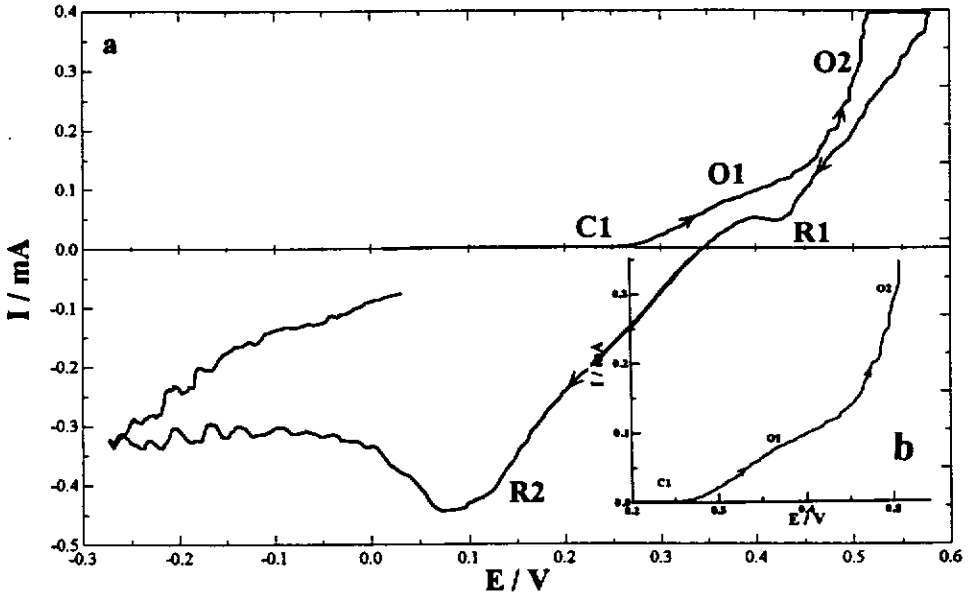

Fig. 7. a) Voltammetric curve of a brownmillerite - type $Sr_2Co_2O_5$ electrode in 1M NaOH solution (RDE 2000 rpm, sweep rate v=1.2 $mV.min^{-1}$, T=300 K, air.)
b) Anodic part of this voltammetric curve.

estimate the apparent oxygen overvoltage in such conditions. The value was estimated to be about 0.15 V. This fact confirms the previous observations of the mixed reaction above 0.45 V during the anodic sweep on the $Sr_2Co_2O_5$ electrode.

The Tafel plot recorded under these conditions is shown in Fig. 8. The value of the slope was found to be 29 $mV.dec^{-1}$. This result well confirms the result found during the faster sweeps and indicates once again the fourth step - the transfer of the second electron - to be the rate determining step.

The dependence of log(I) on E in the region O_2 (after subtracting the current corresponding to the pseudo - plateau O_1 revealed the behavior that did not allow to determine the reaction pathway corresponding to this part of I - E curve.

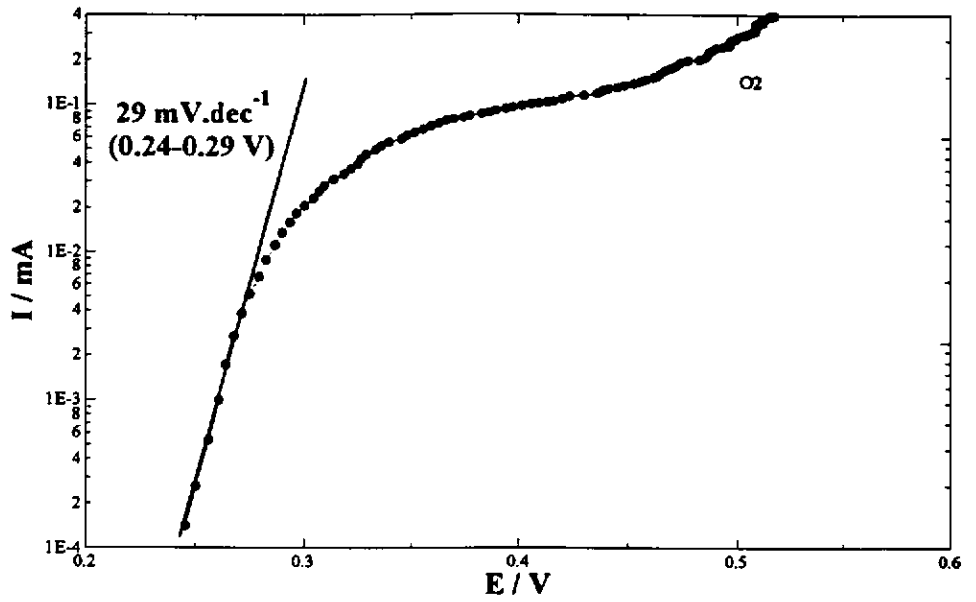

Fig. 8. log I vs. potential plot of the anodic part of the voltammetric curve shown in Fig. 7b.

III.3.3. Determination and optimization of the conditions for the oxidation of the brownmillerite - type $Sr_2Co_2O_5$.

III.3.3.1. Potentiostatic mode.

On the basis of the previous results of studies concerned with the chemical stability of the $Sr_2Co_2O_{5\pm x}$ material and the cyclic voltammetric experiments, referring to the results of previous studies of Lagueyte et al. [24], Arrouy et al. [25] and Park [36] the experimental conditions for oxidizing $Sr_2Co_2O_5$ should be postulated according to the following requirements:

1) The choice of the optimal oxidation potential.

2) The determination of the polarization time required to oxidize completely the total mass of the electrode material.

3) The choice of the proper concentration of the hydroxide solution.

To determine these conditions we have to use some criteria according to which we will follow the progression of the oxidation reaction.

As it was shown previously by Park [36], the variation of the rest potential with the polarization time seems to be a simple and non destructive measure of the rate of the oxidation reaction and therefore may indicate the end of the oxidation reaction.

The coulometric determination of the charge passed through the electrochemical cell, also in fact a non destructive method, assuming 100% current efficiency, provides a relevant information.

The XRD analysis and the chemical analysis of the Co^{4+} content (and consequently of the oxygen content), both destructive methods, after the end of the polarization, may finally validate the results of the rest potential measurements or of the coulometry.

According to these assumptions the study leading to the determination of the suitable conditions for the oxidation of $Sr_2Co_2O_5$ was carried out as follows:

III.3.3.1.1. The choice of the oxidation potential

Lagueyte et al. [24] showed that the oxidation potential should be placed in the limiting part of the oxidation plateau (cf. Fig 5 b O_1). But she also observed, similarly to our measurements, that the mixed electrochemical reaction appears in this region and it is therefore impossible to avoid some contribution of the oxygen evolution reaction.

But as such a contribution appears to be very important in the case of the polarization of $Sr_2Co_2O_5$ electrodes, it implies to determine empirically the polarization potential for the reaction.

Hence the samples of brownmillerite - type $Sr_2Co_2O_5$ were polarized for 100 hours at various potentials in the range from 0.35 V to 0.55 V, keeping constant all other parameters (e.g. polarization time, temperature, rotation speed). The rest

potentials after each polarization reaction were measured for 15 min. They revealed a steady value of 0.485 V when samples were polarized at 0.50 V or above (Fig. 9).

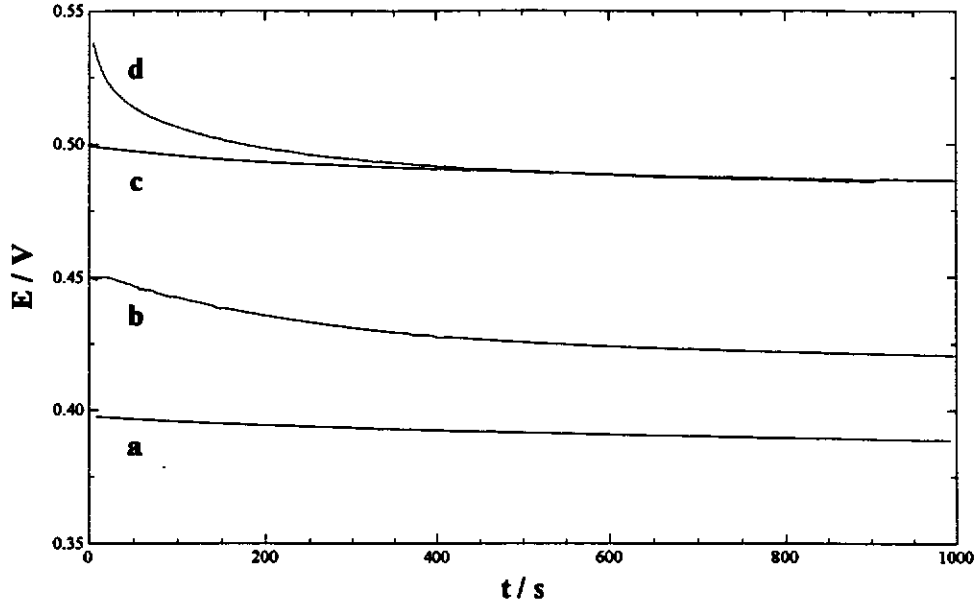

Fig. 9. Time dependence of the rest potential as a function of polarization potential: a) E=0.40 V, b) E= 0.45 V, c) E = 0.50 V and d) E = 0.55 V.

Finally the potential of E = 0.5 V was chosen for the oxidation experiments in order to avoid as much as possible the oxygen evolution.

III.3.3.1.2. Determination of the polarization time:

III.3.3.1.2.1. The evolution of XRD patterns

The measurement of the oxidation reaction rate as a function of the polarization time was achieved in a second series of experiments. The $Sr_2Co_2O_5$ electrodes were polarized at 0.50 V (1M NaOH, RDE 2000 rpm) for various times. Figure 10 shows the change of the XRD patterns recorded at the surface of the electrodes as a function of the polarization time. It is evident that the surface of the electrode material

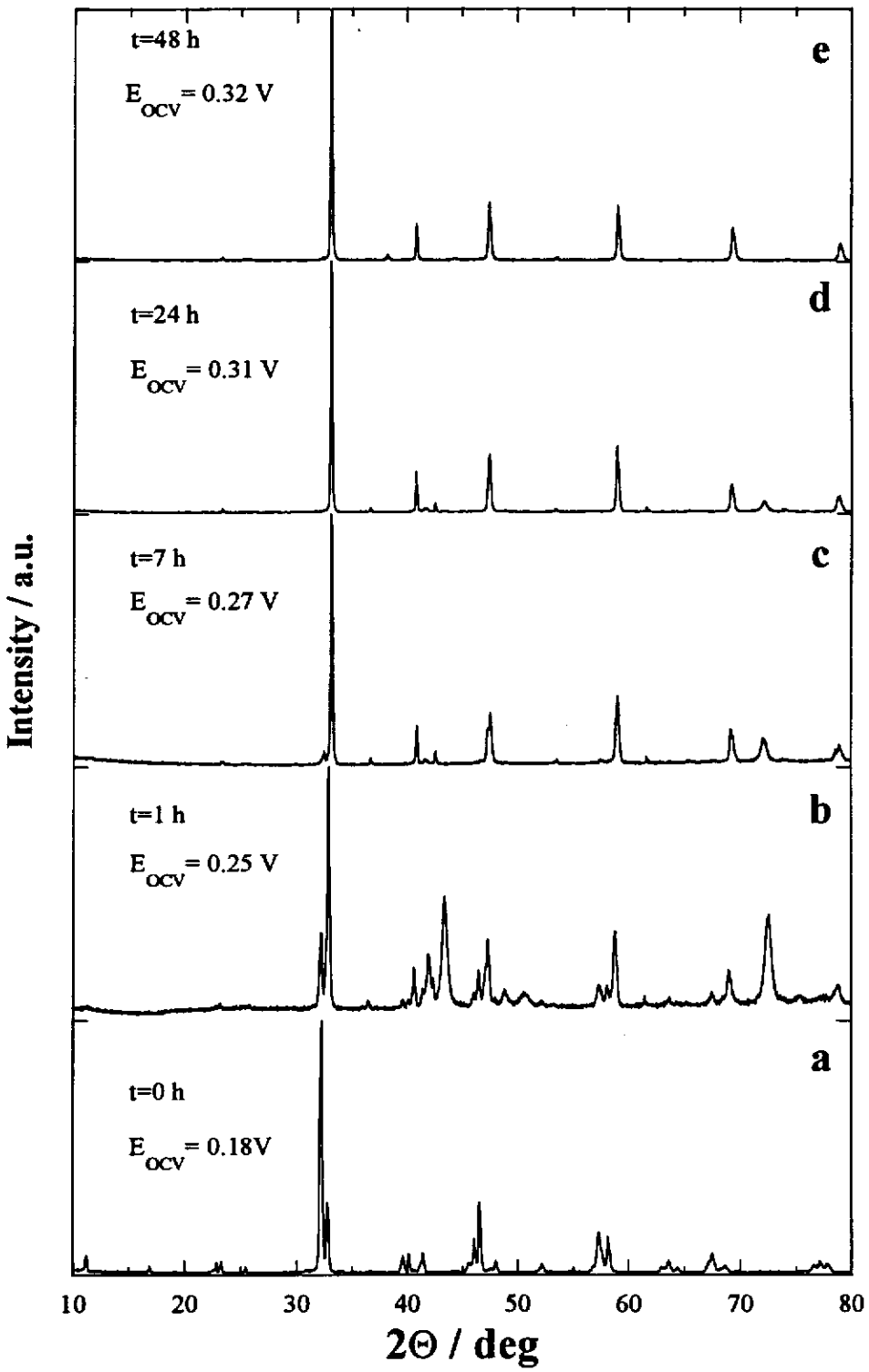

Fig. 10. XRD pattern recorded at the surface of the brownmillerite - type $Sr_2Co_2O_5$ electrodes after various polarization times

undergoes very rapidly significant changes. After 48 hours of polarization, the surface is converted into the cubic perovskite phase.

III.3.3.1.2.2. The rest potential.

A similar variation characterizes the values of the rest potential, measured after each experiment for 15 min. The values of E_{ocv} as a function of the polarization time are plotted in the figure 11 and its time dependence reveals a logarithmic behavior in

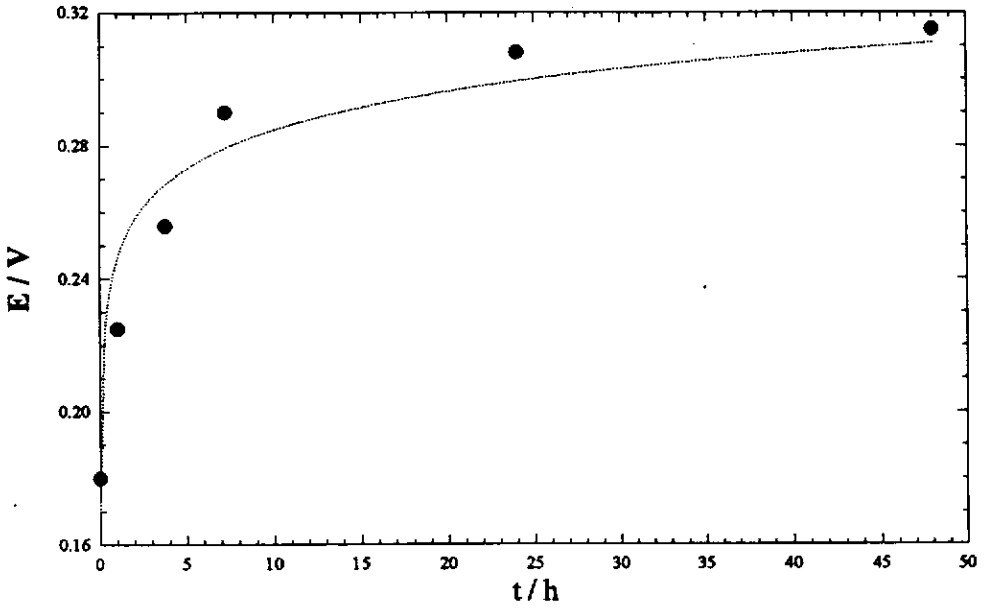

Fig. 11. Time dependence of the rest potential as a function of the polarization time (values of E_{ocv} recorded after 15 min.).

spite of that they were not measured until a thermodynamic equilibrium was reached.

Therefore we carried out another series of experiments dealing with the determination of the rest potential as a function of the composition of $SrCoO_{3-y}$ prepared by different thermal treatment. The rest potential of each sample was measured for 15 minutes and the value at t = 15 min was taken for plot. The resulting dependence of the rest potential on x (degree of nonstoichiometry) is shown in Fig. 12.

In this case the dependence of the rest potential on the composition of the $Sr_2Co_2O_{5\pm x}$ samples reveals also a logarithmic character:

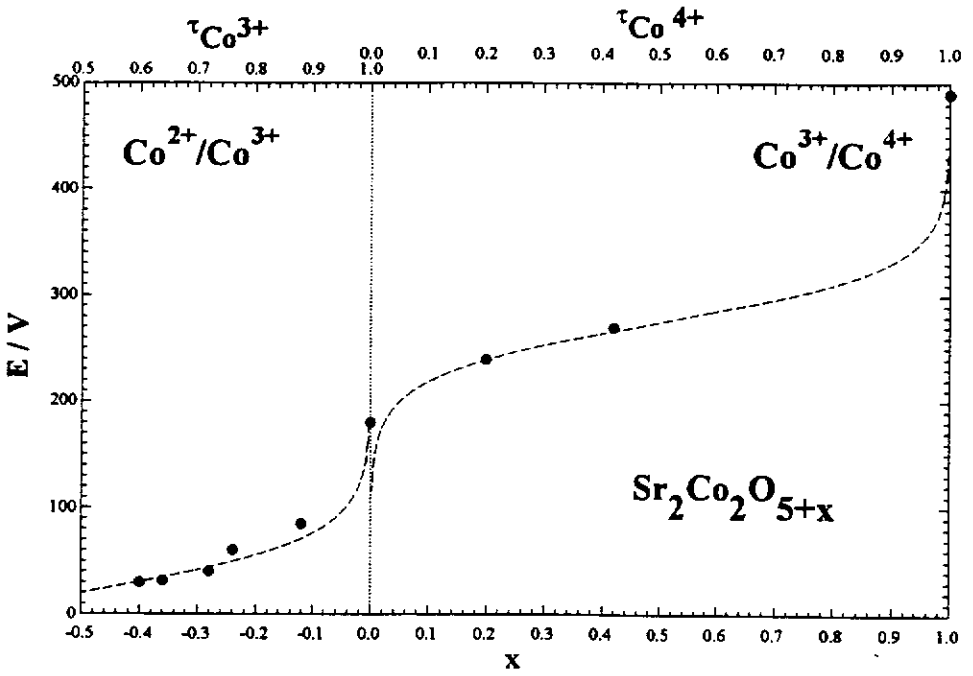

Fig. 12. Dependence of the rest potential on x (amount of nonstoichiometry). (values of E_{ocv} recorded after 15 min.).

$$E_{ocv} = f(x) \propto \log \frac{x}{1-x}$$

It may be explained similarly as in the case of the intercalation of alkaline ions into CoO_2, MnO_2 or other oxides on the basis of the Armand equation (cf. § A2.4.3.4.). But in our case we cannot describe quantitatively our result using this equation (the rest potential does not reflect the thermodynamical equilibrium, the values were recorded at very short relaxation times). But in any case we can estimate that the end of the polarization reaction is reflected by a drastic increase of the rest potential and not by a constant value. It implies that the polarization time should be longer than 48 hours as used in the series of experiments described above.

III.3.3.1.2.3. Determination of the thickness of the oxidation front

After ending the polarization we noticed that the color of the surface of electrodes has changed. The starting material was grey and during the oxidation it became brown. This change initiated the idea to check the progression of the oxidation front. Therefore the cross section of each pellet was polished and the oxidation front was observed with respect to the change in color.

Introducing *l* to be equal to the distance between the surface of the electrode and the boundary of the oxidation front we found that *l* is linearly proportional to the square root of the polarization time (Fig. 13).

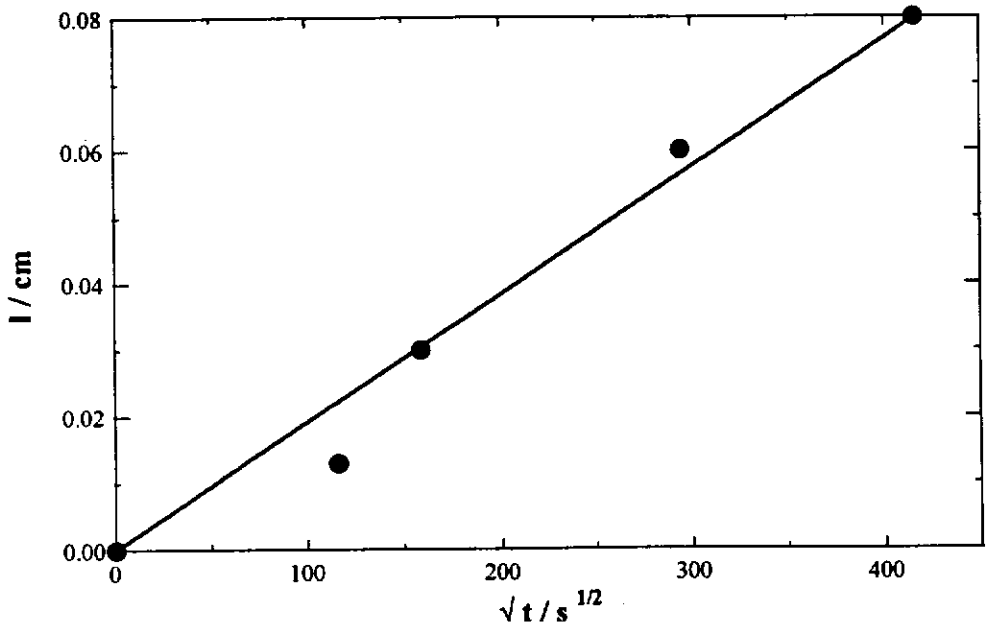

Fig. 13. Dependence of the thickness of the oxidation front on the square root of the polarization time.

It has been found that various rate laws may fit the increase in the thickness *l* of layers formed on the surface of solids as a function of the reaction time at a constant chemical potential of the oxidant. More especially, several authors e.g. Tamman [37], Rickert [38] and Fellner et al. [39] showed that the dependence $l=f(\sqrt{t})$ (so called parabolic law) is expected if diffusion processes leading to the increase of thickness of such layers are rate determining.

References page 133

Using the formulation of Rickert [38]

$$\frac{dl}{dt} = \frac{k}{l}$$

or in the integrated form $l = k'\sqrt{t}$ where $k' = \sqrt{k/2}$ it is possible to estimate the duration of the electrolysis necessary to oxidize the whole bulk of the pellet. For the pellet with the thickness about 1.7 mm (after the polishing procedure) the required polarization time was estimated to be about 180-200 h.

This estimation was finally proved by an experiment carried out in the same conditions (E = 0.5 V, 1 M NaOH, RDE 2000 rpm) for 180 h. The rest potential of 0.485 V and the cubic XRD pattern were found for the final product even after grinding the electrode. Moreover, the chemical analysis of the material revealed a bulk oxidation and a composition corresponding to $SrCoO_3$.

III.3.3.1.2.4. Estimation of the diffusion coefficient

The current I as a function of $1/\sqrt{t}$ for the polarization of $Sr_2Co_2O_{5\pm x}$ at 0.50 V (1 M NaOH , disk electrode, no rotation) is plotted in Fig. 14. According to the Cottrell equation (cf. § A2.3.) the current density is proportional to $1/\sqrt{t}$, i.e. a plot of I versus $1/\sqrt{t}$ may be approximated with a straight line. The slope is proportional to the product of $A.c.\sqrt{D}$, where c represents the concentration of electroactive species, D is the diffusion coefficient and A represents the electroactive surface area, which is defined as $A=r.S_g$. S_g is the geometrical surface area of the electrode and r is the roughness factor. This r factor may vary for perovskite - type ceramic electrodes in the range of (5 - 200) according to the type, preparation and consequently the density of a given oxide [25]. For density close to 80 % its value is close to $r \cong 10$.

The concentration (c) of electroactive species (i.e. oxygen species that diffuse into the $SrCoO_{3-y}$ lattice) can be estimated by the following way [40]. The maximal fraction x which can be inserted, represents for $Sr_2Co_2O_5$ the value x =1. The concentration can be then calculated using the theoretical density of the host material, (0.014 $mol.cm^{-3}$) based on the unit cell parameters, which leads to the maximal concentration c = 0.014 $mol.cm^{-3}$.

Finally the diffusion coefficient D was calculated on the basis of the slope of the dependence I = f(1/√t) (see Fig. 14.). The resulting estimated value of D was

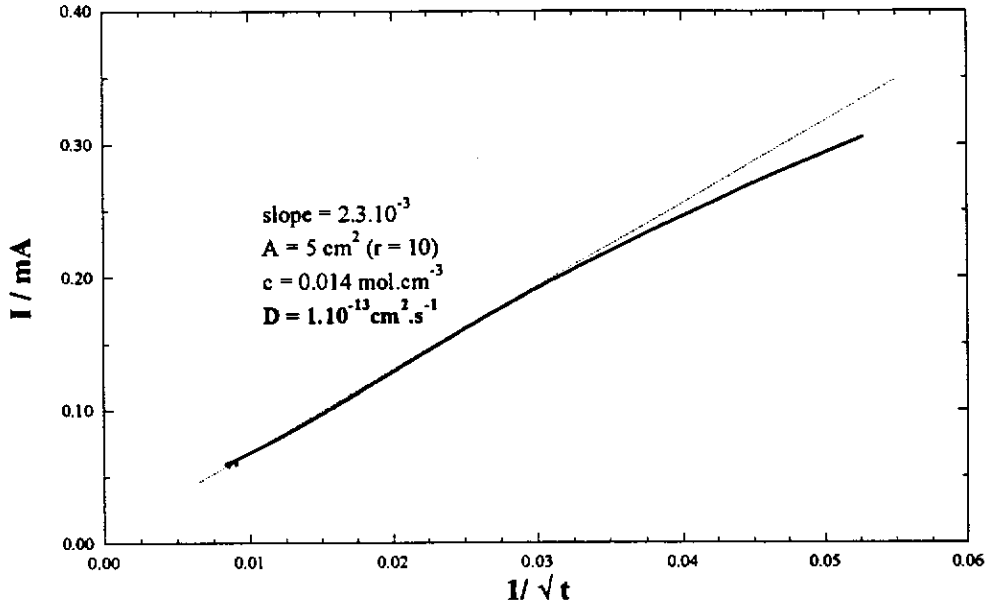

Fig. 14. Current I as a function of square root of the polarization time recorded for $Sr_2Co_2O_5$ at 0.50 V (1M NaOH, disk electrode, no rotation).

$1.\cdot10^{-13} cm^2 s^{-1}$. This value agrees well with those found by Lagueyte et al. [24] and Arrouy et al. [25] for the oxygen intercalation into the La_2CuO_4 and $La_{2-x}Nd_xCuO_4$ oxides respectively.

References page 133

III.3.3.1.3. Influence of pH on the oxidation process: corrosion of the electrode material

As it is usual, the first ex situ characterization after the electrochemical oxidation is the XRD analysis. Figure 15 shows a typical XRD pattern characterizing the cubic perovskite. However, some additional diffraction lines are observed. As expected (cf. § III.3.1.), some of them can be assigned to $SrCO_3$. But there are still some lines they did not correspond neither to $SrCoO_3$ nor $SrCO_3$. They were finally attributed to CoO oxide.

Therefore some additional experiments were carried out for explaining the nature of this corrosion.

III.3.3.1.3.1 Influence of the polarization potential on the stability of the $Sr_2Co_2O_5$ phase

A series of potentiostatic experiments at various potentials, using the RDE electrode and with the constant polarization time of 10 hours were carried out. After each run, the pellet of the studied material was removed from the electrode support and then, its surface was analysed. The concentration of strontium, cobalt and oxygen as a function of the distance from the surface was measured by means of the Auger spectroscopy coupled with the Ar ions sputtering method. Typical results are shown in figures 16 a-d. Fig. 16a shows the concentration profiles of Sr, Co and O in the $Sr_2Co_2O_{5\pm x}$ starting material. The ratio of Sr/Co is equal to 1, which confirms the correct cation stoichiometry of the oxide. The results of each subsequent polarization at potentials of 0.40, 0.55 and 0.70 V respectively are represented in Figs 16 b-d.

The following facts emerged from this series of experiments:

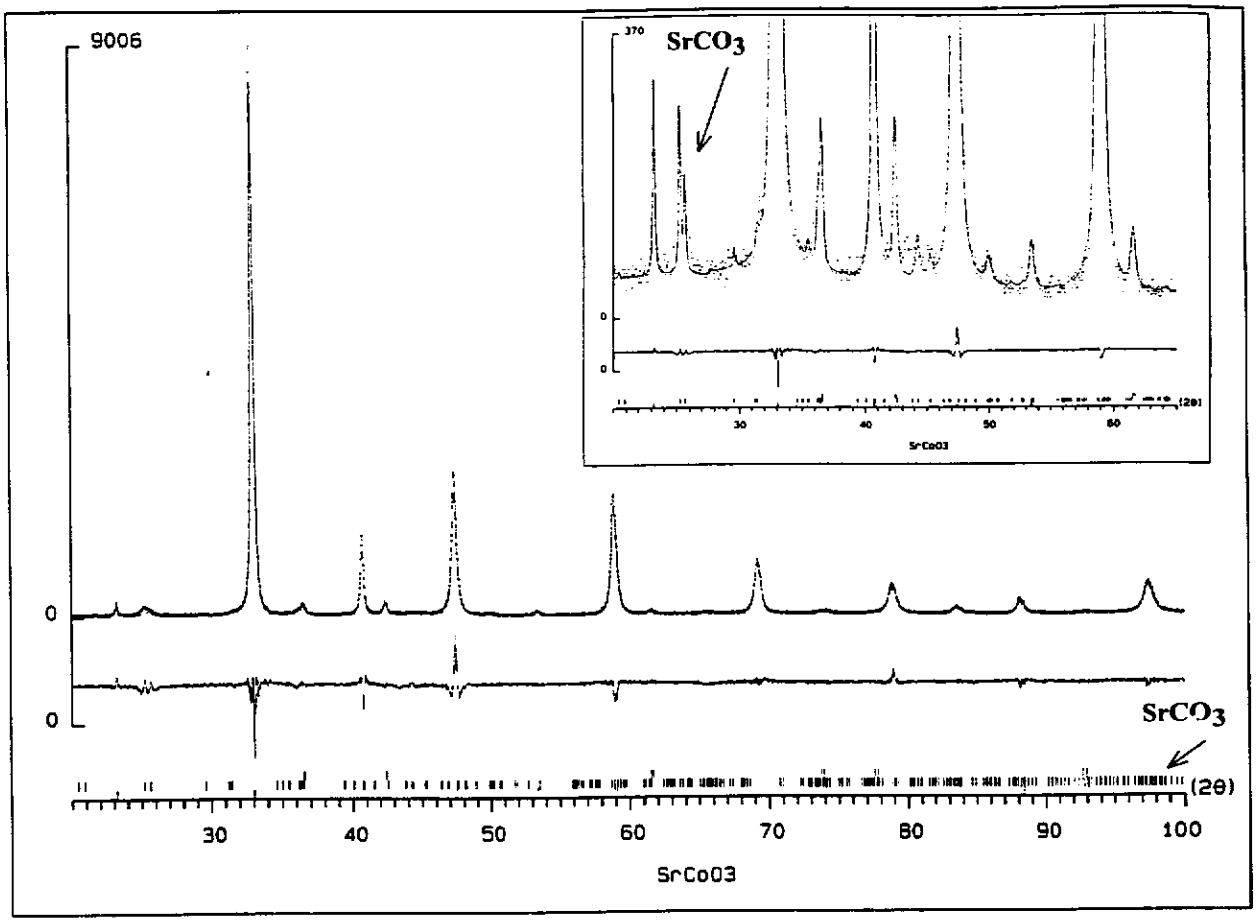

Fig. 15. XRD pattern characterizing cubic $SrCoO_3$ with additional difraction lines of $SrCO_3$ and CoO.

References page 133

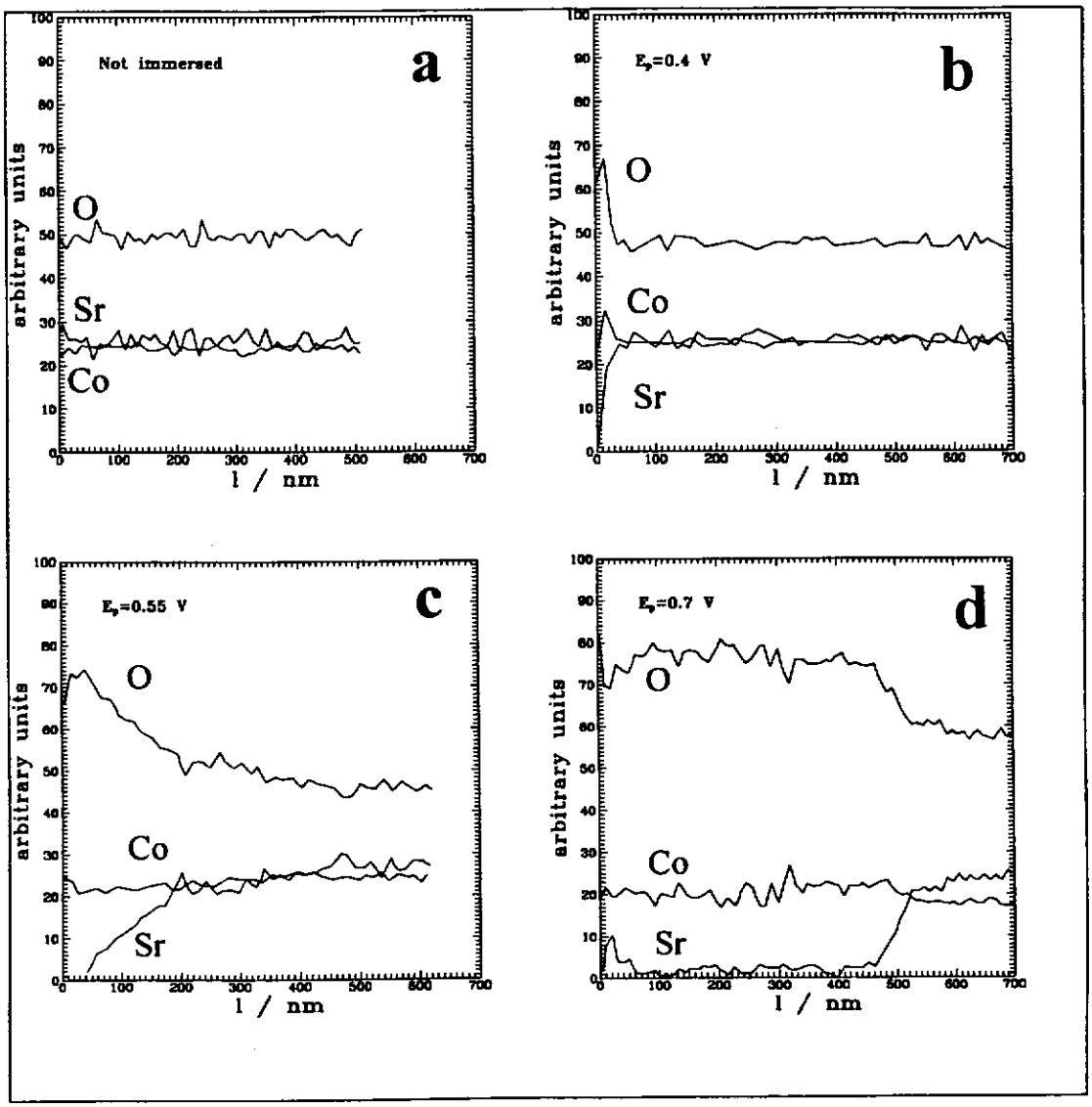

Fig. 16. Concentration profiles of Sr, Co and O in the $Sr_2Co_2O_5$ material as a function of polarization potential (RDE 2000 rpm, t = 10 h.)

- the depletion of Sr on the surface, the slight increase of the Co concentration and the increase of the oxygen concentration were found. This agrees well with observations of Kobussen et al. [20]. They also found the surface depletion of La and Sr when they studied the oxygen evolution on $La_{1-x}Sr_xCoO_{3-y}$ electrodes in 1 M KOH.

- when the electrode is polarized at higher potentials, the attacked region is larger.

III.3.3.1.3.2. Influence of pH on the oxidation reaction

In this series of experiments, four different concentrations of sodium hydroxide were used. The results of the potentiostatic electrolyses carried out at the constant potential of 0.50 V for 160 hours are summarized in Table II.

Table II: The oxidation of $Sr_2Co_2O_5$ as a function of pH.

c [mol.dm^{-3}]	pH	E_{ocv}(*) (before)	E_{ocv}(*) (after)	ΔE_{ocv}	x
6.1	14.9	0.045 V	0.445 V	0.400 V	0.64
1	13.9	0.055 V	0.482 V	0.427 V	0.82
0.1	12.9	0.243 V	0.496 V	0.253 V	0.10
0.01	12.0	0.287 V	0.500 V	0.213 V	0.02

(*) the values taken after 15 minutes of relaxation.

It follows from Table II that the value of the rest potential before the polarization changes drastically with the change of the sodium hydroxide concentration. It can be explained by the change of the stability of the electrode

material in the alkaline solutions especially when pH ≤ 13 or pH ≥ 14 (cf. .§ III.3.1.). The values of the difference between the rest potential before and after the polarization show a maximum for the experiment performed at pH 13.9. It is in a good agreement with the results of the chemical analyses which reveal the same tendency. It can be concluded from these experiments that the concentration of 1M NaOH (pH=13.9) gives the best compromise between the reaction rate and the stability of the electrode material.

III.3.3.1.3.3. Origins of the instability of the electrode material

Based on the previous observations of the surface degradation during the potentiostatic electrolysis on the RDE and the influence of pH on the polarization reaction, the following conclusions concerned with the stability of the electrode material can be drawn:

Referring to the Pourbaix diagrams [31] (cf. § III.3.1., Fig 4 a-c), two different effects may promote or slow down the corrosion processes:

1) When the polarization potential increases cobalt changes its behavior from the corrosion ($HCoO_2^-$ region) into the passivation (Co_3O_4, $Co(OH)_3$, CoO_2 regions). But strontium, when the pH is lower than 14, remains still in the corrosion domain. Anyway, the increase of potential provokes the increase of current and it may give rise to the Sr^{2+} concentration in the electrolyte and therefore the corrosion rate increases following the equation as pointed below:

$$2H_2O + Sr_2Co_2O_5 \xrightarrow{\text{corrosion},OH^-} 2Sr^{2+} + 2CoO + 4OH^- + \frac{1}{2}O_2(\uparrow)$$

$$Sr^{2+} + CO_3^{2-} \longrightarrow SrCO_3$$

2) when pH decreases cobalt shifts again from the corrosion domain to the passivation one (pH ≤ 13, $Co(OH)_2$ region). In comparison with cobalt, strontium corrosion is again sped up at decreasing pH. It means that also in this case the corrosion would be promoted by the attack of strontium atoms on the surface of the electrode material.

At pH ≥ 14 the corrosion attack is mainly caused by the instability of cobalt with the subsequent formation of the soluble $HCoO_2^-$ ion.

$$H_2O + Sr_2Co_2O_5 \xrightarrow{\text{corrosion},OH^-} 2\,HCoO_2^- + 2\,Sr^{2+} + O_2(\uparrow)$$
$$Sr^{2+} + CO_3^{2-} \longrightarrow SrCO_3$$

On the contrary in this region strontium exist preferably in the form of $Sr(OH)_2$ and is therefore passivated.

In addition, the electrode material being a ceramic, its corrosion strongly depends on its porosity. The electrolyte which penetrates within the pores and participates in the electrochemical reaction may change its pH because of the consumption of OH^- ions during the reaction. As the exchange (and therefore the compensation of these changes of pH) of the electrolyte inside and outside the pores is slower than the reaction rate, the corrosion rate increases within the pores, which is microscopically the same effect as the global change of pH previously described.

Moreover, when oxygen is evolved it may partially fill the pores (it is in fact due to the mixed reaction mechanism occurring during the oxidation). In such a case new equilibria are established within the pores (the formation of "gas porous electrodes"): The real electroactive surface is changed. The formation of the gaseous oxygen within the pores increases the ohmic drop in the electrode circuit. Finally all these effects influence the current density and therefore all reactions occurring within the pores are influenced. Additionally the oxygen gas bubbles may also erode the material within the pores.

References page 133

This attack (caused by the porosity of the electrode material) is well represented by the SEM micrograph in Fig. 17. It shows that the grains after

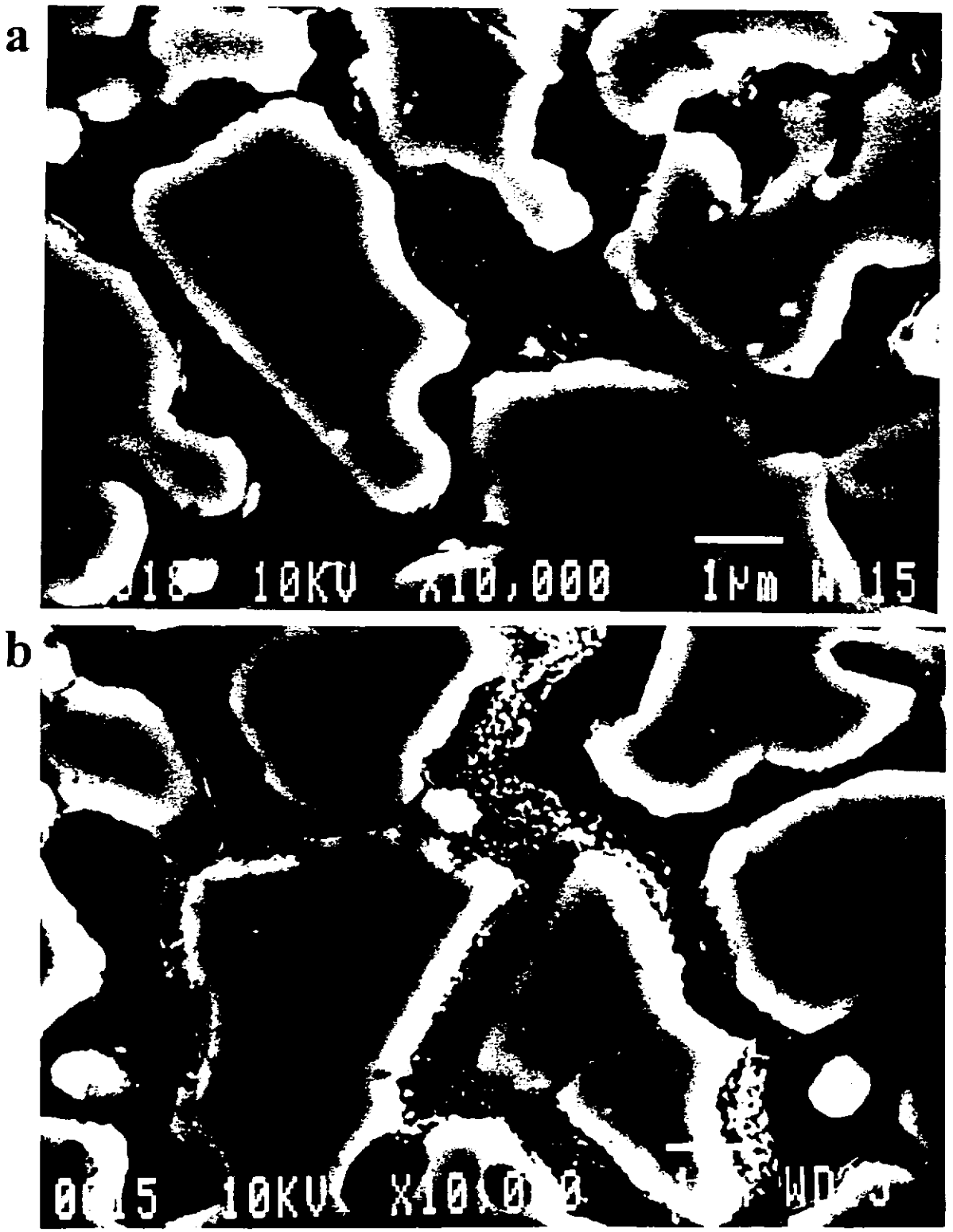

Fig. 17. SEM photographs of grains in the cross section of the brownmillerite - type $Sr_2Co_2O_5$ electrode a) nonoxidized part, b) grains within the oxidation front, revealing effects similar to etching.

polarization at 0.50 V reveal cracks which may be caused by effects of the oxidation reaction and the corrosion reactions. This figure also documents that the corrosion occurs only on the surface of grains (having the effect similar to etching) and does not represent the significant contribution to the studied electrochemical oxidation of $Sr_2Co_2O_5$.

III.3.3.1.4. The conditions for preparing $SrCoO_3$ in potentiostatic mode

Finally, regarding all results of different series of experiments in potentiostatic mode, the best conditions for the preparation of $SrCoO_3$ material are those reported in Table III.

Table III: The conditions for preparing $SrCoO_{3.00}$ in potentiostatic mode.

Working electrode	B - type $Sr_2Co_2O_5$ ceramic
Relative density	80 - 85 %
Weight	about 300 mg
Final polishing	alumina 20 nm
Rotation speed	2000 rpm
Electrolyte	1M NaOH (1M KOH)
Atmosphere	air
Temperature	300 K
Oxidation potential	500 mV (vs. HgO/Hg 1M OH^- ref. electrode)
Polarization time	180 h

III.3.3.2. Galvanostatic mode.

The possibility to use the galvanostatic method for the preparation of high oxidation states in the transition metal oxides was firstly reported by Rudolph et al. [29] for preparing the $La_2CuO_{4+\delta}$ (δ up to 0.07). They supposed that this method can allow to study all reaction pathway between the starting and the final material and to investigate the reversibility of the process.

We considered to be very interesting to perform the same study on the $Sr_2Co_2O_5$. The results of a series of experiments in which we studied the influence of the magnitude of polarization current, keeping all other parameters unchanged in regards to those of potentiostatic experiments, are presented below.

All experiments were carried out in 1 M NaOH electrolyte using a RDE with the rotation speed of 2000 rpm. The polarization currents were chosen on the basis of the voltammetric curves (cf. Fig 5 b). The following currents were selected:

- 250 μA - the current corresponding approximately to the limit between the wave O_1 and the gaseous oxygen evolution domain O_2,
- 100 μA corresponding to the limiting current of the oxidation plateau (Fig 5 b, part O_1),
- 40 μA - slightly less than the half wave current for the same plateau.

The results of the galvanostatic experiments, carried out in conditions as described above, are plotted in the Figure 18. The time dependence of the potential was converted into the potential as a function of the degree of nonstoichiometry (x) on the basis of the Faraday law considering the 100% current efficiency before the onset of the oxygen evolution (part V). It may be expressed by the following relation:

$$x = \frac{M \cdot I \cdot t}{2 \cdot F \cdot m}$$

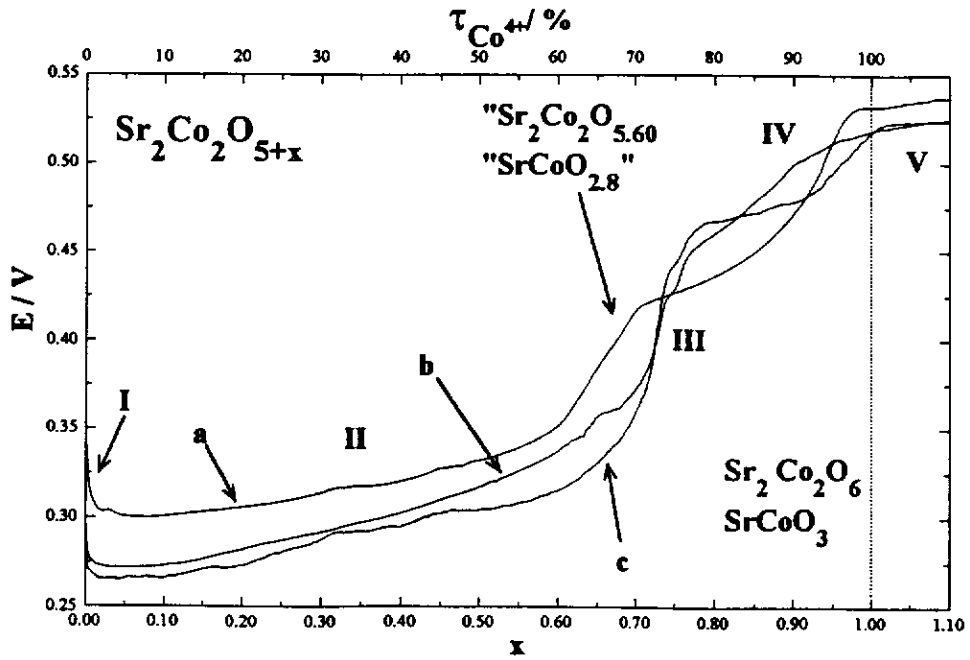

Fig. 18. Potential as a function of the amount of oxygen overstoichiometry x (i.e. $\tau_{Co^{4+}}$) during the constant current electrolysis of the brownmillerite - type $Sr_2Co_2O_5$ electrode using a) 250μA, b) 100μA and c) 40μA.

where M is the molar weight of $Sr_2Co_2O_5$, m is the mass of the sample, I is the polarization current, t is the polarization time and F is the Faraday constant.

The validity of this relation was supported by the results of the chemical analyses revealing values of the oxidation state of cobalt within the range 96 to 100 % of Co^{4+}. Finally it implies that the oxidation current $I_{ox} >> I_{O_2}$ at least within the studied range of current (40 μA ≤ I ≤ 250 μA).

Moreover, the curves show several interesting features.

The part I appearing immediately after each polarization began reveals an inverse tendency of the variation of the potential with the oxidation state. It is probably due to interfacial phenomena in the very beginning stage of the polarization (the double layer charging, the penetration of the electrolyte into the pores, the corrosion reaction).

The part II corresponds to the typical change of potential in the region without the existence of a well defined composition.

References page 133

It is not clear to which composition the first wave (part III) could correspond. It is probably due to the existence of a phase with a composition around "$Sr_2Co_2O_{5.60}$" but additional investigations are necessary.

The stoichiometry of $SrCoO_3$ is surprisingly reached at the end of the second wave (part IV, Fig. 18). It follows from the theory of the constant current electrolysis that the presence of a defined compound changes drastically the potential, in other words, that the halfwave potential should correspond to a defined compound. In the case of $SrCoO_3$ the difference could be explained by the fact that the contribution of the oxygen evolution reaction appears, in galvanostatic conditions, when the electrode material is almost saturated by oxygen.

At this moment (part V, Fig. 18) the gaseous oxygen evolution becomes the predominant reaction and the potential stabilizes at a quite constant value. The slope of the wave occurring on the E = f(x) curve just before this stabilization differs significantly from the theoretical one. It may be explained in terms of non - steady state effects i.e. that system is still far from the equilibrium conditions and a homogenization of grains needs some additional time which causes difference.

III.3.3.3. Comparison between the potentiostatic and galvanostatic modes

Based on the results of the previous series of potentiostatic and galvanostatic experiments, the following comparison of both potentiostatic and galvanostatic modes of the anodic oxidation of $Sr_2Co_2O_{5\pm x}$ can be done in the following summary:

Potentiostatic mode (E_{ox} = const., $I = f(t)$):

- better reproducibility, the oxidation potential is independent of the relative density of the electrode material.

- the oxidation potential should be placed between E_{OCV} of the starting material and E_{O_2}, which may be followed by problems with the mixed electrochemical reaction. Frequently it is quite impossible to distinguish between the oxidation and oxygen evolution reactions on the basis of the shape of the oxidation plateau.

- in such a case the oxidation potential should be determined empirically, for given density (c% = const). and given polarization time (t = const).

- generally the potentiostatic oxidation kinetics is rather fast. It allows to prepare the oxidized materials within some days.

- in combination with the fixed electrode, it allows to oxidize rather important quantities of the electrode material (0.4 g ≤ m ≤ 10 g, 8 mm ≤ ∅ ≤ 32 mm)

- The problem of inhomogeneous composition of the studied materials after the oxidation reaction may occur. The inhomogeneities in the oxygen stoichiometry may be caused by the relatively high reaction rate either on the intergranular or intragranular level. This is the reason why the end of the reaction should be carefully checked.

Galvanostatic mode (I_{ox} = const., $E = f(t)$):

- it is more difficult to attain the reproducibility of the galvanostatic experiments

- it requires relatively well defined ceramics or at least a larger series of pellets prepared at identical conditions, to have a possibility to compare the results of different series of experiments.

- the RDE is required in preference to keep constant the electroactive surface and the hydrodynamic conditions in the electrochemical cell.

- the use of the RDE determines the quantity of the studied material to be about 0.4 g (∅ = 8 mm).

-the use of small polarization currents requires large polarization times.

References page 133

- but it insures a relatively well homogeneous samples because of comparable rates of the generation of the electroactive species and their diffusion inwards the bulk of the electrode.

III.4. Electrochemical behavior of the rhombohedral $Sr_2Co_2O_5$ phase

III.4.1. Voltammetric experiments

On the contrary the voltammetric curves measured on the $Sr_2Co_2O_5$ rhombohedral material reveal a different behavior (Fig 19) than that of the

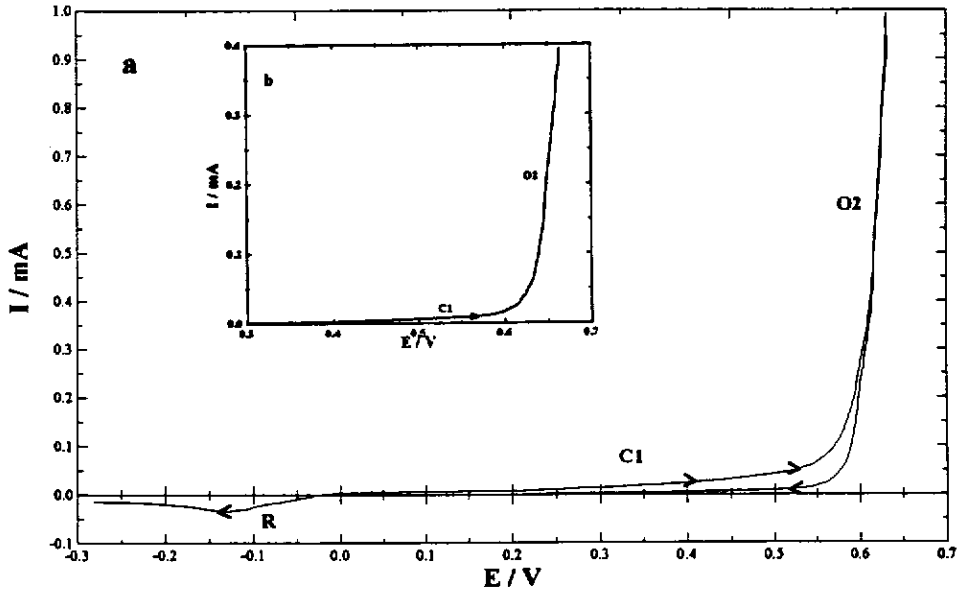

Fig.19. a) Voltammetric curve of a rhombohedral $Sr_2Co_2O_5$ electrode in 1M NaOH solution (RDE 2000 rpm, sweep rate v=150 mV.min^{-1}, T=300 K, air.)
b) Anodic part of this voltammetric curve.

brownmillerite - type electrode (c.f. Fig 5). There are only two phenomena appearing in the anodic part of the voltammetric curve. The current starts to increase linearly in the domain C_1 - it corresponds similarly to the previous cases to the charging of the double layer. The wave (O_1) which appeared on the brownmillerite - type electrode material, corresponding to the oxidation reaction of the electrode, is absent. and the

gaseous oxygen evolution reaction (part O_2) takes only place when the electrode is polarized above 0.55 V. As shown in Fig 20, the Tafel slope in the region of the

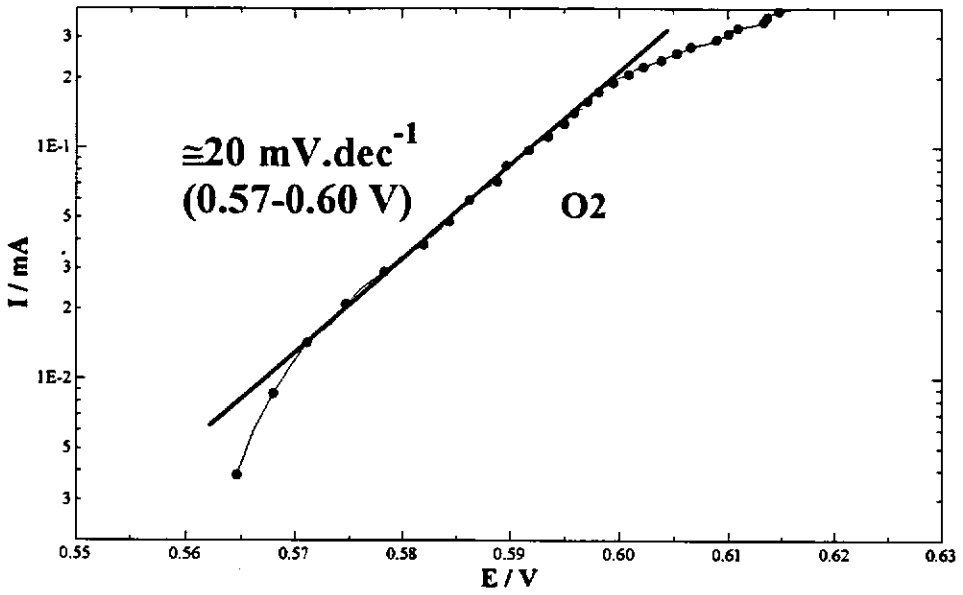

Fig.20. log I vs. potential plot of the anodic part of the voltammetric curve presented in Fig. 19 b.

reaction O_2 is about 20 $mVdec^{-1}$. This clearly confirms that the gaseous oxygen is generated according to the fifth reaction of the mechanism proposed by Wattiaux [22] (Table I). On the cathodic sweep only a small peak is observed.

The fact that the wave O_1 is absent may indicate the impossibility to oxidize the mentioned material.

III.4.2. The potentiostatic electrolyses of $Sr_2Co_2O_5$ rhombohedral electrode material.

In the absence of the plateau O_1, it was impossible to carry out similar studies to those of the brownmillerite - type phase for determination of the experimental conditions of the anodic oxidation of the rhombohedral phase. Therefore the same conditions as for the brownmillerite - type phase were used for the oxidation of rhombohedral $Sr_2Co_2O_{5\pm x}$.

References page 133

The results of the chemical analyses revealed that, as expected, the rhombohedral $Sr_2Co_2O_{5\pm x}$ phase does not undergo the oxidation.

III. 5. References

1) Tarasevich M.R., Efremov B.N., in: *Electrodes of Conductive Metallic Oxides*, (Trasatti S., ed.), Part A, 221, Elsevier, Amsterdam, 1980.

2) Trasatti S., Lodi G., in: *Electrodes of Conductive Metallic Oxides*, (Trasatti S., ed.), Part B, 521, Elsevier, Amsterdam, 1980.

3) Tarasevich M.R., Efremov B.N., Elektrokhimiya **17**, 1672, 1981.

4) Tamura H., Yoneyama, Matsumoto Y., in: *Electrodes of Conductive Metallic Oxides*, (Trasatti S., ed.), Part A, 261, Elsevier, Amsterdam, 1980.

5) Tseung A.C.C., Bevan H.L., J. Electroanal. Chem., **45**, 429, 1974.

6) Otagawa T., Bockris J. O'M., J. Electrochem. Soc., **129**, 2391, 1982.

7) Balej J., Int. J. Hydrogen Energy, **10**, 89, 1985.

8) Meadowcroft D.B., Nature, **226**, 847, 1980.

9) Tseung A.C.C., J. Electrochem. Soc., **125**, 1660, 1978.

10) Kudo T., Obayashi H., Genjo T., J. Electrochem. Soc., **122**, 159,1975.

11) Kudo T., Obayashi H., Yoshida M., J. Electrochem. Soc., **124**, 321, 1977.

12) van Buren F.R., Broers G.H.J., Boesveld C., Bouman A.J., J. Electroanal. Chem., **87**, 353, 1978.

13) van Buren F.R., Broers G.H.J., Bouman A.J., Boesveld C., J. Electroanal. Chem., **87**, 381, 1978.

14) van Buren F.R., Broers G.H.J., Bouman A.J., Boesveld C., J. Electroanal. Chem., **87**, 389, 1978.

15) Kobussen A.G.C., van Buren F.R., van den Belt T.G.M., J. Electroanal. Chem., **96**, 123, 1979.

16) Kobussen A.G.C., Mesters C.M.A., J. Electroanal. Chem., **115**, 131, 1980.

17) Kobussen A.G.C., J. Electroanal. Chem., **126**, 199, 1981.

18) Kobussen A.G.C., Broers G.H.J., J. Electroanal. Chem., **126**, 221, 1981.

19) Kobussen A.G.C., Willems H., Broers G.H.J., J. Electroanal. Chem., J. Electroanal. Chem., **142**, 67, 1982.

20) Kobussen A.G.C., Willems H., Broers G.H.J., J. Electroanal. Chem., J. Electroanal. Chem., **142**, 85, 1982.

21) Bockris O'M. J., Otagawa T., Young V., J. Electroanal. Chem., **150**, 633, 1983.

22) Wattiaux A., Grenier J.C., Pouchard M., Hagenmuller P., J. Electrochem. Soc., **137**, 1714, 1987 and **137**, 1718, 1987.

23) Wattiaux A., Grenier J.C., Pouchard M., Hagenmuller P., Nouv. J. Chimie, **10**, 247, 1986.

24) Lagueyte N., Wattiaux A., Park J.C., Grenier J.C., Fournès L., Pouchard M., J. Phys. III, **1**, 1755, 1991.

25) Arrouy F., Wattiaux A., Cros C., Demazeau G., Grenier J.C., Pouchard M., Etourneau J., Physica C, **175**, 487, 1991.

26) Wattiaux A., Fournès L., Demourgues A., Bernaben N., Grenier J.C., Pouchard M., Solid State Commun., 77, 489, 1991.

27) Demourgues A., Weill F., Grenier J.C., Wattiaux A., Pouchard M., Physica C, **192**, 425, 1992.

28) Bennet J.C., Olfert M., Scholz G.A., Boswell F.W., Physical Review B, **44**, 2727,1991.

29) Rudolf. P., Paulus W., Schöllhorn R., Advanced Materials, **3**, 438, 1991.

30) Chou F.C., Cho J.H., Johnston D.C., Physica C, **197**, 303, 1992.

31) Pourbaix M., *Atlas of Electrochemical Equilibria in Aqueous Solutions*, Pergamon Press, New York, 1966.

32) Charlot G., *Les Méthodes de la Chimie Analytique*, Masson, 1961.

33) Matsumoto Y., Manabe H., Sato E., J. Electrochem. Soc., **127**, 811, 1980.

34) Bockris J. O'M., Otagawa T., J. Electrochem. Soc., **131**, 290, 1984.

35) Carapuca H.H., da Silva Pereira M.I., da Costa F. M. A., Mat. Res. Bull. **25**, (1990) 1183.

36) Park J.C., *Doctoral Thesis*, University of Bordeaux, 1990.

37) Tamman G., Z. Anorg. Chem., **111**, 78, 1920.

38) Rickert H., *Electrochemistry of Solids*, Springer, Berlin, 1982.

39) Fellner P., Chrenková M., Matiašovský K., Surface Technol., **8**, 501, 1979.

40) Vondrák J., Jakubec I., Bludská J., Skácel V., Electrochim. Acta, **35**, 995, 1989.

Chapter IV

RESULTS & DISCUSSION

IV.I. Discussion

Electrochemical oxidation of $Sr_2Co_2O_5$ was successful in the case of the brownmillerite - type starting compound that undergoes the oxidation rather reproducibly.

The mechanism of the electrochemical oxidation of this material may be postulated as follows:

- the rate determining step of the oxygen evolution on this material may be expressed by the following relation:

$$M(O^-)_{ads} \longrightarrow M(O)_{ads} + e^-$$

which was estimated from the I - E curves measurement (cf. § III.4.2.). This rate determining step implies a maximal coverage of the surface of the studied material with the intermediate oxygen species O^-_{ads} ($\theta \cong 1$).

When the material is polarized in the region of the limiting current of the pseudo - plateau O_1 (cf. § III.4.2., Fig 7b), the activity of the intermediate oxygen species on the surface may be considered to be constant and close to unity. It should involve that the electrochemical reaction is limited by the diffusion of the intermediate oxygen species into the bulk of the electrode. This hypothesis may be reinforced by the features of the electrochemical responses e.g. the independence of the limiting current of I- E curves on the rotation speed of the working electrode (RDE) [1], or the current response on the potential step supported by the estimated value of the diffusion coefficient $D_x = 1.10^{-13}$ $cm^2.s^{-1}$. This value well agrees with those found by Kudo [4], van Buren [5], and Takeda [6] on several cobalt containing oxides. This diffusion, as supposed from the accumulation of these species on the surface, is not easy.

The magnitude of this diffusion coefficient shows clearly that it cannot be ascribed neither to the diffusion of OH^- species from the solution to the surface of the

electrode(D_{OH^-} = $5.10^{-5}cm^2.s^{-1}$) [2] nor the diffusion of O^{2-} species into the bulk of the electrode ($D_{O^{2-}}$ = $10^{-15}cm^2.s^{-1}$) [3]. Therefore, one can consider the species that diffuse into the bulk of the studied material would be those of O^-.

Moreover this value of the diffusion coefficient (D_X = 1.10^{-13} $cm^2.s^{-1}$), rather elevated one, may be explained in terms of the charge transfer:

$$Co^{3+} + O^- \longleftrightarrow Co^{4+} + O^{2-}$$

occurring in the bulk of the material.

It corroborates also previous observations [7] in which the authors supposed the same species to diffuse into the bulk of the perovskite - type oxides.

From the crystallographic point of view, the intercalation of the oxygen species is facilitated in the case of brownmillerite - type $Sr_2Co_2O_5$ by the existence of "channels" of ordered oxygen vacancies along the $[101]_C$ direction. Supposing the $r_{O^{2-}}$ to be 140 pm and $r_{Co^{3+}_{IV}}$ to be 42 pm (cf. § II.2.4.3) the maximal radius of species fitting to these channels should be r = 110 pm (Fig. 1). The calculated electrostatic potential, (Madelung potential) [8], is positive within all area of the channels (Fig. 1), and is therefore attractive for the negative charged species.

The size of the channels (110 pm) may reject the O^{2-} anions ($r_{O^{2-}}$ =140 pm) to be the oxygen species that diffuse through these channels.

Finally, based on all above mentioned facts, it seems reasonable to conclude that the species which intercalate into the bulk of the brownmillerite - type structure are likely O^-.

In the case of the low temperature phase which in fact does not exist as $Sr_2Co_2O_{5+x}$ but, as it was found in § II.2.6.4., may be formulated with the composition $Sr_6Co_5O_{15-y}$, no oxidation was observed.

References page 149

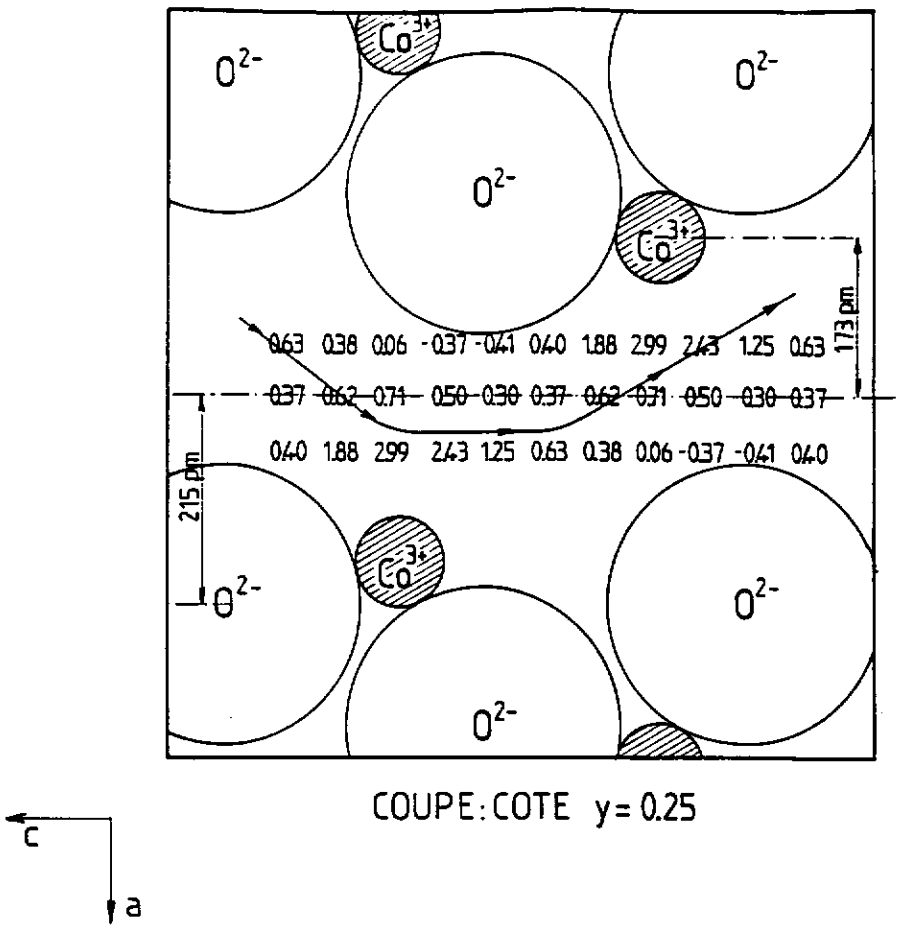

Fig. 1. Electrostatic potential within the channel in the brownmillerite - type $Sr_2Co_2O_{4.96}$ material.

The absence of the oxidation plateau O_1 and the fact, that the rate determining step found on the base of I - E curves measured on this material (cf. § III.5.) is that of the gaseous oxygen evolution:

$$2\,M(O)_{ads} \longrightarrow 2\,M + O_2$$

indicate clearly, that this material does not undergo the oxidation reaction. It was confirmed by the subsequent chemical analyses.

From the crystallographic point of view, these materials are in fact already in highly oxidized form, according to the results of chemical analyses to the compositions ($Sr_6Co_5O_{14.05}$ (22 % of Co^{4+}) and $Sr_6Co_5O_{14.45}$ (38 % of Co^{4+}), respectively). The fully stoichiometric material would be formulated $Sr_6Co_5O_{15}$, with 60 % of Co^{4+}. Although the oxygen vacancies in this type of material are located on a given crystallographic site (O(5), cf. § II.2.6.4.), they appear isolated in the network, which likely increases the energy required for the intercalation of oxygen species into the lattice of this phase. This emphasises the role of the structure of the starting material which should be appropriate for oxygen intercalation, i.e. presence of vacancies or at least interstitial sites in "direct vicinity".

The electrochemical method, at least as it was used in this study, does not provide enough energy to the species and therefore the oxygen gas evolution takes place (which is in fact always in competition with the oxidation reaction). and therefore this material does not undergo the oxidation.

The remaining question concerning the electrochemical behavior of the $Sr_6Co_5O_{15-y}$ phase is that of the role of cobalt oxides occurring in the material because of decomposition of $Sr_2Co_2O_{5\pm x}$ during the phase transition.

As mentioned above, the electrochemical oxidation of $Sr_2Co_2O_5$ was successful in the case of the brownmillerite - type phase. The characterization of the oxidized material will be presented below.

References page 149

IV.2. Characterization of the oxidized material $SrCoO_3$

IV.2.1. Chemical analysis

The final stoichiometric $SrCoO_3$, prepared either by means of the potentiostatic electrolysis or using the galvanostatic method, was characterized by several physical and chemical methods. The chemical analysis, provided as described before by means of bichromatometric titration (with the excess of Mohr salt), revealed the oxygen content corresponding to the stoichiometric compound within the accuracy of this analytical method so that the composition may be formulated as $SrCoO_{3.00\pm0.03}$.

IV.2.2. XRD pattern

The XRD pattern (cf. § III.3.3.1.3) be indexed as expected it in the Pm3m cubic space group, with the refined unit cell parameter being a = 383.5±0.2 pm. This value is in very good agreement with that extrapolated by Taguchi [9,10] for a stoichiometric compound (a = 383.6 pm).

Assuming anionic radius of oxygen $r_{O^{2-}}$ = 140 pm, one can therefore calculate $r_{Co^{4+}}$ = 51.8 pm in the octahedral coordination of the perovskite structure.

In addition, comparing the mean reduced parameter of the brownmillerite-type starting compound ($a_C \cong 391.2$ pm) and the cubic unit cell parameter of $SrCoO_3$, one should point out the significant change of the unit cell volume ($\Delta V/V \cong -5.8$ %) due to the oxidation process, as previously observed for $SrFeO_3$ [7] ($\Delta V/V \cong -6.6$ %).

IV.2.3. Transport properties

The $Sr_2Co_2O_{5\pm x}$ brownmillerite - type phase before oxidation exhibits a semiconducting behavior (Fig 2a). After electrochemical oxidation the $SrCoO_3$ compound is metallic (Fig. 2b).

Thermoelectric power measurements reported in Fig. 3 show small negative values typical of electron carriers.

IV.2.4. Magnetic properties

As expected from previous publications, the magnetic properties of the final compound $SrCoO_3$ characterize a ferromagnetic behavior. The Curie temperature ($T_c \cong 280$ K) was determined either from the thermal evolution of the magnetic moment (Fig. 4) or from the thermal behavior of the magnetic susceptibility. At each temperature the magnetic moment was calculated using the Belov-Kouvel method [11,12]. The extrapolated value of the saturation magnetic moment at 0 K is 2.1 μ_B (Fig. 4). One should point out that this moment as well as the Curie temperature of $SrCoO_3$ are somewhat higher than those previously reported by Taguchi [9,10] for nearly stoichiometric materials.

IV.2.5. Discussion of the physical properties

In an oxygen environment the Co^{4+} ($3d^5$) ions should adopt a low spin configuration ($t_{2g}^5 e_g^0$) (Fig 5a, $10D_q > E_{ex}$) [13].

However, the 3d levels of this cation and the O_{2p} levels are very close, which involves the following electron transfer:

References page 149

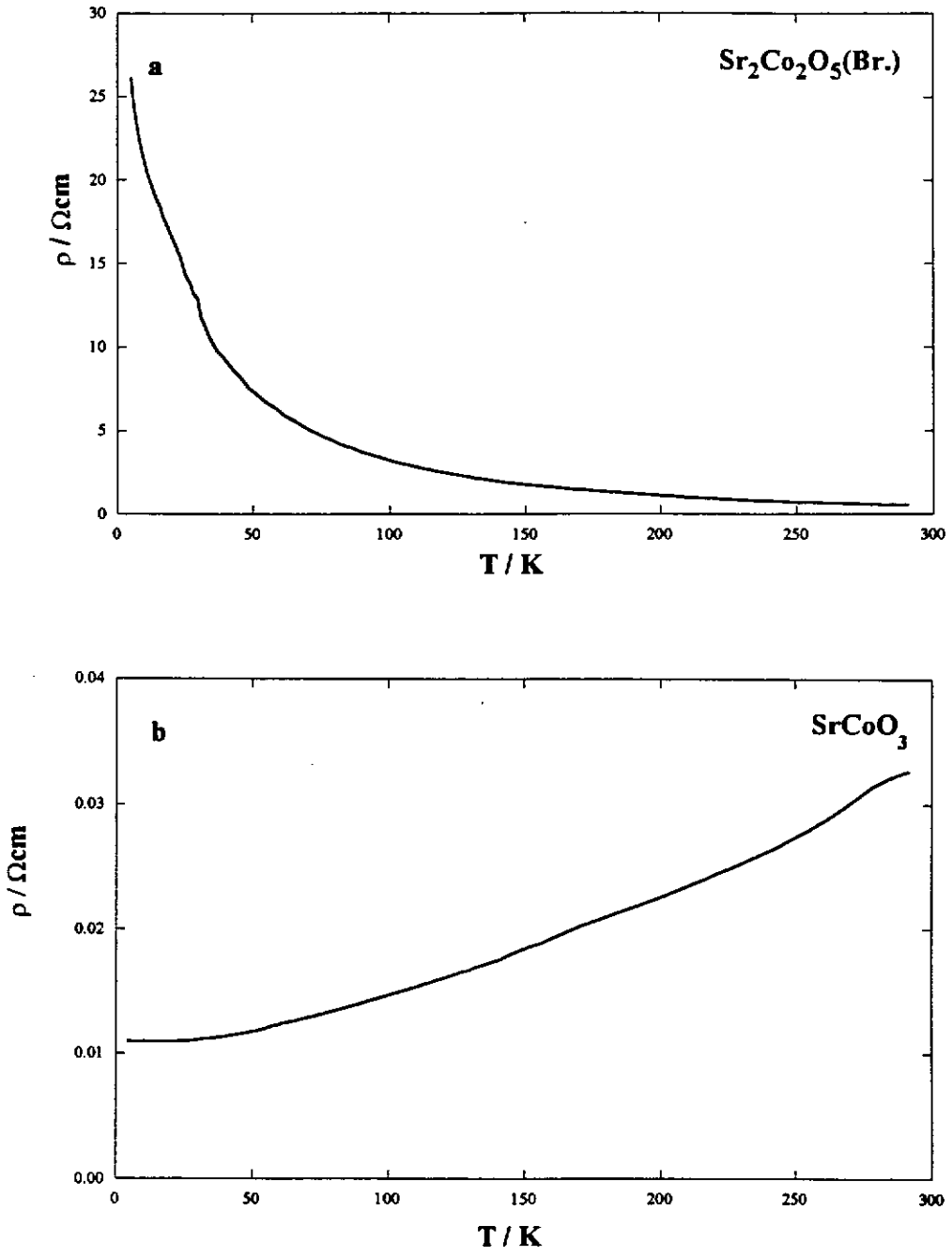

Fig. 2. Temperature dependence of the electrical resistivity a) of $Sr_2Co_2O_5$ before polarization. b) of $SrCoO_3$ after polarization.

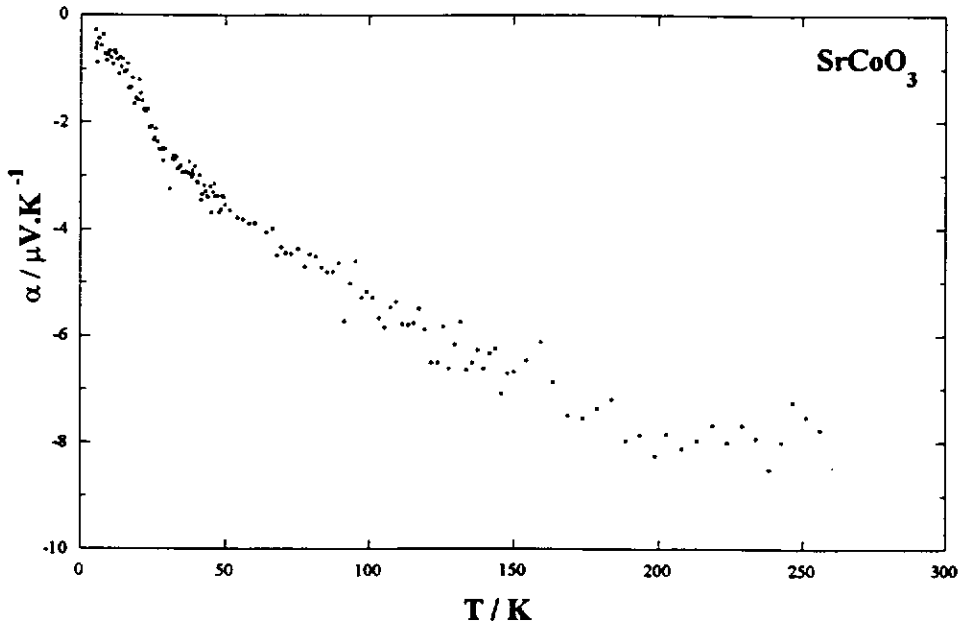

Fig. 3. Temperature dependence of the Seebeck coefficient of $SrCoO_3$ after polarization.

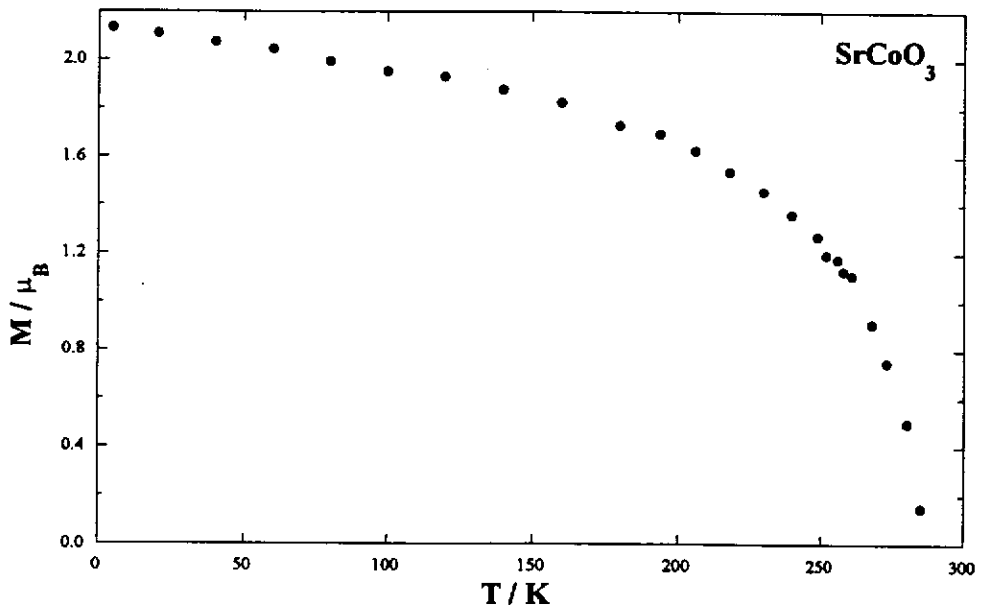

Fig. 4. M - T curve for $SrCoO_3$ after polarization measured at 2 T.

References page 149

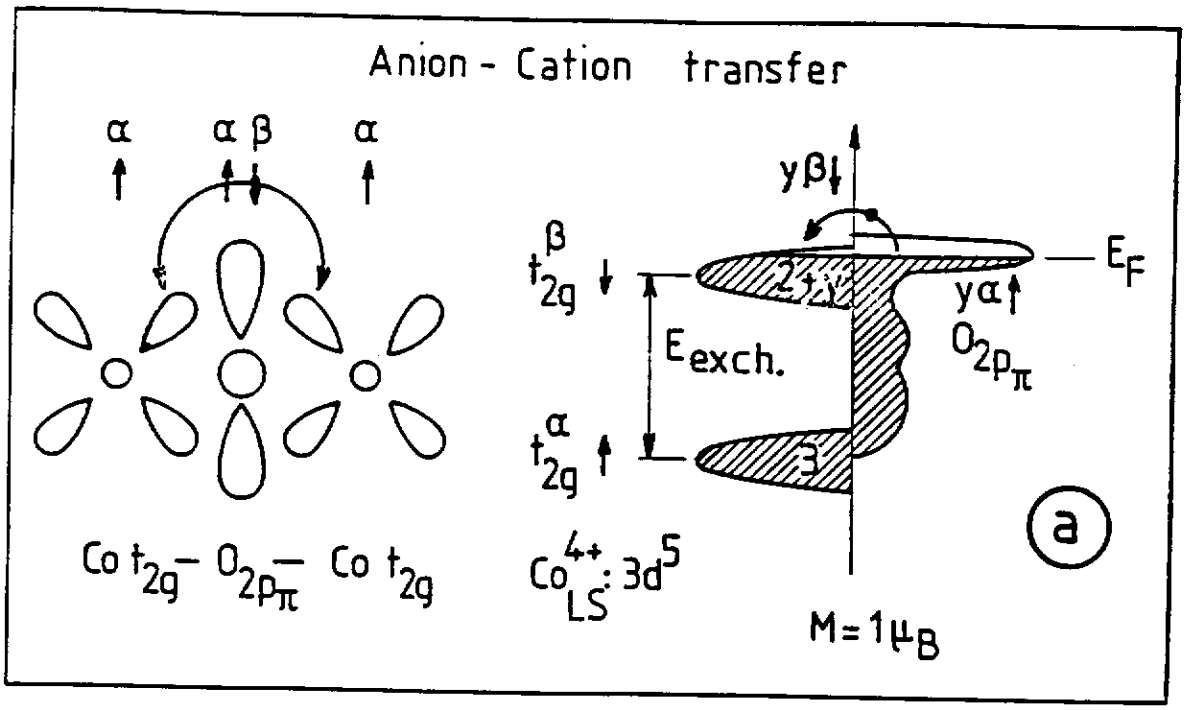

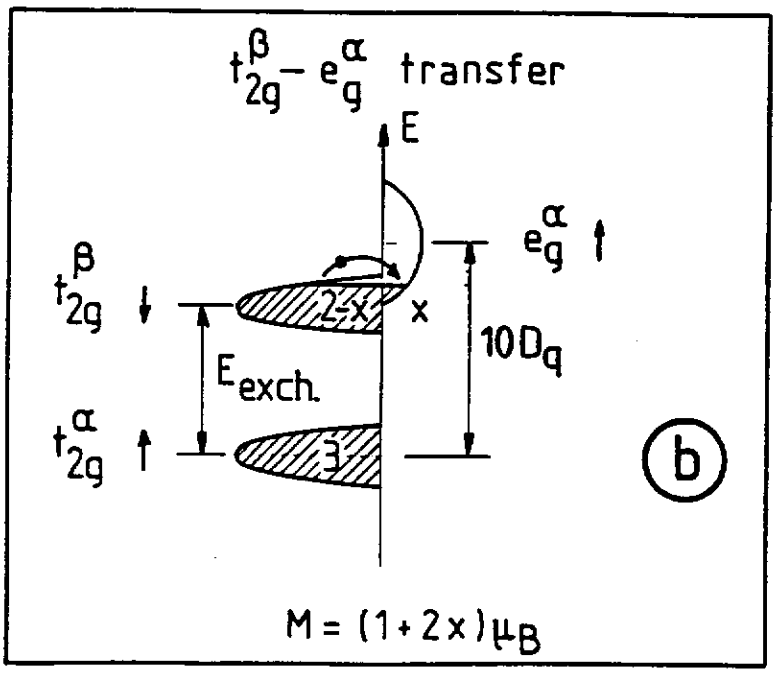

Fig. 5. Schematic representation of a) the anion - cation transfer, b) the partial electron transfer in e_g^{α} orbitals in $SrCoO_3$.

$$O^{2-} + Co^{4+} \Longleftrightarrow O^{-} + Co^{3+}$$

This transfer characterizes materials whose charge - transfer parameter Δ is low and implies the occurrence of mixed valence states.

In a recent work based on an ionic model described by Zaanen et al. [14], using the two physical parameters U, (Hubbard energy) and Δ, (charge transfer energy), Torrance et al. [15] have proposed a classification of oxides showing that $SrCoO_3$ is indeed a metal, or rather a semimetal, with overlapping of the $O_{2p\pi}$ and 3d metal bands.

The charge transfer resulting from the low value of the calculated Δ ($\Delta \cong 3eV$ [7]) should correspond to a partial electron transfer (y) from the $O_{2p\pi}$ band (a very narrow antibonding O-O band) toward the Co_{t2g} band (of similar symmetry). Evidence of such a charge transfer, requiring the presence of a certain spin density on the oxygen atoms, was previously given by a neutron diffraction investigation on stoichiometric $SrFeO_3$ ($\cong 0.3\ \mu_B$/oxygen) [16].

Nevertheless one should point out that this transfer of (y) electrons does not change the total magnetic moment M. For instance, assuming, in a first approximation that there is no overlap between $\sigma^*_{eg}\alpha$ and $\pi^*_{t2g}\beta$ (Fig. 5a) one may write:

$$M = (3 + y)_\alpha - (2 + y)\beta = 1\ \mu_B$$

However, the value of the experimental magnetic moment is somewhat higher (2.1 μ_B), which can be only explained by a partial transfer ($t^{\beta}_{2g} \rightarrow e^{\alpha}_{g}$) resulting in an intermediate spin configuration $t^{5-x}_{2g} e^{x}_{g}$. This configuration, usually unstable in an ideal O_h environment for localized systems is stabilized by the delocalization of the d electrons in the $\sigma^*_{eg}\alpha$ band in agreement with the metallic character of this compound ($\lambda_\sigma > \lambda_c$).

References page 149

Therefore, the value of the magnetic moment becomes:

$$M = (3 + x)_{\alpha} - (2 - x)_{\beta} = 1 + 2x\ \mu_B$$

x being the fraction of electron in the e_g^{α} orbitals. On hand of the experimental value of $M \cong 2.1\ \mu_B$, x should be close to 0.50.

Assuming that the electron mobility in the $\sigma^* e_g^{\alpha}$ bands is higher than that of the holes in the $\pi_{t2g}^{*\beta}$ or $O_{2p\pi}$ bands [10], a low negative value of α may be expected. It is indeed observed but the nonlinear temperature dependence suggests that the thermal evolution of both bands likely change the number of negative carriers at rising temperature.

In addition, the ferromagnetic behavior of stoichiometric $SrCoO_3$ results obviously from the coupling between the itinerant $\sigma^* e_g^{\alpha}$ electrons with the quasilocalized t_{2g} ones.

IV.3. References

1) Arrouy F., Doctoral Thesis, University of Bordeaux, 1992.

2) Besson J., Guitton J., *Introduction à la théorie et à la pratique de la cinétique*, Masson, Paris, 1972.

3) Kingery W.D., Pappis J., Doty M.E., Hill D.C., J. Amer. Ceram. Soc.,**42**, 393, 1959.

4) Kudo T., Obayashi H., Genjo T., J. Electrochem. Soc., **122**, 159,1975.

5) van Buren F.R., Broers G.H.J., Bouman A.J., Boesveld C., J. Electroanal. Chem., **87**, 381, 1978.

6) Takeda Y., Kanno R., Takada T., Yamamoto O., Z. Anorg. Allg. Chem., **540 / 541**, 259, 1986

7) Grenier J.C., Wattiaux A., Doumerc J.P., Dordor P., Fournès L., Chaminade J.P., Pouchard M., J. Solid State Chem., **96**, 20, 1992.

8) Villesuzanne A., private communication.

9) Taguchi H., Shimada M., Koizumi M., J. Solid State Chem., **29**, 221, 1979.

10) Taguchi H., Shimada M., Koizumi M., Mat. Res. Bull., **15**, 165, 1980.

11) Belov K.P., Gonyaga A.N., Fiz. Met. Metall., **2**, 3, 1956.

12) Kouvel J.S., *Gen. El. Lab. Report N 57, RL*, 1799, 1957.

13) Buffat B., *PhD Thesis, University of Bordeaux*, 1984.

14) Zaanen J., Sawatzky G. A., J. Solid State Chem., **88**, 8, 1990.

15) Torrance J.B., Lacorre P., Asavaroengchai C., Metzger R.M., J. Solid State Chem., **90**, 168, 1991.

16) Oda H., Yamaguchi Y., Takei H., Watanabe H., J. Physique, **38**, C1, 1977.

CONCLUSION

Nous nous étions fixés pour but d'étudier les phénomènes d'oxydation électrochimique sur des oxydes de cobalt plus particulièrement sur l'oxyde $Sr_2Co_2O_5$ qui cristallise sous deux variétés cristallines selon la configuration électronique du cobalt trivalent, avec l'espoir de préparer deux variétés allotropiques de la perovskite $SrCoO_3$.

Dans une première partie de ce mémoire nous avons précisé les domaines de stabilité thermique de ces deux phases afin de préparer des céramiques de bonne qualité destinées aux traitements électrochimiques. Les matériaux trempés brutalement depuis des températures supérieures à 1273 K cristallisent avec la structure brownmillerite; ses caractéristiques cristallographiques ont été affinées avec le groupe d'espace Icmm et nous avons montré l'existence de larges files susceptibles d'accueillir par intercalation des espèces oxygénées. La phase de basse température était supposée dérivée de la perovskite hexagonale de type 2H. Les études par microscopie électronique nous ont conduits à adopter une maille rhomboédrique mais les divers essais d'affinement des données de diffraction X ou de neutrons n'ont pu conduire à des facteurs de confiance corrects. En revanche nous avons été amenés à conclure que, lors de la transition de spin, une décomposition partielle de la brownmillerite se produisait pour donner un composé déficitaire en cobalt dont la formule est proche $Sr_6Co_5O_{14.04}$. Dans cette phase le cobalt dont le degré d'oxydation est relativement élevé (3.22 +) occupe essentiellement des sites octaédriques et en fait le taux de lacunes d'oxygène y est relativement faible (1 oxygène sur 15 est manquant).

Dans la deuxième partie de ce mémoire, les études électrochimiques ont été menées afin de déterminer les possibilités d'oxydation électrochimique de ces deux phases. Le comportement observé est très différent, la brownmillerite subit une oxydation de coeur alors que la phase rhomboédrique semble inerte et conduit uniquement au dégagement de l'oxygène par électrolyse de l'eau. Les conditions optimales d'oxydation ont été ensuite étudiées pour la phase de type brownmillerite en fonction de divers paramètres (type d'électrode, pH, etc...) pour des traitements potentiostatiques ou intentiostatiques. L'évolution du potentiel de repos a permis de

contrôler l'état d'avancement de la réaction et une phase complètement oxydée $SrCoO_3$ a pu être préparée et caractérisée par diverses techniques. Plus particulièrement les propriétés magnétiques ont révélé une température de Curie très élevée (Tc = 280 K), traduisant un composé métallique très stoechiométrique. La valeur du moment magnétique n'a pu être expliquée que par l'existence d'une configuration électronique du cobalt intermédiaire de l'état spin fort et de l'état spin faible.

Enfin sur la base des études électrochimiques et de considérations cristallographiques nous avons proposé un mécanisme réactionnel mettant en jeu la diffusion d'espèces O^-. Nous avons pu également expliquer sur la base de considérations cristallographiques pourquoi la phase de basse température ne pouvait s'oxyder.

Des résultats encourageants ont été obtenus en milieu non aqueux; ils devront être confirmés et seront susceptibles de nous permettre de mieux comprendre le mécanisme réactionnel.

APPENDIX 1

Experimental techniques

A1.1. X-ray powder diffraction

(coworkers: *P. Gravereau*, LCS CNRS, *J. Rodriguez Carvajal*, LLB CNRS, *Ľ. Smrčok*, Inst. Inorg. Chem. SASc., Bratislava)

The powdered samples have been analysed using X-ray powder diffraction method. The Philips PW 50 goniometer equipped with graphite monochromator that uses the Bragg-Bretano geometry and $Cu_{K\alpha}$ tube as the source of X-rays served to perform all experiments.

The stepwise counting up to 40 s was used for subsequent refinement analyses using Rietveld [1-3] method.

Neutron diffraction data were collected at room temperature on a powdered sample contained in a vanadium holder using the diffractometer D1a at ILL Grenoble. Data were collected at 2θ intervals of 0.05^{o} throughout the angular range $5 < 2\Theta < 180°$, the mean neutron wavelength was 195 pm.

The high temperature X-ray diffraction method was used to determine the temperature dependence of cell parameters and phase transitions in the studied specimens. The goniometer was equipped with a high temperature chamber that allows to carry out the measurements up to 1500 K The sample is placed on a Pt40Rh support that serves in the same time as a sample holder and a heating element as well. The temperature in the furnace is determined from the calibration using known phase transitions of standard samples. These experiments were done either in air or in purified spectral grade nitrogen atmosphere ($p_{O_2}=10^{-2}$ Pa).

A1.2. High resolution transmission electron microscopy.

The different samples were studied by means of high resolution transmission electron microscopy using JEOL 2000 FX microscope. The microscope was equipped with a double tilting ($\pm 40^{o}$) sample holder

The sample was finely grinded in alcohol. The resulting suspension was deposited on a graphite membrane then attached to the sample holder before placing into the microscope.

A1.3. The Auger electron spectroscopy analysis.

(coworker: *M. Lahaye*, LCS CNRS)

Elemental analysis was performed by Auger electron spectroscopy [4] (AES) using the scanning Auger microprobe PHI - 590 , Perkin Elmer with Ar^{+} sputtering gun. The apparent atomic concentrations were derived from intensities of the SrMNN (110 eV), CoLMM (775 eV) and OKLL (512 eV) Auger electron transitions, using the derivative mode that these concentrations are only semiquantitative.

A1.4. Magnetic measurements

Two types of magnetic determinations were carried out:

- The magnetic moment under various magnetic fields ($1T \leq H \leq 2T$) was measured as a function of temperature using a Foner - type magnetometer (PAR) [5]
- The paramagnetic susceptibility was determined under 1.8 T with an automatic susceptometer (Manics, DSM8) [6]

References page 161

A1.5. Electrical measurements

(Coworkers: P. Dordor, E Marquestaut, LCS CNRS)

The electrical conductivity was measured using the four probe method in the range of 4.2 K to 300 K. [7,8]

Thermoelectric power data were obtained using an equipment described elsewhere [9]

A1.6. Thermal analyses

(Coworkers: *L. Rabardel, J. Villot*, LCS CNRS, *J. Krajčovič, M. Kubranová*, Inst. Inorg. Chem. SASc, Bratislava)

Thermogravimetric analyses under various atmospheres (e.g. nitrogen -10% hydrogen, argon, air, vacuum) were performed for determination of total oxygen amount and/or oxygen stoichiometry as a function of the temperature. The experiments were carried out using an automatic microbalance (MTB 10-8, Setaram) connected to an HP 9826 computer. The temperature range of this equipment is 25 - 1200°C.

The differential thermal analysis to determine the phase transitions at increasing or decreasing temperature was carried out either using the system which was set up in LCS CNRS or DuPont DTA apparatus in IIC SASc.

A1.7. Total amounts of elements

(Coworker: *V. Kliment,* Inst. Physics SASc, Bratislava)

The total amounts of the present cationic elements were determined using two independent methods.

Classical gravimetric analysis [10] by means of sulphuric acid in the presence of alcohol was used for determination of the total amount of strontium in the sample. The chelatometric titration [10] with a standard solution of EDTA in a solution of NH_4OH/NH_4Cl buffer with a Eriochrome T black indicator was achieved to analyse the total amount of cobalt.

ICP-AES spectroscopy [4] was used to determine the concentration of these elements by means of another independent method. This analytical technique allows to examine also the traces of other elements in the same solution. The presence of platinum and aluminium, possible pollution during sample preparation, was therefore checked in the analysed powders.

A1.8. Determination of the Co^{4+} content in the studied samples

The Co(IV) content in the samples was obtained by bichromatometric titration after dissolution in 1 M HCl in presence of an excess of Mohr's salt as described by Wattiaux [11].

References page 161

A1.9. Electrochemical experiments.

(Coworker: *J. Vondrák*, Inst. Inorg. Chem. ASCR, Prague)

Electrochemical experiments were carried out using a two compartment electrochemical cell with a three electrode system (cf. Appendices 2 & 3).

The reference electrode was a HgO/Hg electrode filled with 1 M NaOH (E_T = 0.098 V/SHE, 298 K). All potentials quoted in this thesis are referred to this electrode.

The auxiliary electrode was a platinum foil.

A rotating disk electrode made of the ceramic of the starting material was used as the working electrode. The samples were mounted on the holder as described elsewhere [12]. A rotating support, EDI 101 T (Tacussel), was used to realize the whole working electrode arrangement.

A Tacussel PJT 24-1 potentiostat was used for the electrochemical experiments. This potentiostat was piloted by an IBM PC computer equipped with an ADDA converted (Keithley DAC 8) as described in Appendix 3.

A1.10. References

1) Rietveld H.M., J. Appl. Cryst., **2**, 65, 1969.

2) Rodriguez-Carvajal J., *program Fullprof, ver. 2.2.1*, private communication.

3) Smrčok Ľ., *PhD Thesis*, Slovak Academy of Sciences, Bratislava 1990.

4) Christian G.D., O'Reilly J.E. eds., *Instrumental Analysis*, 2nd ed., Prentice Hall, Englewood Cliffs, New Jersey, 1987.

5) Dance J.M., Doctoral Thesis, University of Bordeaux, 1973.

6) Dupeyron M., DESS, University of Bordeaux, 1988.

7) Laplume J., L'onde electrique, **335**, 113, 1985.

8) Dordor P., Marquestaut E., Sadulcci C., Hagenmuller P., Rev. Phys. Appl., **20**, 795, 1985.

9) Dordor P., Marquestaut E., Villeneuve G., Rev. Phys. Appl., **15**, 1607, 1980.

10) Charlot G., *Les Méthodes de la Chimie Analytique*, Masson, 1961.

11) Wattiaux A., *PhD Thesis*, University of Bordeaux, 1985.

12) Wattiaux A., Grenier J.C., Pouchard M., Hagenmuller P., Rev. Chim. Miner., **22**, 1, 1985.

13) Moya Pizarro T., *Doctoral Thesis,* University of Bordeaux, 1983.

APPENDIX 2

Electrochemical reaction

A2. Electrochemical reaction

An electrode reaction is a heterogeneous chemical process involving the transfer of electrons to or from a surface, generally a metal or semiconductor.

Although the basic electrochemical laws were established using this kind of electrodes (commonly considered to be inert and as smooth as possible), the majority of these laws has a more general validity.

But in most cases of applied electrochemistry (e.g. electrocatalysis, fuel cells, industrial electrolysis) we have to deal with solid electrodes. The interfacial structure of these electrodes is extremely difficult because there are great difficulties for reproducing a surface and keeping it clean. Another difficulty is the existence of pores in the electrode material and consequently the spatial distribution of phenomena occurring on the surface of such electrodes.

Keeping in mind these facts, a brief survey of basic electrochemical laws will be presented below. A special interest will be paid to particular problems of electrochemistry of ceramic materials which may undergo significant changes during the electrochemical process and which may be classified as "inorganic modified electrodes".

A2.1. Faraday law

The current through the external circuit, I given by I=Aj, when A is the electroactive surface area and j the current density, is a convenient measure of the rate of the cell reaction, and the charge q passed during a period t indicates the total amount of chemical reaction which may have taken place: indeed, the charge required to convert m moles of the starting material into the final product in an electrode reaction involving the transfer of n electrons/molecule is readily calculated using the Faraday law [1,2]

$$q = \int_0^t I \cdot dt = m \cdot n \cdot F$$

A2.2. Basic laws for an electrochemical reaction: transfer of an electron

An electrode reaction is a heterogeneous chemical process involving the transfer of electrons to or from a surface, generally a metal or a semiconductor. The electrode reaction may be an anodic process whereby a species is oxidized by the loss of electrons to the electrode, e.g.

$$4\ OH^- \longleftrightarrow O_2\ (g) + H_2O + 4\ e^- \qquad E^o = 0.303\ V\ /\ HgO/Hg,\ 1M\ NaOH$$

Such an electrochemical reaction occurs at the interface electrolyte / electrode at a given potential E^o(E^o is the standard electrode potential).

In the case of a simple electrochemical reaction, the dependence of the electrode potential on the concentrations of the electroactive species present at the interface obeys the Nernst equation [3]

$$E = E^\circ + \frac{RT}{nF} \ln \frac{a_{Ox}}{a_{Red}}$$

where a_{Ox}, a_{Red} are the activities of the oxided and reduced species on the surface of the electrode, respectively. R is the gas constant, F is the Faraday constant and n is the number of electrons exchanged during the electrochemical reaction.

Generally an electrochemical reaction (e.g. oxidation) [4] occurs at a given potential E ($E > E^o + RT/nF.\ln\{a_{Ox}/a_{Red}\}$). The electrochemical process involves various steps, as follows:

References page 183

1)	Red_{sol}	$\Longleftrightarrow$	Red_{el}^{*}	Transport to the interface
2)	Red_{el}	$\Longleftrightarrow$	$Ox_{el} + n\,e^{-}$	Charge transfer
3)	Ox_{el}	$\Longleftrightarrow$	Ox_{sol}	Transport from the interface
(3a)	Ox_{el}	$\Longleftrightarrow$	Ox_{bulk}	(Intercalation reaction)

*) el - surface of the electrode, sol - solution, bulk - bulk of the electrode.

The difference $E - E_0$ is usually called the overvoltage η.

It has been shown that in the case of a charge transfer reaction (it requires a well stirred solutions to prevent the changes due to the mass transfer) the current is directly connected with the electrode overvoltage by an exponential function commonly known as the Butler - Volmer equation [2]:

$$I = I_o\left[\exp\left(\frac{-\alpha nF}{RT}\eta\right) - \exp\left(\frac{(1-\alpha)nF}{RT}\eta\right)\right]$$

cathode anode

where $I_o = n \cdot F \cdot A \cdot k^{o}[Ox]_{sol}^{(1-\alpha)} \cdot [Red]_{sol}^{\alpha}$ (exchange current), $\eta = E - E_0$ (overvoltage), A = surface of the electrode, α = charge transfer coefficient, k^o = rate constant of the electron transfer reaction.

By convention, the current I for such an anodic process is a positive quantity.

The Butler - Volmer equation must be regarded as the fundamental equation of electrode kinetics, and it shows the way in which current varies with the exchange current, the overvoltage, and the transfer coefficients.

When the overvoltage η is sufficiently large, $|nF\eta/RT| >> 1$, one of the exponential terms in Butler-Volmer equation will be negligible compared with the other. The anodic current is thus given by:

$$\log I = \log I_o + \frac{(1-\alpha)nF}{2.3RT}\eta$$

This equation is known as the Tafel equation [6] and suggests the means by which the exchange current and the transfer coefficient may be determined.

The same mechanism can be applied for an electrode process which consists of several electron-transfer steps, one of them is slow and rate limiting, the others are fast and can be assumed to be essentially at equilibrium [7,8].

A2.3. Diffusion controlled process

The reaction rate, proportional of current passing through the cell, increases with the increasing overvoltage. In the case of diffusion controlled reaction it can increase only until the limiting current is reached. This is for example the case when the reaction rate is limited by the transport of Red species to the electrode, i.e. every Red species that arrive at the electrode will be oxidized. Making the potential more positive cannot make the current any larger because it is limited by the rate of mass transport of Red to the electrode. The limiting current is then defined by the following equation known as Cottrell equation [9]:

$$I_L = n \cdot F \cdot S \cdot [Red]_{sol} \sqrt{\left(\frac{D_{Red}}{\pi t}\right)}$$

In such a case the potential dependence of the current may be clearly seen from the rearrangement of the previous equations as follows

$$E = E_{\frac{1}{2}} + \frac{RT}{nF} \ln \frac{I_L - I}{I}$$

where

$$E_{\frac{1}{2}} = E^{\circ} - \frac{RT}{2nF} \ln \frac{D_{Ox}}{D_{Red}}$$

This equation was derived by Heyrovský and Ilkovič [10]. $E_{1/2}$ is called the half-wave potential, I_L is the limiting current, D_{Ox} and D_{Red} are the diffusion coefficients of oxidized and reduced species respectively.

This system of equations constitutes the fundamental basis of the electrochemistry. The theoretical description of various electrochemical techniques is connected in any particular case with the solution of these basic equations.

A2.4. Electrochemical cell

A2.4.1 Three electrode system

By setting an external voltage of magnitude E_{appl} with a power supply, a current is forced through the cell and the potential of the working electrode is shifted to a new value

$$E_{appl} = E + IR = E_{eq} + \eta + IR$$

The term IR is the ohmic drop in the electrochemical cell. In experiments where IR may be large, a three-electrode cell arrangement is preferable. In this arrangement the current is passed between the working electrode and an auxiliary (or counter) electrode [11] (Fig. 1). This arrangement is required because of keeping the stability of the reference electrode. To operate correctly, the current passing between the working and the reference electrodes should be $I \cong 0$.

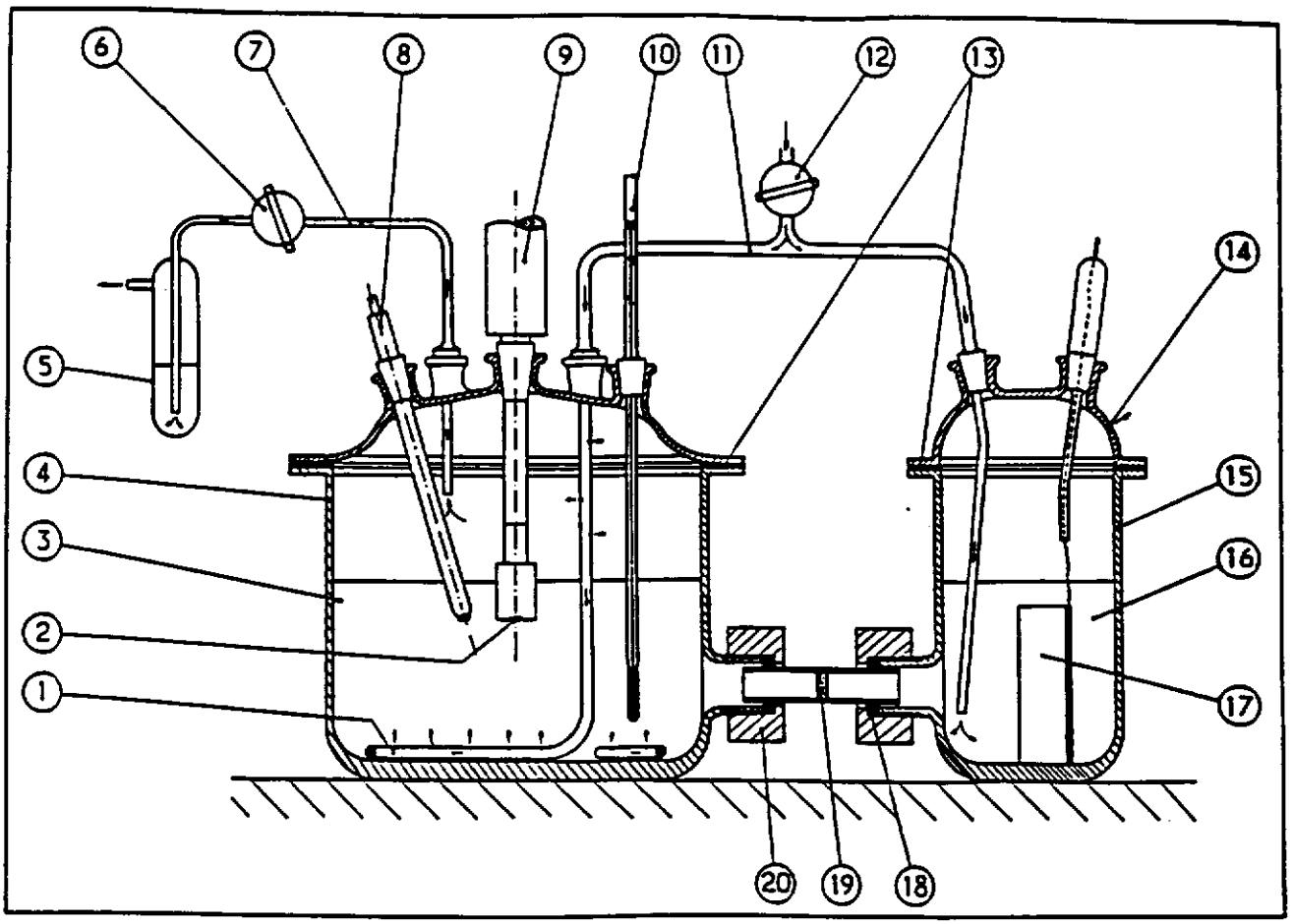

Fig. 1. Electrochemical cell.:

1) gas inlet, 2) rotating disk, 3) electrolyte, 4) main compartment, 5) gas outlet, 6) tap, 7) gas evacuation, 8) reference electrode, 9) rotating disk electrode, 10) thermometer, 11) gas inlet tubing, 12) tap, 13) teflon ring, 14) gas outlet, 15) auxiliary electrode compartment, 16) electrolyte, 17) auxiliary electrode, 18) teflon ring, 19) glas frit, 20) screws.

References page 183

A2.4.2. Components of an electrochemical cell

A2.4.2.1. The working electrode

The most important part of the electrochemical cell is the working electrode; it is usually a metal electrode. But, when a ceramic made of an oxide material is used as a working electrode, its properties differ significantly from those of metallic plane electrodes. The real structure of such a ceramic plays a very important role in the electrochemical behavior of the studied working electrodes that are named "porous electrodes". Therefore it is obvious to speak briefly about the porous electrodes which we deal with in this work.

A2.4.2.1.1. Porous electrodes

Two kinds of porous electrodes can be basically distinguished: two-phase or *"drowned"* porous electrodes [12], where an electrolyte solution fills entirely the pores of the solid phase, and the three-phase or *"gas"* porous electrodes, where an electrolyte solution comes into contact both with a gas and a solid phase. The latter electrodes may be further divided into a hydrophilic class, where the electrolyte wets the inner pore surface and a gas overpressure is necessary to prevent their drowning, and a semihydrophobic class, where the electrolyte wets only certain parts of the inner pore surface, so that flooding of the pores cannot normally occur.

The structure and composition of porous electrodes should ensure a sufficient electrical conductivity, both in the solid and liquid phases, and at the same time a minimum overvoltage for the electrochemical reaction. These conditions are closely related to the theory of transport of charge and mass in porous systems, and their fulfilment is the main object of theoretical calculations and of many experiments. Good conductivity of the solid phase is achieved with electrodes prepared by sintering

powdered materials or by the mixing with an adequate additive, i.e. graphite. Good electrical conductivity in the liquid phase of porous electrodes can be attained by a proper choice of the electrolyte, preferably KOH or H_2SO_4 at an optimum concentration, if possible.

Generally speaking, a smooth electrode can be represented by elements such as resistivities (both ohmic and non-linear, attributed to electrode reactions), double layer capacity, etc. These elements are localized on the surface (to the point x = 0 in the case of planar system). On contrary, any real surface of a solid body is never ideally smooth and is always a three - dimensional object. This aspect being much more pronounced in the case of porous electrodes. Therefore, the elements mentioned above (including resistivities of electrode material and electrolyte) are distributed within some space, and partial differential equations must be used for their mathematic description, simple algebraic or differential equations instead. Several theories of highly developed three dimensional electrode surfaces have been created.

A parallel series of cylindrical single pores with uniform cross-section filled with the electrolyte is one of the simplest model of the porous flooded electrode [13].

So far only the steady- state response has been only considered [13]. However, the attainment of the steady state in porous electrodes may take quite a long time. Grens and Tobias [14] indicate times of the order of 10 - 10^4 sec. Due to the double layer charging in the porous electrode some transient phenomena are observed.

A typical current response on the potential step (Fig 2.) corresponds to the double layer charging and may be used, in absence of the faradaic processes to determine the pore depth, pore diameter, double layer capacitance and exchange current density. Serious complications occur when a faradaic process occurs at the same time (it is in fact very often). In such a case because of the ambiguity in correcting for this faradaic process, this method looses its physical sense.

This model has proven to be highly successful; however, calculations and experimental results have shown that these models become unreliable for shallow

References page 183

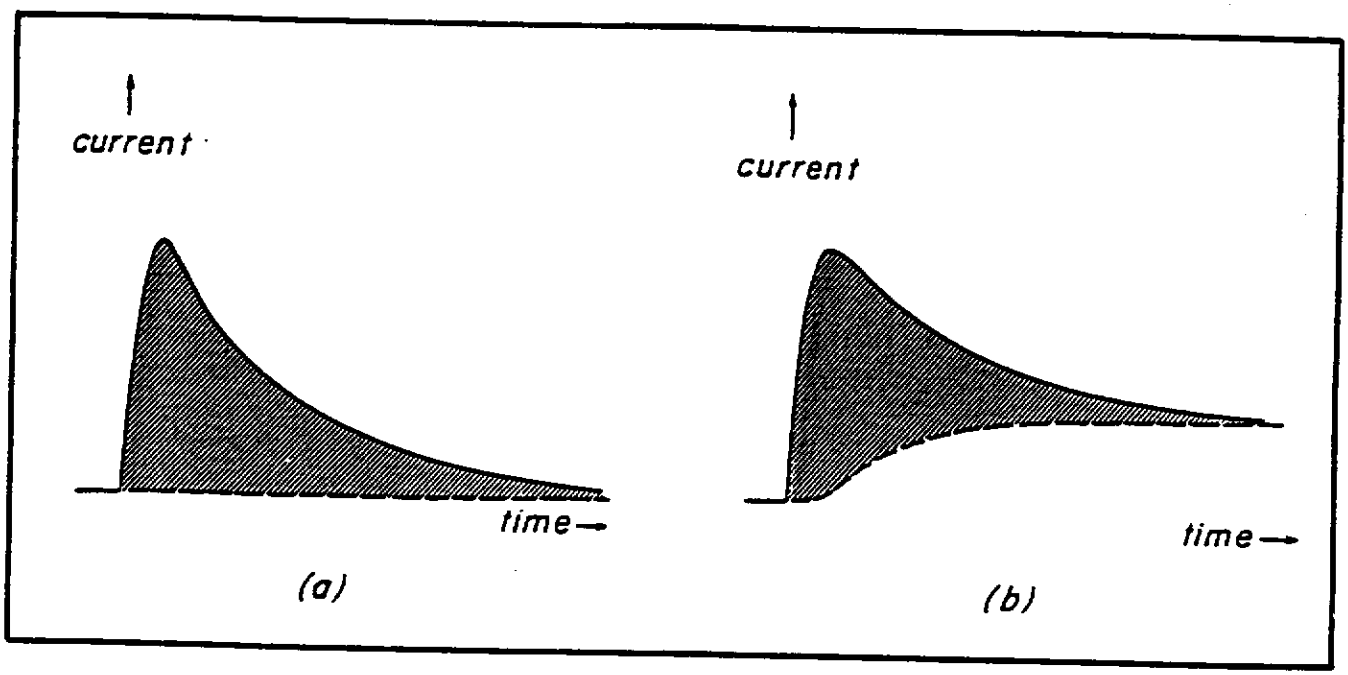

Fig. 2. The electrical response following a potential step. a) Current (solid line) and double - layer charge (shaded area) in absence of faradaic interference (horizontal baseline, broken). b) Same in presence of faradaic response. The (broken) baseline due to the faradaic current is not measurable separately. [15].

pores, i.e. when the pore diameter becomes larger than the effective penetration depth, $\sqrt{(Z/R_i)}$ [15].

A2.4.2.1.2. Rotating Disk Electrode.

As it follows from the theory of the rotating disk electrode (RDE) the hydrodynamical conditions, when the electrode operates, insure the constant electrolyte flow to the electrode surface and therefore the constant activity of the electroactive species on the surface of the RDE [16-18]. It necessitates an appropriate ratio between the rotating disk and the electrochemical cell diameters [18]. From the point of view of the ceramic electrode material (a typical arrangement of a ceramic RDE is shown in Fig. 3), these conditions limit the electrolyte penetration into the pores of the ceramic. It may be regarded as a case of a rough electrode and all basic electrochemical laws may be applied for this electrode.

Because only the upper surface of the ceramic pellet is exposed to the electrolyte (the electrode material is coated in a polymer resin to prevent the exposure of the whole electrode surface), all phenomena occurring in the bulk of the electrode are unidirectional. This fact determines the reaction rate of the anodic oxidation of the ceramic material mounted to a RDE. The reaction time necessary to oxidize the whole bulk of the electrode is much more longer than that of the fixed electrode. But on the other hand it permits to evaluate some quantitative conclusions about the diffusion rate of the intercalated species in the bulk of the ceramic RDE [19].

References page 183

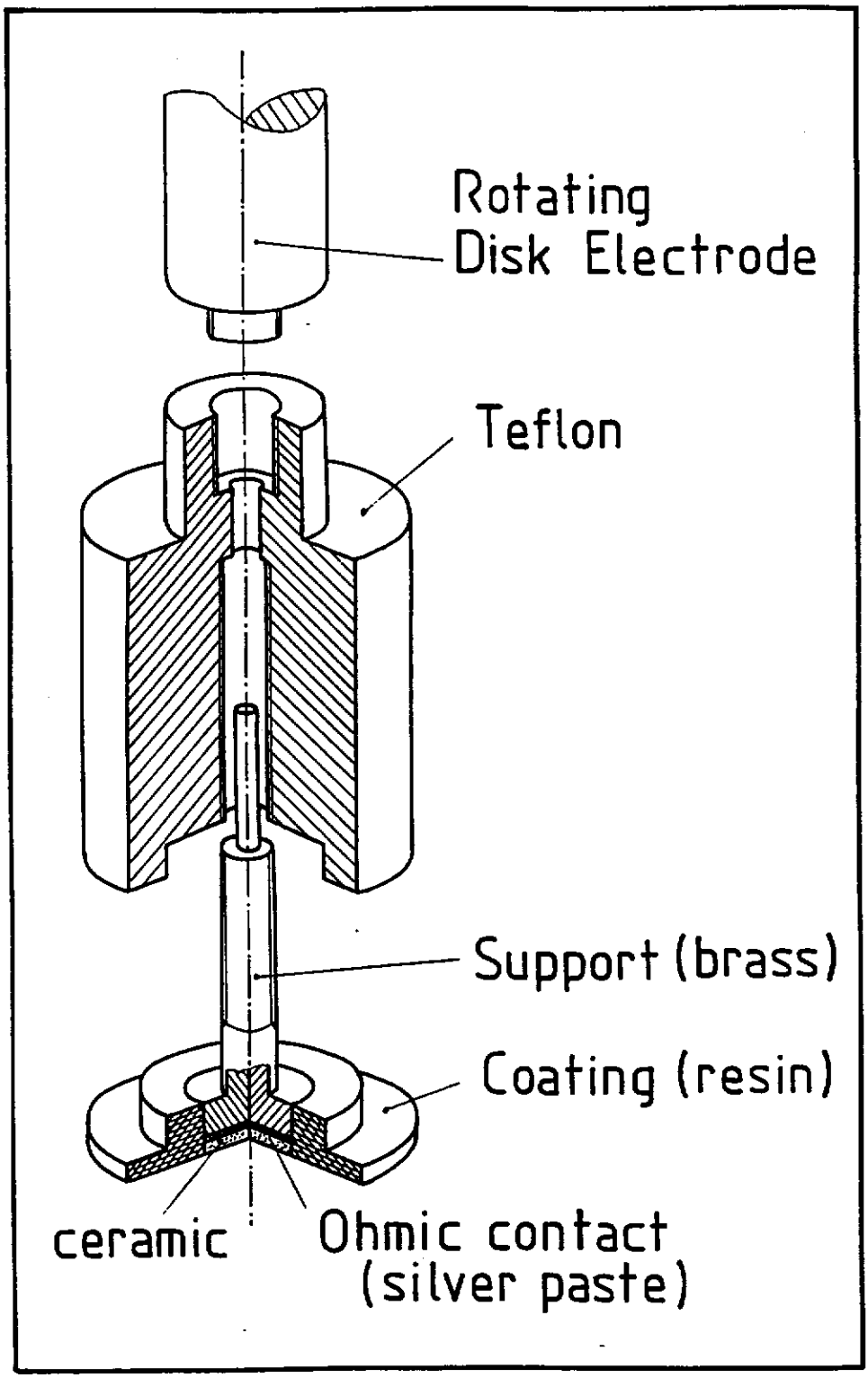

Fig. 3. Rotating disk electrode.

A2.4.2.1.3. The Fixed Electrode

This is a typical case of a porous electrode. The main advantage of the fixed electrode (Fig. 4) is the simplicity of the preparation of such an electrode. Contrary to the RDE, the fixed electrode could be prepared in the simplest way as a pellet of the ceramic material immersed in the electrolyte with the electric contact made by a croc-jack or a silver varnish with a copper or platinum wire. The hydrodynamic conditions in such a case are not well defined, therefore, this electrode cannot be used for accurate quantitative experiments. The most convenient use of the fixed electrode is the case of the necessity to prepare a rather big quantity of the final product (e.g. a pellet of ∅ 32 mm, mass ≈ 10 g ,e.g. for neutron diffraction analysis).

A2.4.2.2. The reference electrode.

The role of the reference electrode is to provide a fixed potential which does not vary during the experiment (e.g. it should be independent on the current density). [20] In most cases, it is necessary to relate the potential of the reference electrode to other scales, for example to the normal hydrogen electrode, the agreed standard for thermodynamic calculations.

In our case the best results may be obtained using the mercury - mercuric oxide electrode (HgO/Hg). This electrode is easy to prepare and is recommended for use in alkaline solutions because of its excellent stability in this media.

The standard potential of this electrode is 0.098 V against SHE (T = 298 K, $a_{OH^-} = 1$) , or 0.925 V against the hydrogen electrode immersed in the same solution.

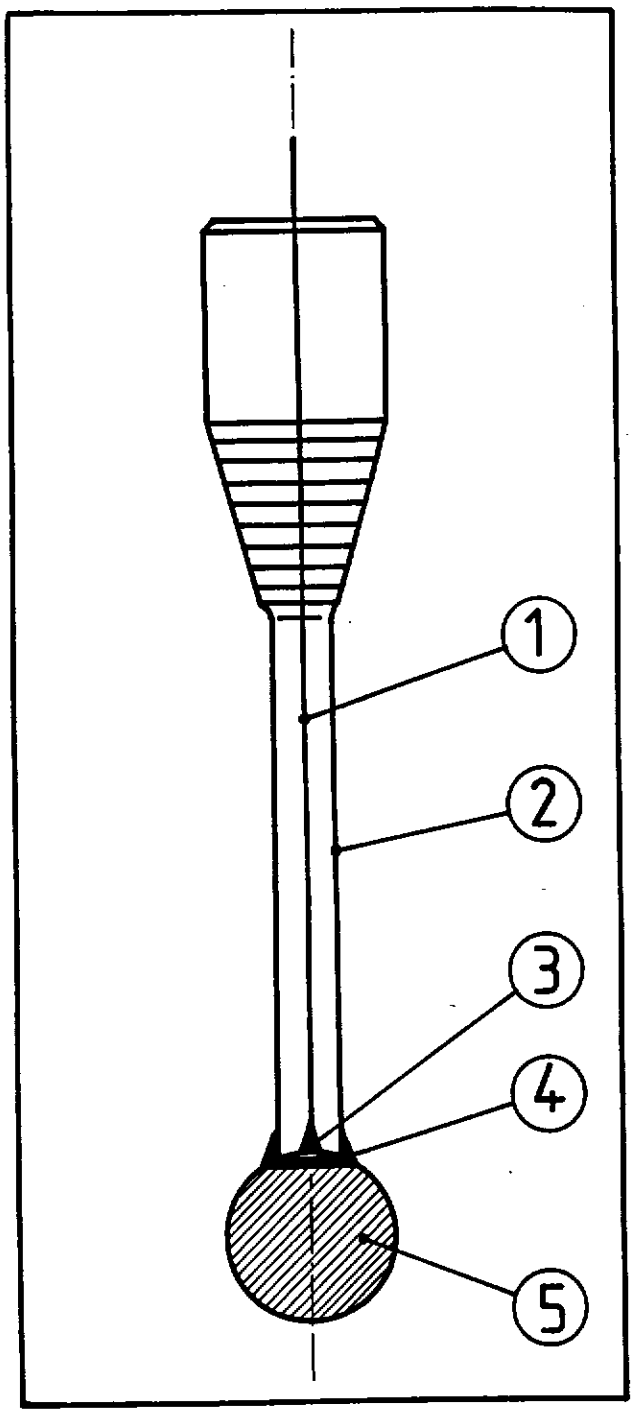

Fig. 4. Fixed electrode.

1) Pt wire, 2) Glas tube, 3) Contact (Ag), 4) Protective coating, 5) Ceramic pellet.

A2.4.2.3. The auxiliary electrode

The purpose of the auxiliary (or counter) electrode is to supply the current required to the working electrode without any way limiting the measured response of the cell.

The auxiliary electrode can be any desired electrode. One should note that this counter electrode must not impose any characteristics on the measured data, and consequently it should have a large area compared to the working electrode. Moreover, its shape and position are important since they determine whether the working electrode is an equipotential surface. It is usually chosen to be an electrode that does not produce substances interfering with the working electrode and is usually placed in a compartment separated from the working electrode by a sintered-glass ring.

It is essential that the electrode process is either the decomposition of the electrolyte medium or oxidation/reduction of a component of the electrolyte so that current flows readily without the need for a large overpotential.

The most commonly used materials for the auxiliary electrode are those of platinum, gold or glassy carbon.

A2.4.3. Operation modes of an electrochemical cell

A2.4.3.1. Constant potential electrolysis (E = const., I = f(t))

The electrochemical experiments which require control of the working electrode potential have been done with the instrumentation built around a potentiostat. [21-23] The potentiostatic control requires a rather complicated experimental device, keeping a constant value of the potential between the working and the reference electrodes disregarding ohmic losses in the electrolyte and electrode processes occurring on the auxiliary electrode. It is based on the negative feedback principle.

In practice, a chronoamperometric experiment (the alternate name for the constant potential electrolysis) is done by stepping the potential applied to a cell from an initial value where negligible current flows to a final value well beyond the half-wave potential. The current-time response (I = f(t)) is then recorded. The course of the controlled potential electrolysis (in fact based on Cottrell equation cf. §.A2.2) is shown in Fig. 5a

This experimental technique allows to obtain sufficient overpotential so that the electrochemical reaction appears at the half- wave potential but it limits the occurrence of another electrochemical reactions provided that its electrochemical characteristics are more positive than the applied potential. This control of the potential yields to increase significantly the selectivity of the electrochemical experiments.

A2.4.3.2. Constant current electrolysis (I = const., E = f(t))

On the contrary the galvanostatic method requires a more simple instrumentation.

If a constant current is applied on the electrode, then the concentrations at the electrode surface start to change due to the 1st Fick law:

$$I = \text{const.} = n \cdot F \cdot A \cdot D_{Ox} \frac{dC_{Ox}}{dx} = -n \cdot F \cdot A \cdot D_{Red} \frac{dC_{Red}}{dx}$$

and this change is accompanied by corresponding change of electrode potential (e.g. according to Nernst equation). Hence, the gradients of concentration at the surface are constant. The potential shifts towards an extreme value (positive if current positive), this shift being accomplished if one of the concentrations sinks to zero (Red if $I > 0$).

However, the potential rise is limited to finite values in real systems (the evolution of hydrogen or oxygen in aqueous solutions).

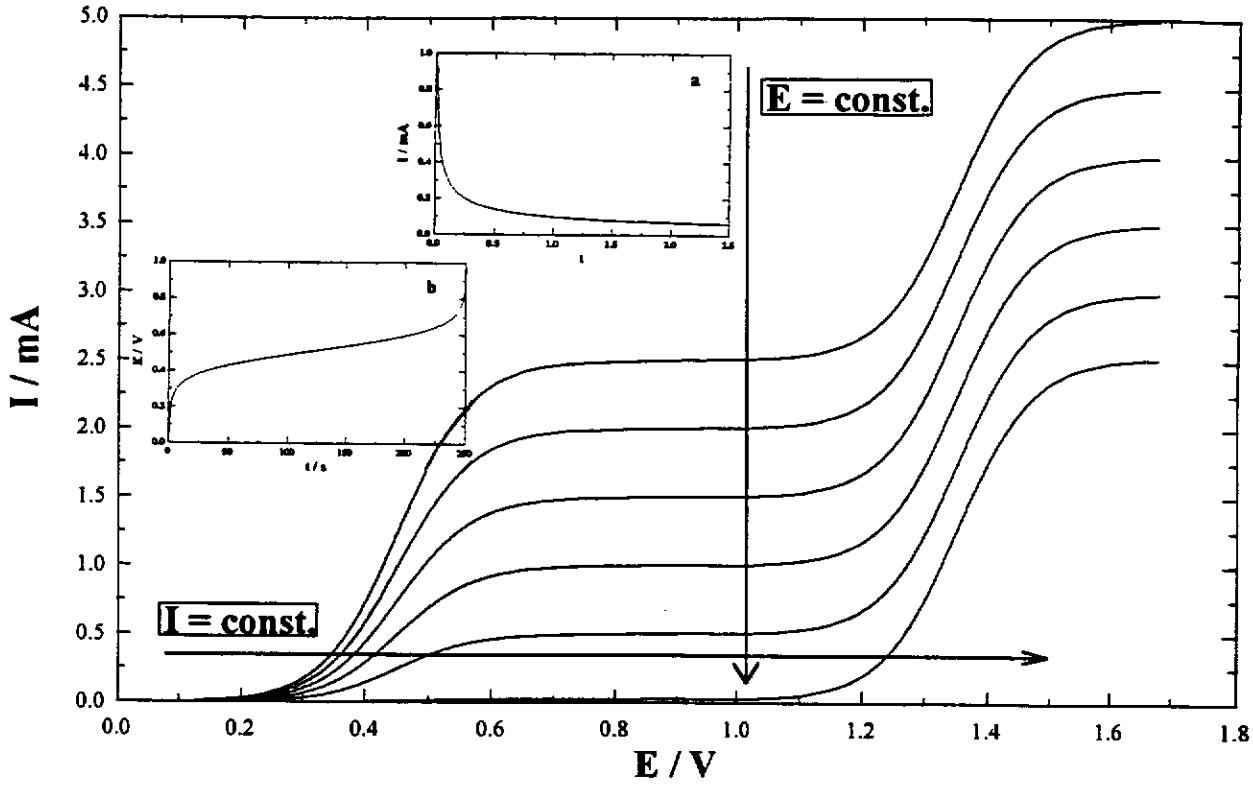

Fig. 5. Schematic representation of a) the constant potential electrolysis, b) the constant current electrolysis.

References page 183

The number of electrons related to the quantity of material involved in the electrode reaction can be determined rather easily on the basis of the Faraday law (cf. A2.1.)

The course of the constant current electrolysis is sketched in Fig 5.b.

A2.4.3.3. Voltammetry

Voltammetry is the class of electrochemical measurements in which the controlled parameter, the potential of the working electrode, varies with time and in which the current flowing through the working electrode is the measured parameter.

Classical (or linear sweep) voltammetry is that subclass of voltammetry in which the rate of change of potential with time is sufficiently slow so that the observed phenomena can be quantitatively described by equilibrium or quasi-equilibrium theories.

Fast voltage scan techniques whose scan is reversed, are called cyclic techniques. In these techniques a ramp is applied over the full voltage-scan range and then reversed so that a descending ramp returns, almost invariably to the original potential. The scan rate in the forward and reverse directions is normally the same, so that the excitation waveform is actually a triangle.

When using cyclic voltammetry to study a system for the first time it is usual to start by carrying out qualitative experiments in order to get a feel for the system, before proceeding to semi-quantitative and finally quantitative ones from which kinetic parameters may be calculated (i.e. to measure the CV curves until the decomposition of the electrolyte solution occurs). In a typical qualitative study it is usual to record voltammograms over a wide range of sweep rates and for various values of potentials. Commonly, there will be several peaks, and by observing how they appear and disappear as a function of the potential limits and sweep rate, and also by noting the differences between the first and subsequent cycles, it is possible to determine which

kind of electrochemical processes represented by the peaks takes place. At the same time, from the sweep rate dependence of the peak amplitudes, the role of adsorption, diffusion, and coupled homogeneous chemical reactions may be identified. The difference between the first and subsequent cyclic voltammograms frequently provides useful mechanistic information. It must, however, be pointed out, that kinetic data can only be accurately obtained from an analysis of the first sweep, especially in the case of ceramic electrodes that may modify (oxidation, reduction) during the CV sweep.

The simplest case of the reversible charge transfer occurring on the surface of a plane electrode was at first solved by Randles and Ševčík in 1948 [24,25]. The solution, quite difficult because of the time dependent potential term, is expressed in the following relation:

$$I_p = -0.4463 \cdot n \cdot F \cdot [Red]_{el} \cdot \sqrt{\frac{nF}{RT} \cdot D \cdot \nu}$$

where I_P is the peak current, D is the diffusion coefficient and ν is the scan rate.

The theoretical evaluation of the equations corresponding to various more complicated reaction mechanisms is very complex and exceeds the scope of this short overview. The reader may refer to more fundamental articles, such as that of Nicholson and Shain [26].

A2.4.3.4 The rest potential (open circuit voltage) , Armand equation

In the case of the intercalation of ionic species into the host lattice of an oxide electrode material, the open circuit voltage is an important parameter related to the amount of intercalated or deintercalated species in the host lattice. In that case the Nernst equation (cf. §.A2.2) cannot be used for correlating the experimentally measured potential with the concentration of the electroactive species because it is

References page 183

valid only for species occurring at the electrolyte/electrode interface in the electrolyte solution.

The relation between the open circuit voltage and the amount of species present in the host lattice was studied at first by Crandall and Faughnan [27]. Similar considerations were reported also by Armand [28] who gave the following relation:

$$E = E^{\circ} + Ky - \frac{nRT}{F} \cdot \ln \frac{y}{1-y}$$

for the dependence of the open circuit voltage on the concentration of the intercalated species y in the host lattice, in fact some kind of extension of the Nernst equation involving the solid phase. E^{O} is the standard potential of the intercalation reaction.

The K factor (called also the Darken, or thermodynamic factor [29]), relies the concentration and the activity of the inserted ions

$$K = \frac{\partial \ln a}{\partial \ln c} = -\frac{yF}{RT}\frac{\Delta E}{\Delta y}$$

A2.5. References

1) Bard A.J., Faulkner L.R., *Electrochemical Methods*, Wiley, New York, 1980.

2) Bockris O'M. J., Reddy A., *Modern Electrochemistry*, Plenum, New York, 1970.

3) Nernst W., Z. Phys. Chem., **4**, 129,1889.

4) Vetter K., *Electrochemical Kinetics*, Academic Press, New York, 1967.

5) Butler J.A.V., Trans. Faraday Soc., **19**, 734, 1924

6) Tafel J., Z. Phys. Chem., **50A**, 641, 1905.

7) Charlot G., Badoz-Lambling J., Tremillon B., *Electrochemical Reactions*, Elsevier, Amsterdam, 1962.

8) Albery W.J., *Electrode Kinetics*, Oxford University Press, London, 1972.

9) Cottrell F.G., Z. Phys. Chem., **42**, 385, 1903.

10) Heyrovský J., Ilkovič D., Coll. Czech. Chem. Commun., 7., 198, 1935.

11) White R.E., *Electrochemical Cell Design*, Plenum, New York, 1984.

12) Micka K., Coll. Czech. Chem. Commun., **30**, 2288, 1965.

13) Daniel' - Bek V.S., Zh. Fiz. Khim., **20**, 567, 1946.

14) Grens. E.A., Tobias C.W., Z. Elektrochem., **68**, 236, 1964.

15) deLevie R., *Electrochemical Response of Porous and Rough Electrodes*, in *Advances in Electrochemistry* (ed. Delahay P.), Vol. **6**, 329, New York, Interscience Publishers, 1967.

16) Levich V.G., *Physicochemical Hydrodynamics*, Englewood Cliffs, NJ: Prentice Hall, 1962.

17) Albery W.J., Hitchmann M.L., Ring - Disc Electrodes, Clarendon Press, Oxford, 1971.

18) Riddiford A.C., Rotating Disk System, in Advances in Electrochemistry and Electrochemical Engineering, (Delahay P., Tobias T., eds.), Vol. **4**, Interscience Publishers, New York, 1966.

19) Arrouy F., Doctoral Thesis, University of Bordeaux, 1992.

20) Ives D.J.G., Janz G.J., Reference Electrodes, Theory and Practice, Academic Press, New York, 1961.

21) MacDonald D.D., Transient Techniques in Electrochemistry, Plenum, New York, 1977.

22) Delahay P., *New Instrumental Methods in Electrochemistry*, Interscience, New York, 1954.

23) Greef R., Peat R., Peter L.M., Pletcher D., Robinson J., Instrumental Methods in Electrochemistry, Ellis Horwood, Chichester, 1985.

24) Randles J.E.B., Trans. Faraday Soc., **48**, 828, 1952.

25) Ševčík A., Coll. Czech. Chem. Commun., **13**, 349, 1948.

26) Nicholson R.S., Shain I., Anal. Chem., **36**, 706, 1964.

27) Crandall R.S., Faughnan B.W., Phys. Rev., **B16**, 175, 1977.

28) Armand M., *Intercalation Electrodes* in *Materials for Advanced Batteries* (ed. Murphy D.W.), 145, Plenum, New York, 1980.

29) Darken L.S., Trans. AIME, **175**, 184, 1948.

APPENDIX 3

The interface for Electrochemical Experiments

A.3. The Interface for Electrochemical Experiments Controlled by an IBM PC Computer

Simple and Succinct Description

The main idea leading to the interface between a computer and a potentiostat is to improve the performance of the existing electrochemical device already available for the electrochemical experiments. Such an interface can be rather flexible, the programs written in a relevant programming language (such as the Microsoft Quick BASIC) are easily modifiable to the needs of the experimental conditions of the research work.

Thus far, all on microcomputer based electrochemical experiments [1-9] use to control a conventional potentiostat (or galvanostat). The computer based instrumentation replace usually the function generator and the recording device. The interface between the digital part (represented by the computer) and the analog part (the potentiostat and the cell) are achieved by A/D and D/A converters (ADC and DAC respectively).

DAC enables a microcomputer to be used as a function generator. Thus by successively converting a series of binary numbers, theoretically every desired waveform can be generated. The major limitation is the resolution of the DAC, which depend on two factors: the output voltage range and the number of bits which are converted. Output ranges of 1V, 2.5V, 5V and 10V are common, both unipolar and bipolar. For electrochemical purposes a bipolar 5V DAC is probably the optimal one. The cost of DACs increases with the increase of the number of bits converted, and a good compromise is therefore a 12-bit resolution. A 12-bit, ±5V converter will have a resolution of 2.4 mV, which satisfy most purposes.

The ADC is used for conversion of the cell voltage to machine interpretable, digital form. Again, these devices are available similarly as DAC in different input ranges, which should be matched as closely as possible to the maximum output range

of the electrochemical system under investigation. Generally 12-bit resolution will be again sufficient, provided that the input range is well chosen.

First part, the electrochemical measuring system, is based on a classical potentiostat. The another part is represented by IBM PC compatible computer with peripherals and corresponding software. This part operates as a controller for potentiostat and data acquisition unit as well.

The hardware and software described in this appendix provide the control of the common potentiostat available earlier and as well as the computer-aided evaluation of the resulting voltammograms, chronopotentiograms (E = f(t), I = const.) or chronoamperograms (I = f(t), E = const.).

A3.1. Computer and interface cards

The system consists of two major parts: a personal computer (PC) with peripheral devices (parallel printer, HPGL compatible plotter) and electrochemical device. The PC is an IBM PC compatible computer based on an Intel 80x86 microprocessor supported by the Intel 80x87 coprocessor and equipped with at least 640 kB memory, hard disk and an graphic card. The communication with the electrochemical device is provided by the commercial ADDA 12-bit card installed in a PC's expansion slot.

The pilot voltage for the potentiostat is applied directly from the DAC output. The DAC output was wired for bipolar operation.

The ADC was made using the Keithley DAS8/PGA card [10]. This card permits to measure voltages in 12-bit resolution mode with several gains up to ±10mV/full scale. The input is achieved using differential amplifiers to improve the signal/noise ratio and to increase satisfactorily the input impedance of the input channels.

References page 196

A3.2. Potentiostat

A Tacussel PJT 24-1 potentiostat was operated using the PC based interface. This potentiostat has been designed to be easily adaptable to different types of the electrochemical devices [11]. It is due to its main advantage - the low impedance outputs of all signals provided by a potentiostat (E, I, $I_{filtered}$, V_{aux}) and the external voltage input for piloting the operation by several external sources.

A3.3. Software

Software for voltammetric, constant potential, constant current experiments and the measurement of the open circuit potential, was written in Microsoft Quick BASIC version 4.5.

All programs are divided into three parts: input part, "electrochemical" routine and output data to disk.

A3.4. Voltammetry.

The first part allows to input all necessary parameters for the curve (e.g. initial potential, potential range, scan rate, expected current range, and the identifications of the experiment). A complete set of input parameters can be stored in the input data field and/or as an option in the separate description file. This gives the opportunity of repeating experiments under standardized conditions (see Tables I and II).

Table I: Program CVPJT.EXE - Main menu.

Main menu		
Description of experiment		
Number of cycles		: 1
Initial potential	(V)	: 0
Maximum potential	(V)	: 1
Minimum potential	(V)	: -1
Scan rate (V/s)		: 1
Sign of polarisation (+/-)		: +
Shunt resistance (Ω)		: 1000
Name of file		: SRC
Run sweep		
Read parameters from a file		:
Exit		

Table II: Program CVPJT.EXE - description of experiment.

Cyclic voltammetry
Working electrode : $SrCoO_{3-y}$
Electrolyte : NaOH 1 M
Reference electrode : HgO/Hg 1M NaOH
Rotation speed : 2000 rpm
Conditions : electrode 31/12/93 - 1
Particular : none
Return to main menu

References page 196

When the experiment is completed the last part of the program starts (Table III).

Table III: Program CVPJT.EXE - Data treatment.

Data treatment
Smoothing
Data storage
Set up the limits
Back to main menu

There are three useful facilities presented:

- a convenient graphical representation
- a data smoothing routine
- measured data sets could be optionally stored for later retrieval.

The graphs on the screen can be hard-copied by means of a graphics printer.

General least-squares smoothing procedure according to the Savitzky-Golay method [12] incorporating the improvements presented by Gorry [13] was used. This subprogram uses 9-point cubic fit, which includes initial-point smooth.

A3.5. The Open Circuit Potential, Potentiostatic and Galvanostatic electrolyses

The essential parts of this program are presented in Tables IV - VI.

Table IV: Program OCPA.EXE - Main menu.

Main menu
Time increment : 1
Number of points (max. 32500) : 3600
Name of file : SRC
Constant potential (I = f(t))
Constant current I ≥ 0 (E = f(t))
Run
Read data file
Exit

Table V: Program OCPA.EXE - Constant potential experiment.

Constant potential experiment
Working electrode : $SrCoO_{3-x}$
Electrolyte : NaOH 1M
Reference electrode : HgO/Hg 1M NaOH
Rotation speed : 2000 rpm
Conditions : electrode 31/12/93 - 2
Particular : none
Potential : 0.5 V
Shunt resistance (Ω) : 1000
Name of file : SRC.CHA
Return to main menu

References page 196

Table VI: Program OCPA.EXE - Open circuit voltage measurement, Constant current experiment.

Open circuit voltage measurement
Working electrode : $SrCoO_{3-x}$
Electrolyte : NaOH 1M
Reference electrode : HgO/Hg 1M NaOH
Rotation speed : 2000 rpm
Conditions : electrode 31/12/93 - 3
Particular : const. current 250 μA
Name of file : SRC.OCP
Return to main menu

The program allows to measure the desired quantities as a function of time, with the step lying between 1 second and 1 day. The quantities are on line visualized on the screen and stored (if the step is superior to 5 seconds) in the file. If the step is equal of inferior to 5 seconds, the measured curve is stored on the disk after the experiment had been finished. The latter options of program are the same as for the previous programs.

A3.6. Limits of the interface.

Theoretically the limits of such an interface are given either by the limits of used potentiostat or by limits of used DAC, ADC converter.

In the case of the our device, the potentiostat Tacussel PJT 24-1 can operate within the ± 5 V between the working and reference electrode and within ±24 V between the working and auxiliary electrode. The maximal allowed current is 1 A.

The converter card can produce the piloting voltage within ±10 V. The input ranges are programable between the gains of ±10 V (resolution 4.88 mV) and ±10 mV (resolution 4.88 μV).

It implies in fact that the main limitation of this device is given by the operating conditions of the potentiostat Tacussel, PJT 24-1.

On the contrary the maximal scan rate is limited by the configuration of the PC.

A3.7. Conclusions

The main benefits of the described apparatus are:

- Each potentiostat which has an external pilot voltage input can be used

- Scan rates up to $1Vs^{-1}$ are reached with the 10 MHz IBM PC/XT in the on line monitoring mode (The increase of the scan rate depends only on the configuration of the PC).

- Easy adaptation for different hardware configuration by program modification.

- Easy use of the software also for electrochemists who are not familiar with the computers.

References page 196

A3.8. References

1) Tommasino J.B., *Doctoral Thesis*, University of Toulouse, 1992

2) Osteryoung R.A. in *Computers in Chemistry and Instrumentation*, Ed. J.S. Mattson, H.B. Mark and H.C. Macdonald., Vol. 2, p.353, Marcel Dekker, (1972).

3) Smith D.E., in *Computers in Chemistry and Instrumentation*, Ed. J.S. Mattson, H.B. Mark and H.C. Macdonald., Vol. 2, p.369, Marcel Dekker, (1972).

4) Perone S.P., in *Computers in Chemistry and Instrumentation*, Ed. J.S. Mattson, H.B. Mark and H.C. Macdonald., Vol. 2, p.423, Marcel Dekker, (1972).

5) Kirschenbühler P., Latscha H.P., Chemiker Ztg., **112**, 169, 1988.

6) Kirschenbühler P., Kellerbauer R., Latscha H.P., Chemiker Ztg., **113**, 147, 1989.

7) Thomsen K.N., Skov H.J., Kryger L., Anal. Chim. Acta, **219**, 105, 1989.

8) *Autolab / General Purpose Electrochemical System*, ECO Chemie Ltd., Utrecht, Netherlands.

9) *Z-computeur / General Purpose System for Electrochemical Measurements*, Tacussel, Solea Ltd., Villeurbanne, France.

10) *Keithley DAS8/PGA card, User Guide*, Keithley Inc., USA, 1990.

11) *Tacussel PJT 24-1 potentiostat, User Guide*, Solea Ltd., Villeurbanne France

12) Savitzky A., Golay M.J., Anal. Chem., **36**, 1627, 1964.

13) Gorry P.A., Anal. Chem., **62**, 570, 1990.

Figure Captions

Chapter I

Chapter II

Figure Captions

Chapter III.

Chapter IV

Figure Captions

Appendix 2